

**ELUCIDATING THE BIOMECHANICAL FACTORS
THAT INFLUENCE FLUID LOSS AND RECOVERY
IN ARTICULAR CARTILAGE**

by

Steven Voinier

A dissertation submitted to the Faculty of the University of Delaware in partial fulfillment of the requirements for the degree of Doctor of Philosophy in Mechanical Engineering

Summer 2023

© 2023 Steven Voinier
All Rights Reserved

**ELUCIDATING THE BIOMECHANICAL FACTORS
THAT INFLUENCE FLUID LOSS AND RECOVERY
IN ARTICULAR CARTILAGE**

by

Steven Voinier

Approved: _____
Ajay K. Prasad, Ph.D.
Chair of the Department of Mechanical Engineering

Approved: _____
Levi T. Thompson, Ph.D.
Dean of the College of Engineering

Approved: _____
Louis F. Rossi, Ph.D.
Vice Provost for Graduate and Professional Education and
Dean of the Graduate College

I certify that I have read this dissertation and that in my opinion it meets the academic and professional standard required by the University as a dissertation for the degree of Doctor of Philosophy.

Signed:

David Burris, Ph.D.
Professor in charge of dissertation

I certify that I have read this dissertation and that in my opinion it meets the academic and professional standard required by the University as a dissertation for the degree of Doctor of Philosophy.

Signed:

Jill Higginson, Ph.D.
Member of dissertation committee

I certify that I have read this dissertation and that in my opinion it meets the academic and professional standard required by the University as a dissertation for the degree of Doctor of Philosophy.

Signed:

X. Lucas Lu, Ph.D.
Member of dissertation committee

I certify that I have read this dissertation and that in my opinion it meets the academic and professional standard required by the University as a dissertation for the degree of Doctor of Philosophy.

Signed:

Christopher Price, Ph.D.
Member of dissertation committee

I certify that I have read this dissertation and that in my opinion it meets the academic and professional standard required by the University as a dissertation for the degree of Doctor of Philosophy.

Signed:

Lynn Snyder-Mackler, Sc.D.
Member of dissertation committee

ACKNOWLEDGMENTS

To all of the funding sources that supported me during my time at Delaware, including the National Science Foundation and the Delaware Space Grant.

To my advisor, David Burris, who taught me that if I am going to say or write something, to make sure it's worth listening to.

To my past and present lab mates who have supported (and hopefully I have also lent support to): Axel, Viraj, Aman, Istiaque, Arnab, Nick, Farida, Subrata, Abdulmalik, and my cartilage buddy, Jamie. Additionally, thank you for the undergraduate researchers who volunteered their time to perform experiments and complete data analysis in my absence.

To my friends Dana and I have found outside of the University of Delaware. Thank you for not judging us (publicly) for pursuing the PhD. Furthermore, thank you for lending your support whenever you could, no matter how large or small.

To my dissertation committee, who have graciously volunteered their efforts and time to ensure that I earn this degree.

To my teachers and mentors, starting from kindergarten. Thank you for encouraging me to struggle mentally, and never curtailing my creativity when approaching problems.

To my parents, Elaine and Randy who always told me that my extra education would never be wasted and respected my time when I was just too busy. To my brothers (Chris and Greg) and in-laws (Kathy, Manda, Tom, Christine, Thomas, and Christian), who provided the foundation for Dana and me to finish our degrees.

To my daily wolf pack in Teddy, Max, and Bear. You will never learn to read this, but know that I enjoyed the company as much as you did.

And finally to my rock, Dana. You know the depths of my character many times more than I do and know how bring out my best qualities to help this world. Now that we finished school...let's do this!

TABLE OF CONTENTS

LIST OF TABLES	x
LIST OF FIGURES	xi
ABSTRACT	xxi

Chapter

1	CARTILAGE BIOMECHANICS AND ITS RELATIONSHIP TO FUNCTION	1
1.1	Cartilage function and structure	1
1.2	Articular Cartilage cells upkeep ECM integrity	2
1.3	How does cartilage maintain its function?	3
1.4	What happens when cartilage breaks down?	4
1.5	Can we save our cartilage and reduce the risk of OA?	5
1.6	The mechanical response of cartilage and dynamics of fluid flow	6
1.7	Applying biphasic theory to explain cartilage mechanics	8
1.8	Cartilage fluid strain in the context of human movement	11
1.9	Objectives	15
2	AIM 1—CAN A RANGE OF CONTACT STRESSES BE PREDICTED FOR A RANGE OF PHYSIOLOGICAL LOADS?	19
2.1	Introduction	19
2.2	Methods	21
	Experimental Details	21
2.2.1	Sample Extraction	21
2.2.2	Experimental Procedure	22
2.3	Data Analysis	24
2.3.1	Experimental Contact Mechanics	24
2.3.2	Theoretical Contact Mechanics Framework	24
2.4	Results	26
2.4.1	Experimental results	26

	2.4.2	Contact Model Results	29
	2.4.3	Discussion.....	32
3		AIM 2—EXUDATION CHARACTERISTICS OF CARTILAGE IN PHYSIOLOGICAL CONDITIONS.....	37
	3.1	Introduction	37
	3.2	Methods	41
	3.2.1	Materials and specimen preparation.....	42
	3.2.2	Testing Instrument.....	42
	3.2.3	Exudation Testing Procedure and Data Curation	44
	3.2.4	Model Development	46
	3.2.5	Data Analysis.....	50
	3.3	Results	51
	3.3.1	Effect of load and preload	53
	3.3.2	Simulating the effect of indentation-based permeability.....	59
	3.4	Discussion.....	60
4		AIM 3—THE MODES AND COMPETING RATES OF CARTILAGE FLUID LOSS AND RECOVERY	69
	4.1	Introduction	69
	4.2	Methods	72
	4.2.1	Materials	72
	4.2.2	Instrument and Measurements.....	74
	4.2.3	Fluid Recovery Measurements	74
	4.2.4	Data Analysis.....	78
	4.3	Results	79
	4.4	Discussion.....	84
5		AIM 4—HYDRODYNAMIC DRIVEN REHYDRATION: HOW TO REACH FUNCTIONAL EQUILIBRIUM.....	92
	5.1	Introduction	92
	5.2	Methods	96
	5.2.1	Materials and specimen preparation.....	96
	5.2.2	Instrument and Measurements.....	97

5.2.3	Measuring the Dynamic Equilibrium with varying Sliding Speeds and Load.....	98
5.2.4	Measuring the Fluid Load Support at Dynamic Equilibrium....	100
5.2.5	Measuring the Dynamic Equilibrium at Sub-physiological Sliding Speeds	101
5.3	Results	103
5.3.1	Dynamic Equilibrium with varying Sliding Speeds and Load..	103
5.3.2	Fluid Load Support at Dynamic Equilibrium.....	105
5.3.3	Dynamic Equilibrium at Low Sliding Speeds	106
5.4	Discussion.....	107
6	DISCUSSION AND CLOSING REMARKS	117
6.1	Summary of Aims.....	117
6.2	How can this dissertation inform activity recommendations?	120
	REFERENCES	123
Appendix		
A	SUPPLEMENTAL METHODS.....	152
A.1	Darcy Flow Model Development	152
A.2	Model Iterative Algorithm and Fit	156
A.3	Exudation Model Image processing	157
B	SUPPLEMENTAL RESULTS.....	159
B.1	Exudation Model Results	159
B.2	Rehydration Rates Comparison.....	160
B.2.1	Comparing Cartilage-on-Cartilage rehydration vs. Free Swelling and Passive Swelling.....	160
B.2.2	Quantifying Applied Contact Pressures	162

LIST OF TABLES

Table 1:	The predicted model material properties separated by sample and preload. For each sample and preload condition, mean and standard deviation of E_c , E_t , k_0 and M are reported for imparted loads 2,3,4, and 5 N. Although an increase in load yielded a statistical change in material properties, these data demonstrate a more substantial sample-based effect on material properties. Additionally, the effect of preload only significantly reduces the tensile modulus of the tissue, while the remaining tissue properties remain indistinguishable.	57
----------	---	----

LIST OF FIGURES

- Figure 1-1: Cartilage tissue lining our joints consists of a complex collagen matrix to support load and reduce friction while infused chondrocytes maintain biological processes. Most of the tissue is composed of water (~80%) which is drawn in by the negatively charged proteoglycans..... 1
- Figure 1-2: To maintain its functionality, the tissue must maintain its hydration levels to improve lubrication [21], [22], minimize overloading [11], maintain its collagen network and low permeability [24], and sustain metabolic function and regular matrix synthesis [6], [14], [39]. These processes also depend on the regular fluid gain and loss..... 4
- Figure 1-3: A) Confined compression experiments were first used to describe the creep mechanics and fluid exudation of cartilage. B) Unconfined compression experiments more resembled the mechanics of cartilage layers, specifically simulating an impermeable contact interface. At equilibrium, fluid pressure in both unconfined and confined compression ~0. C) Current models of joint contact include cartilage creep models based on the lateral ejection of fluid and impermeable interface as modeled in unconfined compression [11]. However, it is unknown if that contact stress can be predicted and if the interface is indeed impermeable. 10
- Figure 1-4: With the MCA paradigm, cartilage can only exude fluid throughout the day (shown in grey). However, this will equate to significant loading by the end of the day [102]. An alternative thought model includes the realistically high fluid loss (red), but exudation must be equally matched by rehydration (blue) if strains are kept low during movement and by the end of the day..... 13
- Figure 1-5: A) During static loading, contact areas under load will exude fluid. Upon articulation in B), contact areas are directly exposed to the bath for rehydration and hydrodynamics can rehydrate the contact via tribological rehydration [117]. However, due to the periodic motion of joints, joints will always incur some exudation when they return to original contact conditions shown in A). This suggests that cartilage is in a competitive framework of exudation and rehydration during movement. 15

Figure 1-6: The pictorial outline of this dissertation. To understand exudation/rehydration, the contact stress must be predictable (**Aim 1**). The mechanics of inflow and out must be well understood to determine the strain on the tissue (**Aim 2 and 3**). The equilibrium strain defined the “operating conditions” of cartilage, and the physiological parameters that drive the equilibrium strain will be defined (**Aim 4**) 16

Figure 2-1: A) The uniaxial loading apparatus for loading cartilage. While the test sample was submerged in a 1x PBS, an air piston (not shown) loads the cartilage against the plexiglass plate while a camera records the resultant contact area and the load cell records the force. B) A view of the cartilage sample i) prior to loading and ii) a resultant contact area near maximum loading conditions. The contact radius (a) never exceeded the sample radius (9.5 mm). C) The geometrical parameters i) an orthogonal view of a cartilage sample was recorded to define the principal radius of curvature ii) after testing, cartilage samples were sectioned and the thickness was measured at three locations to yield a mean and standard deviation of each plug. 23

Figure 2-2: The contact mechanics of a representative sample of cartilage is visualized in A), B) and C). The measured force (F), contact area (A), and contact stress (P) are displayed with each of the images. The contact area data are shown in D) for the experimental range of loads (0-450 N). The resultant contact stress data are graphed in E). Errors in measurements were consistent across all samples. 27

Figure 2-3: Resultant contact stress vs. input force is separated out for each joint in A) - E). Connected data points represent the response for a single sample. Aggregated results are displayed in G) including binned means (bin size =30 N) with +/- standard deviation lines. 28

Figure 2-4: Theoretical Hertzian corrected contact Modulus vs. input force is separated out for each joint in A) - E). Connected data points represent the response for a single sample. Aggregated results are displayed in G) including binned means (bin size =30 N) with +/- standard deviation lines. 29

Figure 2-5: The mean Hertzian corrected contact modulus for each sample Separating the data by joint illustrates the variability of modulus within a joint, and thus, constant modulus should not be assumed for a unique joint. The error bars represent the standard deviation of the modulus over the range of experimental loads. 30

Figure 2-6: A) With the average contact modulus, the predicted Hertzian substrate corrected contact stress is plotted against experimental data for a representative sample. The power law fit is also provided. The percent error ($\% \text{Err}_i$) was calculated at each data point to yield the RMSPE from the fit. B) The RMSPE for all samples separated by joints tested.. 31

Figure 2-7: A histogram plot of the power law coefficients from the Hertzian corrected model and the experimental results. The larger range in the experimental power law coefficient (0.6-0.9) likely demonstrates that there are sample specific stiffening effects. 32

Figure 3-1: A) In Aim 2.1, we will determine the exudation characteristics of a fully hydrated cartilage sample. B) Aim 2.2 will address if interfacial permeability can be reestablished after a passive load..... 41

Figure 3-2: The experimental setup for exudation data collection. The deformation of cartilage could be tracked via the spring/vertical stage/load cell system [18], [28]. India ink infused in the DI bath provided the necessary contrast to discern the changing area of contact. 44

Figure 3-3: The biphasic model of contact and exudation. It was assumed that the fluid within the tissue and the gap laterally ejected through the tissue. Per Darcy’s Law, the pressure in the system was calculated based on streamlines from 1 to 2. See Appendix A for model development. Based on a given contact stress (σ) and change in deformation ($\Delta\epsilon$), the elastic stress (σ_{elastic}), could be calculated. Thus, the resultant fluid pressure could be calculated at future time steps according to Equation 19..... 49

Figure 3-4: The measured deformation (A) and contact radius (B) is plotted vs. time for a single sample and multiple loads. The respective time constants (τ) are shown in light gray circles. For this sample, the average τ_a was 4.6 times larger than average τ_δ 52

Figure 3-5: A representative fit for a single load shown in red. The first data point ($\sim 100 \text{ um}$) was considered the initial elastic deformation. All subsequent deformation accounted for the exudation response. Although this sample did not reach equilibrium within 90 minutes, the model was able to well predict the exudation response. The standard deviation between all simulated fits is non-discernable from the fit shown in red. 53

- Figure 3-6: The predicted permeability curves vs. tissue deformation for the range of tested loads. The permeability at a given tissue deformation was systematically higher for higher loads. For example, at 150 μm , the apparent permeability was 50% higher when comparing 5N to 2N, but also had a $\sim 4\text{X}$ increase in fluid pressure, resulting in a 6X quicker exudation rate at the same deformation..... 54
- Figure 3-7: The generated FLS curves for a representative sample. In this sample, the FLS started at $\sim 96\%$ at initial loading, which is expected since fluid exudation ≈ 0 . The FLS dropped to below 20% after ~ 5000 seconds. Increased load maintained FLS for a longer period..... 55
- Figure 3-8: Comparing the effect of a 60-minute 0.3 N preload on the response of A) deformation, B) contact radius, and generated C) permeability and D) FLS curves for a 5 N contact load. Both the initial deformation and contact area were greater in the preload case, likely due to prior exudation from the 0.3 N load. By 100 seconds, the response was visually indistinguishable, indicating the interface likely repressurized with fluid. Consequently, the permeability characteristics (k_0 and M) were also indistinguishable in this loading case. However, compaction of the interface had limited effect on the fluid pressurization, as depicted in similar FLS curves in D)..... 58
- Figure 3-9: A) The experimental exudation curves (solid lines) are contrasted with the generated exudation curves (dashed lines) with permeability values from literature ($k_0 = 0.00171 \text{ mm}^4/\text{Ns}$, $M = 4.3$). Because the intrinsic permeability is reduced by $\sim 10\text{X}$, the generated exudation curves take $\sim 10\text{X}$ longer to reach the same strains. B) Using the reduced permeability from literature result in an extended FLS decay time. Again, FLS requires 10X the time to reach low FLS..... 59
- Figure 3-10: a) Applying passive load of 0.3N to equilibrium equates to ~ 0 pressure within the interfacial gaps and all of the load is supported by the asperities. b) Once a higher load is introduced, asperities experience more contact pressure as other asperities come into contact, resulting in pressurized fluid into the cartilage gap, thus reopening for the interface for flow. 65

Figure 4-1 Schematic of the experimental apparatus. (a) The cartilage-on-flat configuration (which generates a convergent stationary contact area, cSCA) was used for passive swelling and tribological rehydration tests. The sample was clamped via the subchondral bone and the convex cartilage surface was loaded against a glass disc 21 mm from a rotary spindle. A calibrated water drip added DI water at the same rate as evaporation to maintain osmolarity. (b) The indenter-on-cartilage configuration was used with a porous (60 μm pores, 60% solid, permeability (k) $\sim 2500 \text{ mm}^4/\text{Ns}$) plane-ended stainless-steel indenter (ϕ 6 mm) for free swelling tests. The sample was mounted to a 2-axis tilt stage to align it with the indenter. Schematic sketches of tribological rehydration, passive swelling, and free swelling are shown for reference. 73

Figure 4-2: (a) Methods used to quantify passive and free-swelling rates (δ), which are defined here as the rate of change in thickness or the rate of volume change per unit contact area. Following static exudation at 5 N to a target compression, load was decreased to a tare load of 0.1 N. Time-dependent passive and free swelling rates were quantified using the instantaneous slope of recovery data taken just after reaching the 0.1 N tare load. The term ‘elastic’ denotes active loading and unloading phases where fluid volume is approximately conserved. (b) Methods used to quantify tribological rehydration and exudation rates, also defined based on the change in thickness per unit time. Following static exudation at 5 N to a target compression, fluid recovery accompanied the onset of sliding at 100 mm/s under the constant 5 N load. The time-dependent exudation and recovery rates were quantified using the instantaneous slopes of the exudation and recovery curves as shown. The tribological rehydration (total fluid gained, blue points) rate is the sum of the strain-matched exudation (fluid lost, grey) and recovery (net fluid gained, green) rates as shown. 77

- Figure 4-3: Results of passive and free swelling experiments. (a) Raw end-of-compression and start-of-recovery results from passive swelling measurements for a single representative sample subjected to varying tissue compression; each experiment is labeled with its initial exudation in microns. (b) Raw compression and recovery results from free swelling measurements for a different representative sample with varying tissue compression. The exudation and elastic recovery portions of the curve are highlighted in dark and light grey zones, respectively. (c) Fluid recovery (in microns) for passive and free swelling versus time from the same two representative samples. (d) Passive and free swelling rates (in microns per second) versus time for the same two representative samples..... 80
- Figure 4-4: Results of tribological rehydration experiments conducted with varying tissue compressions for a single representative sample. (a) Raw compression and recovery results from tribological rehydration measurements for a single representative sample subjected to different initial compressions; each experiment is labeled with the initial compression at the onset of sliding minus the elastic compression. (b) Net measured fluid recovery starting from the onset of sliding as a function of time for the same experiments. (c) Tribological rehydration rates and exudation rates for the same experiments as a function of time. The system reached a dynamic equilibrium of zero net flow when exudation (outflow) balanced tribological rehydration (inflow) at $\sim 0.2 \mu\text{m/s}$ each..... 82
- Figure 4-5: Summary of fluid recovery rates for all samples. (a) Mean inflow rates from all measurements for passive swelling (green), free swelling (yellow), and tribological rehydration (blue) as a function of time for the first 100 seconds of recovery (shaded regions represent the 95% confidence intervals for these mean values). All three recovery rates decreased with time but tribological rehydration and free swelling rates were approximately an order of magnitude higher than passive swelling over the entire time course. (b) Average inflow rates for the first 100 seconds of recovery versus compression from exudation prior to recovery for all tested samples. Shaded regions represent the overall means and their 95% confidence intervals. 84

- Figure 4-6: An illustration of the competing rates paradigm for describing cartilage fluid retention in the joint. (a) Exudation occurs during loading and the rates of fluid loss decrease with increasing contact area [9]. (b) Passive swelling occurs during static conditions within the contact area. (c) Free swelling and tribological rehydration occur during articulation outside and inside the contact area, respectively. 87
- Figure 5-1: Activation of the hydration mechanism is dependent on the available wedge based on the curvature of cartilage. Pressure is increased as the fluid is entrained into the wedge and allows fluid to enter the semipermeable membrane. Most of the inflow rate into cartilage is within the pressured wedge, as predicted by hydrodynamics. The pressure and inflow rate data is modified from [248]. 95
- Figure 5-2: The measurements of dynamic equilibrium for a single load. A) After a static load, the load is maintained and slid at 200mm/s until equilibrium. The load was then reduced to 100mm/s and then 50 mm/s. Speeds were repeated 2X per load. B) The dynamic equilibrium is noted in dark blue circles for each sliding speed. 99
- Figure 5-3: A representative test (4N) for cartilage FLS measurements. The force is maintained in part (A) to exude fluid. Cartilage was then slid to recover fluid and achieve equilibrium in part (B). Afterward, sliding ceased and deformation was held constant until force relaxation equilibrium (C). The FLS for cartilage was calculated at dynamic equilibrium deformation (B). 101
- Figure 5-4: A representative test of slow speed testing for a single load. For this test, speeds 30 to 14 mm/s reached equilibrium within 30 minutes. The first order equation was applied for speeds 12 to 6 mm/s to estimate the dynamic equilibrium values. 102
- Figure 5-5 The dynamic equilibrium deformation as a function of load and sliding speed is shown for a single representative sample. The 3 data points displayed in each bar indicate the repeatability of the dynamic equilibrium to conditions. Error bars, albeit small, indicate 1 standard deviation. 104
- Figure 5-6: Representative sample data for A) the dynamic equilibrium, B) dynamic fluid equilibrium, and C) the rehydration rate at the dynamic equilibrium. Error bars shown indicate ± 1 standard deviation..... 105
- Figure 5-7: The FLS as a function of load. Different colors represent unique samples. The circles represent experimental data. 106

- Figure 5-8: Rehydration rate vs sliding speed at 3N and 5N loads. The two base colors (red and blue) represent the two different samples. The rehydration <0.05 from 0-20 mm/s and rapidly increases from 20-100 mm/s. Each sample tends to have a different characteristic curve. 107
- Figure 5-9: Illustration of the rehydration hypothesis at the dynamic equilibrium. After opening of the wedge, the flow into the cartilage interface (Q_{in}) is the sum of the flow into the tissue (Q_T) and through the interface (Q_I). P_y equals the sum of interstitial pressure and osmotic pressure. P_x is the lubricating pressure hydrodynamic pressure. After static loading, initial sliding will cause $dP_y dy \gg dP_x dx$, since interstitial pressures have dropped, and flow will preferentially drive into the tissue. At high-speed sliding, interstitial fluid pressure is restored and $dP_y dy \approx dP_x dx$, such that the flow into the tissue (Q_T) will now compete with flow through the interface (Q_I). An increase in sliding speed will increase $dP_y dy$, but also increase $dP_x dx$ and decrease k_T [185] such that hydrodynamic inflow is limited. 110
- Figure 5-10: Thought model of tribological rehydration. A) The interface is effectively impermeable when speed is slow, an rehydration is insignificant B)The interface becomes permeable. Hydrodynamic pressures at higher speeds begin to push fluid into interfacial gaps, which expand to increase interface permeability. The rehydration rate increases with the rate of flow into the interface. C) The rehydration rate saturates due to tissue absorption limits or because the inflow rate is limited by the tissues ability to absorb fluid. 113
- Figure 5-11: A) Current models predict a large rehydration front near the convergent wedge. B) The current results demonstrate that the rehydration occurs directly at the interface at physiological sliding speeds 114
- Figure 6-1: “Systems approach” to understanding OA initiation and development adapted from Andriacci et al. [278], [279]. Considering the factors of biology, structure, and mechanics, cartilage undergoes a specified amount of activity, which can lead to a healthy environment or disease cartilage. If cartilage cannot withstand activity, it is worsened through a feedback loop until end-stage OA. 121
- Figure 6-2: A modified “systems approach” to account for the role of activity and hydration in the responses of each system and ultimately cartilage health. 122

Figure A. 1: The squeeze film analysis of fluid flow for a given time step. The change in strain (δ) manifests as streamlines as shown. 'r' represents the distance from the center of contact to each streamline. 's' is the axis that accounts for the distance each streamline must travel to be laterally ejected. For an infinitely small section of the tissue (shown on the right), the velocity ($V(r)$) of streamline starting at distance 'r' can be calculated for a given δ . 'dh' represents the change in thickness, or thickness, of the tissue..... 153

Figure A. 2: Looking at the contact area of cartilage, conservation of flow requires that the flow rate for any slice defined by $d\theta$ must equate. Using the relationship, $Vr = 2a \cdot \delta h$, the flow velocity at point $V(r+s)$ can be defined. 154

Figure A. 3: The algorithm to compute the model strain. The model starts at the initial conditions and computes the permeability and strain rate at each time step. The next time steps are then used in subsequent time steps to update permeability and strain rate. The material properties are optimized based on the two objective functions. 156

Figure A. 4: The calculated area for two images in a single test. All data within the white outlines shown was considered the contact area. 158

Figure B. 1: A representative preload at 0.3N is shown before at a 4N load. The preload causes an elastic deformation ($\delta_{elastic\ preload}$) and fluid deformation ($\delta_{fluid\ preload}$). If the accumulated fluid is not accounted for the exudation model (Section 3.2.4), the effective tensile modulus is calculated much softer and the fluid pressurization will be undercalculated. Thus, the $\delta_{fluid\ preload} = \epsilon AF$ for Equation 11 calculations. 159

Figure B. 2: The mean characteristic curves of exudation are compared between pure DI water and same volume of water with 15ml of India Ink (n = 3 repeat tests for each condition, 5 N load for all tests). The overlap of the 2 standard deviation (shaded portions) indicate that the inclusion of India Ink did not significantly alter the exudation mechanics of the cartilage layer. 160

- Figure B. 3: Comparing the rehydration characteristics of unloaded cartilage-on-cartilage with free swelling and passive swelling measurements described in methods Section 4.2. The amount of fluid recovered by the cartilage surface are plotted versus time. In the cartilage-on-cartilage experiment, the total recovery was divided by 2 surfaces to obtain the average rate. A second passive recovery repeat measurement performed after free swelling to demonstrate that contact with the porous indentation had no significant effect on the passive swelling response..... 162
- Figure B. 4: An example comparison of the contact area and contact pressure between static loading and static unloading. Cartilage maintained a relatively constant contact area during unloading. Recovery following exudation is promoted by the reduction in contact pressure but impeded by the contact area. The contact area decreased during recovery such that the contact pressure increased from 0.003 to 0.005 MPa by the end of the experiment..... 163
- Figure B. 5: An example comparison of the contact area and contact pressure between static loading and loaded sliding. Cartilage maintains relatively constant contact pressure during sliding conditions, but tribological rehydration allows for bulk tissue hydration, which stiffens the tissue, reduces the contact area, and increases the contact pressure. Throughout the tribological rehydration process, the contact stress was between 0.15 and 0.16 MPa. 164
- Figure B. 6: Quantification of area during sliding experiments after 15 minutes of static loading. Images of contact area during sliding were captured every 0.1 seconds. Because images were taken during through a port in the POD tribometer, the area was not always well defined (see grey data points). The true area was computed as the maximum area during each rotation, as illustrated by the colored array. 165

ABSTRACT

There has been steady rise in osteoarthritis (OA) incidence rates since the Industrial Revolution. This begs the question, “Why?” With increases in life expectancy, a leading hypothesis is that we are incurring ‘wear and tear’ on our joints for much longer. However, the industrial revolution has also been marked with increasing sedentary behavior. Emerging epidemiological data demonstrates that outcomes of a sedentary lifestyle— which exposes our joints to minimal ‘wear and tear’—implicate cartilage deterioration and OA development, contradicting the ‘wear and tear’ paradigm.

From a mechanical perspective, sedentary behavior insufficiently loads cartilage, leading to excessive, chronic tissue strains through fluid loss—this fluid loss is associated with mechanical and biological dysfunction that can ultimately lead to joint disease. Fortunately, movement is the engine that reverses fluid loss to establish joint function. How much activity is needed, how often, and how those thresholds vary with joint forces depend explicitly on competitive rates of fluid loss and recovery, but these topics remain largely unstudied. Researchers and clinicians must understand the processes contributing to fluid loss/recovery rates to anticipate the influence of an active lifestyle on cartilage function and joint health.

With a well-controlled experimental test-bed, I address the fluid loss/recovery knowledge gap in this dissertation. I leveraged several necessary experimental and theoretical tools pioneered by former researchers to quantify (1) in-situ contact mechanics and fluid loss rates and (2) relative rates of recovery. Because fluid loss

depends on the magnitude of contact stress, my 1st aim investigates the predictability of cartilage contact stress and addresses the potential consequences of assumed cartilage material properties. In Aim 2, I develop an experimentally derived fluid loss model to determine how quickly cartilage loses fluid from a static load (i.e. a sedentary condition). Although cartilage loses fluid from a static load, engaging in activity or unloading the joint can rehydrate the tissue. Therefore, in Aim 3, I quantify the rates of rehydration from both activity and joint unloading to determine what behavior may better restore hydration and function. After a restoration of fluid, cartilage must sustain low fluid loss during activity to maintain its function. In Aim 4, I examine how biomechanical factors, like speeds and loads, affect magnitude of fluid loss during activity. Overall, this dissertation demonstrates that 1) material properties of cartilage must be well-defined to predict contact stresses, 2) cartilage loses fluid much faster than previous models had predicted, 3) activity rehydrates cartilage tissue ~10X faster than a strict unloading of the joint, and 4) cartilage tissue can robustly maintain its function via fluid pressurization, despite increases in contact loads. By connecting physiological biomechanics with fluid loss/recovery, outcomes from this dissertation initiate the foundational bridge between activity and the ability to predict long-term joint function.

Chapter 1

CARTILAGE BIOMECHANICS AND ITS RELATIONSHIP TO FUNCTION

1.1 Cartilage function and structure

Human ambulation requires distribution of forces between articular joints with minimal friction between contacting surfaces. Articular cartilage lines the surface of joints (as shown in Figure 1-1A) to functionally transfer these loads while maintaining low levels of inflammation and joint health. Cartilage remains as a functional load bearing material for decades (1-5MPa) [1], and substantially outperforms synthetic materials currently used to replace cartilage once it fails; a majority of joint replacements last at most 25 years [2]. This suggests that cartilage is a biomaterial more robust than any synthetically derived material.

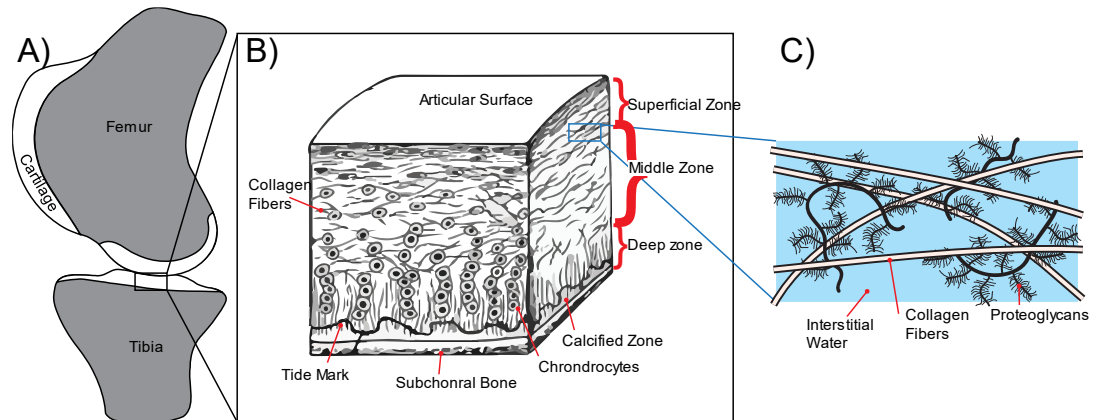


Figure 1-1: Cartilage tissue lining our joints consists of a complex collagen matrix to support load and reduce friction while infused chondrocytes maintain biological processes. Most of the tissue is composed of water (~80%) which is drawn in by the negatively charged proteoglycans.

Articular cartilage is 1-4 mm thick hyaline cartilage lining the end of articular joints. The survivability of cartilage can be attributed to the microstructure of the extracellular matrix (ECM), as shown in Figure 1-1B. The ECM is mainly composed of interstitial fluid (~80% by weight), collagen, and proteoglycans. Negatively charged proteoglycans draw in surrounding fluid, which in turn tensions the collagen matrix to provide its unique mechanical properties. Unlike other regenerative tissues in our body, adult cartilage does not have blood vessels or nerves; cartilage must maintain its structural integrity and functionality for a lifetime [3].

The matrix of collagen changes orientation based on the three zones illustrated in Figure 1-1. The tangential orientation of the superficial layer helps transform compressive loads to tensile stresses of the collagen fibrils. The middle zone, which contains thicker, obliquely organized collagen fibrils, transitions the superficial layer to the deep zone. In the deep zone, collagen fibrils are oriented perpendicular to the cartilage surface to integrate with the subchondral bone, which further stiffens the tissue during loading [4]. As cartilage is loaded, interstitial fluid pressurizes against collagen fibers to stiffen the tissue and distribute load.

1.2 Articular Cartilage cells upkeep ECM integrity

Chondrocytes, shown integrated into the ECM in Figure 1-1, are metabolically active cells that develop, maintain, and repair ECM structure. Each chondrocyte is responsible for the ECM upkeep in its immediate vicinity and cannot readily communicate with other chondrocytes. Therefore, these cells readily depend on mechanical stimuli, like loads and hydrostatic pressures, to synthesize matrix components and maintain ECM metabolism [5]–[7]. Because of its limited capacity

for cellular replication, chondrocytes depend on an optimal chemical and mechanical environment [8], [9]. Cell survival depends on 1) protection from the ECM by external mechanical forces [10]–[12] and 2) nutrition and metabolic waste exchange with the surrounding synovial fluid [13], [14].

1.3 How does cartilage maintain its function?

As stated in Sections 1.1 and 1.2, fluid pressurization and regular fluid exchange with the surrounding synovium is important for a functioning tissue. From a mechanical perspective, pressurization mitigates potentially deleterious stresses [12], [15]–[19] and friction [19]–[22]. Biologically, chondrocytes can only regularly remodel the ECM matrix if they are hydrostatically pressurized [5]–[7] while shear stresses are minimized [23]. The ECM architecture can only provide mechanical protection to the collagen matrix [11], [12] and chondrocytes if stresses and friction are mitigated [24]. Thus, the function of cartilage depends on the symbiosis between the biology, mechanical function, and cartilage structure/architecture, as illustrated in Figure 1-2. However, pressurization is only possible if the tissue is well hydrated. Furthermore, both lubrication [25]–[31] and nutrient transport [32], [33] also depend on regular fluid gain/loss and movement of fluid within the tissue [34]. **Therefore, the function of cartilage depends on its ability to regularly exchange fluid with the surrounding environment while maintaining hydration for pressurization.** This acknowledgement has gained attention from researchers attempting to quantify fluid exchange in vivo [35]–[38], is sparse mechanistic understanding on the fluid inflow and sustained tissue hydration in a physiologically representative setting.

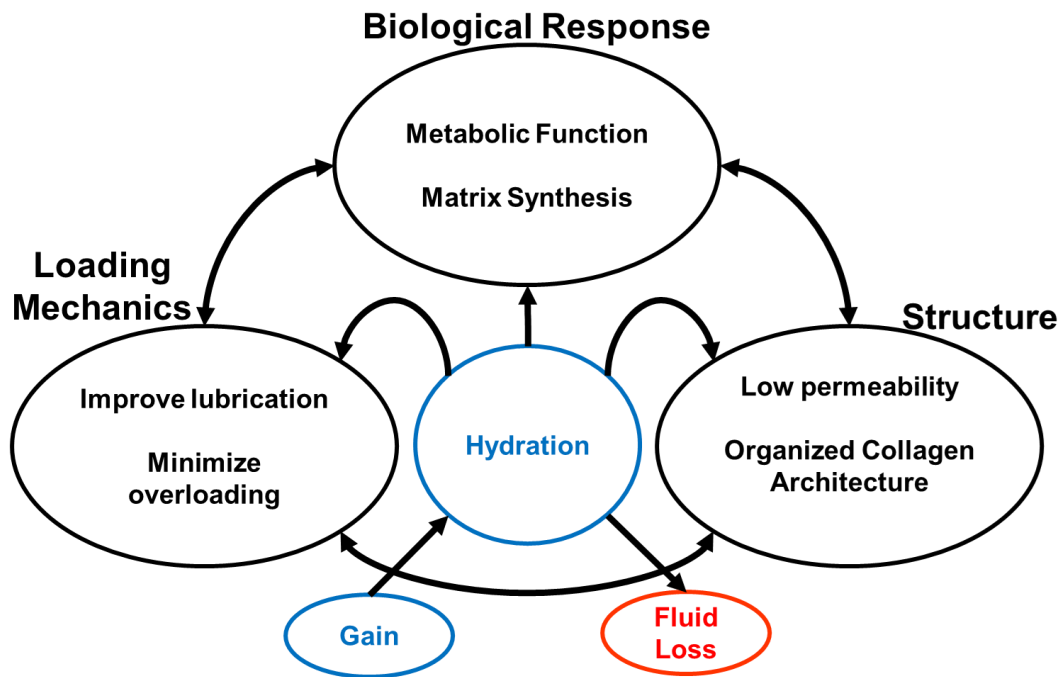


Figure 1-2: To maintain its functionality, the tissue must maintain its hydration levels to improve lubrication [21], [22], minimize overloading [11], maintain its collagen network and low permeability [24], and sustain metabolic function and regular matrix synthesis [6], [14], [39]. These processes also depend on the regular fluid gain and loss.

1.4 What happens when cartilage breaks down?

As stated in Section 1.3, cartilage can optimize its mechanical and biological function if interstitial fluid is regularly recovered and pressurized. However, if the structure of cartilage is mechanically vulnerable, chondrocytes must regularly remodel the ECM until biological and mechanical homeostasis is achieved [7]. If chondrocytes cannot regularly restore homeostasis, remodeling efforts will become catabolic and lead to eventual tissue breakdown. This breakdown, and therefore dysfunctionality, leads to a musculoskeletal impairment known as osteoarthritis.

Osteoarthritis (OA) is the most common form of arthritis, as it affects over 32 million US adults [40]. Symptoms/side effects of the disease are frequent joint pain/aching, stiffness, limited flexibility, and swelling, which leads to lower function and lower quality of life [41]. From the CDC website, “OA is caused by damage or breakdown of joint cartilage between bones...Some people call it degenerative joint disease or “wear and tear” arthritis. It occurs most frequently in the hands, hips, and knees.” [42] With severe OA, many individuals require joint replacement to alleviate symptoms. Nearly, 1 million Americans elect to have knee and joint replacement surgeries, which incurs financial burden on the individual and the economy [43].

1.5 Can we save our cartilage and reduce the risk of OA?

Despite having a complex disease etiology [44], it is clear that rates of OA in the post-industrial age have doubled (when controlling for age, sex, BMI, and ethnicity) as compared to the early industrial age [45]. Because the post-industrial period correlates to longer life expectancies, a leading hypothesis is that longer lifespans equate to more “wear and tear” on joints. For instance, participation in sport (e.g. soccer, football, gymnastics, etc.) increases the risk of development and progression of OA [46]–[50]. Therefore, it’s unsurprising that the general population commonly believes that increased physical activity *of any kind* will initiate and progress the disease [51], [52]. However, the association between sports/activity participation and OA is confounded by prior injury [47], [50], which is known to have a direct relation to OA development [53].

An alternate hypothesis of post-industrial OA rates considers a relationship between OA and the *reduction* of physical activity. With the advent of less rigorous occupations, the post-industrial era has also been marked by a substantial decrease in

overall physical activity [54], [55]. While pre-industrial societies have comparable levels of non-ambulatory time to post-industrial societies, pre-industrial societies spent time in postures still requiring small forms of movement as compared to extended cessation of movement associated with modern lifestyles [56], [57] (i.e. watching TV, sitting in a chair at work, sitting during transportation, etc.). Even if modern adults meet physical activity guidelines, this adopted sedentary behavior has deleterious cardiovascular and metabolic effects [58]. The human body has seemingly evolved to require consistent levels of activity to remain healthy. **The correlation between increased sedentary behavior and increases in OA suggests that cartilage also adopts this paradigm and may not solely be related to the “wear and tear” adage.** In fact, epidemiological studies from the past 10 years demonstrate that activity 1) does not increase OA risk [36], [59]–[63], 2) does not further progress symptomatic or structural OA [63]–[65], and 3) may inhibit disease progression [66], [67]. Furthermore, cartilage tends to atrophy with lack of use [68]–[72]. While these studies can help advocate change in public health policy, they can only provide a solution for a generalized population and provide no insight into the mechanistic risk factors. However, Sections 1.1 - 1.3 demonstrate the importance of fluid exchange and pressurization for long-term cartilage function and health. Thus, **to understand why engagement in activity improves long-term joint health, we must first understand how cartilage fluid loss/gain and interstitial fluid pressurization responds to mechanics of activity.**

1.6 The mechanical response of cartilage and dynamics of fluid flow

Researchers have studied the mechanics of cartilage strains, fluid loss, and fluid pressurization for over 70 years [22], [73]–[80]. Under a zero load condition,

cartilage swells to a specific thickness based on the balance of forces between the osmotic pressure and tensioned collagen fibers in the ECM [81]. Upon an immediate load, interstitial fluid pressurization rapidly increases. The lateral expansion of the ECM is resisted by increased tensioning of the intertwined cartilage matrix, effectively stiffening the tissue [3], [21], [82], [83]. The increased interstitial fluid pressure drives fluid movement within the tissue and exudes fluid to the surrounding synovium. Because of the porous microstructure, the exudation process is slowed due to the frictional drag of interstitial fluid on the ECM [84]. The slow fluid exudation process manifests as a creep and stress-relaxation response. If compressive stress is maintained on the tissue, cartilage rapidly exudes fluid during an initial loading phase, but will eventually slow as the tissue creeps to an equilibrium strain. Conversely, if cartilage strain is held constant, the tissue will relax to an equilibrium stress.

At equilibrium, interstitial fluid pressure vanishes, and stresses are supported entirely by the ECM, which is denoted solid stress. It is important to note that this stress is not purely elastic. Instead, it is due to the osmotic pressure created by the concentration of fixed charges of glycosaminoglycans (GAGs) within the matrix [85]. Osmotic pressure develops whenever a charge or ion concentration difference exists across a permeable membrane [86]. This osmotic pressure difference drives fluid flow from low concentration to high concentration. With higher tissue strains, concentration of charges increases and in turn increases the osmotic pressure. Thus, cartilage behaves according to Hooke's law for elasticity even through the stress response to strain is attributable to an entirely different phenomenon. At the static equilibrium, there is no flow because the externally applied stress exactly matches the osmotic swelling pressure [87], [88].

1.7 Applying biphasic theory to explain cartilage mechanics

Mow and colleagues proposed that cartilage stresses and strains could be explained by biphasic mixture theory [78], [79], [84]. With biphasic theory, the stress response of the tissue (σ) is represented as:

$$\sigma = \sigma_e + P \quad (1)$$

where σ_e is effective stress resulting from strains in the solid matrix and P is the fluid pressure in the system. When cartilage exudation remains low, the interstitial fluid supports most of the load, and the ratio of the fluid pressurization to the total contact stress is known as the fluid load support (FLS):

$$FLS = P/\sigma \quad (2)$$

With an FLS = 100%, the load is completely supported by the fluid constituent, while an FLS = 0% indicates that the ECM completely supports the load. As previously stated, P is dependent on the movement of fluid inside the cartilage tissue, which can be calculated by Darcy's Law:

$$q = \frac{k}{\mu \cdot L} \cdot \nabla P \quad (3)$$

where q is the fluid flux through cartilage, k is the permeability of the tissue, μ is the viscosity of the fluid, L is the distance the fluid is traveling, and ∇P is the pressure drop that drives the fluid exudation.

According to Equation 3, fluid flowing into and out of the tissue is primarily driven by fluid pressure. This fluid pressure is dependent on 1) the applied stress and 2) the relative pressure at the boundary of cartilage. Mow and colleagues first explained flow through cartilage with linear biphasic theory [84]. In their first experiments of confined compression (Figure 1-3A), cartilage tissue was indented with a permeable platen, allowing fluid to drain freely through the contact interface. Although the authors demonstrated that cartilage could achieve high FLS at the initial

loading, the contact interface was considered unphysiological since 1) the tissue is not 'confined' in the joint and 2) the large fluid exudation at the contact interface does not resemble the contact of two cartilage layers. A more “physiological” exudation response—unconfined compression (Figure 1-3B) — imposes impermeability at the contacting interface, which in turn forces cartilage to drive fluid laterally through the tissue and the relaxation time of cartilage would scale with the contact area [89]. This would suggest that a large contact area is beneficial since the exudation time would be extended. However, the maximum fluid load support could theoretically only reach 33% due to the ability of the tissue to laterally expand during compression to conserve volume. In practice, the collagen fibrils confine the tissue, limit lateral expansion, and increase pressurization well-beyond the 33% value predicted for a model biphasic material, due to a tension-compression nonlinearity [17], [90]. When this tension-compression nonlinearity is accounted for in the model cartilage does maintain FLS >80% in unconfined compression, leading to effective stress-shielding of the ECM [79].

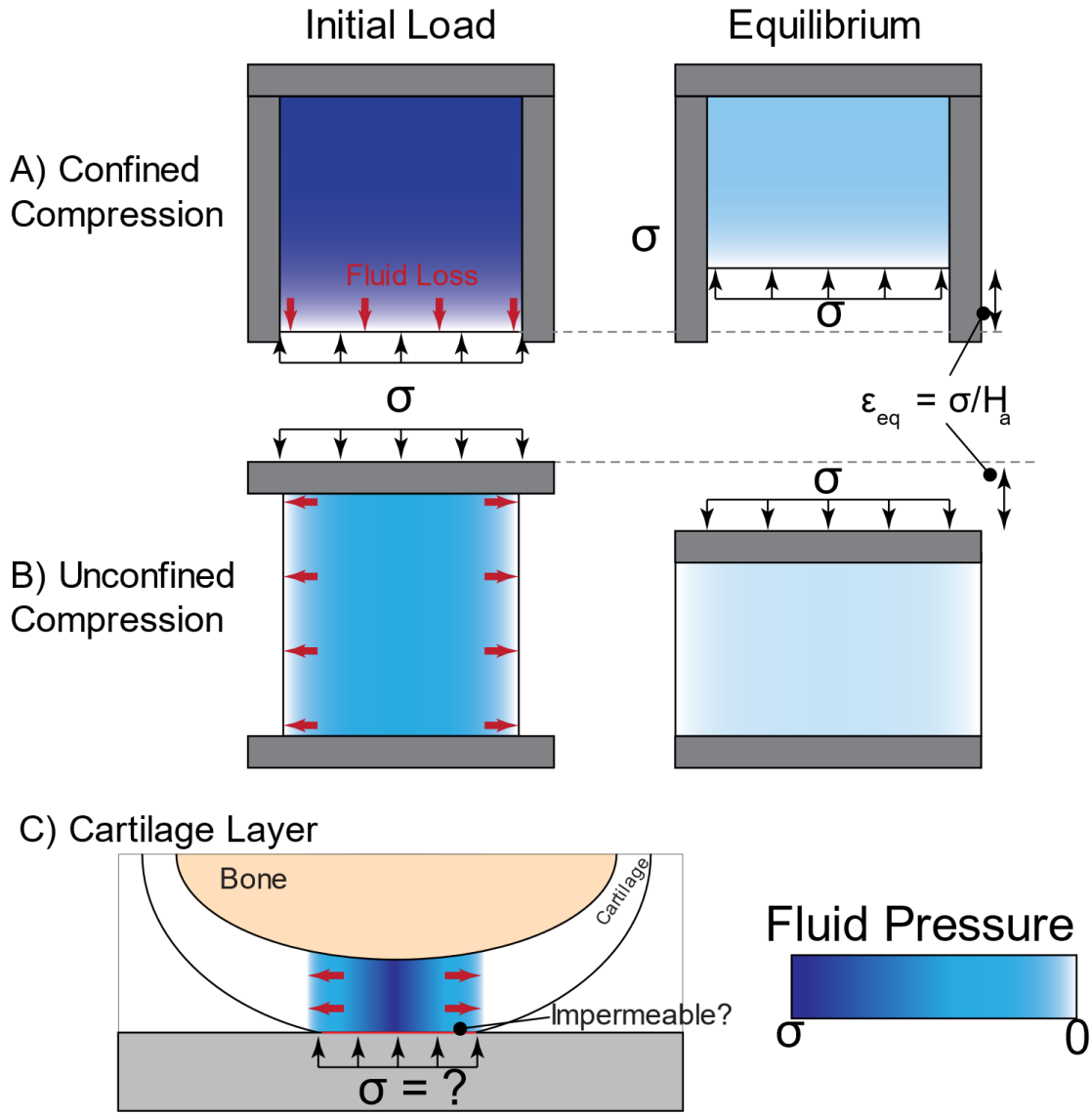


Figure 1-3: A) Confined compression experiments were first used to describe the creep mechanics and fluid exudation of cartilage. B) Unconfined compression experiments more resembled the mechanics of cartilage layers, specifically simulating an impermeable contact interface. At equilibrium, fluid pressure in both unconfined and confined compression ~ 0 . C) Current models of joint contact include cartilage creep models based on the lateral ejection of fluid and impermeable interface as modeled in unconfined compression [11]. However, it is unknown if that contact stress can be predicted and if the interface is indeed impermeable.

Inclusion of tension-compression non-linearity has led to high FLS in models attempting to replicate joint contact [28], [83], as shown in Figure 1-3C. Like unconfined compression, the interface is still considered impermeable to only allow for lateral ejection of fluid and disallow flow into the contact interface. In this case, exudation time depends on contact area size, which has been experimentally verified [91]. In actuality, though, cartilage surfaces are extremely rough [92]–[95], and cartilage-on-cartilage contact would theoretically promote a permeable interface for fluid flow. Although many researchers have modeled the interface as impermeable, Wu and Ferguson showed that the intra-articular gap was at least an order of magnitude more permeable than the bulk tissue, allowing for an alternate flow path during exudation [94], [95]. However, recent research has highlighted that the contact may not be completely sealed, and some fluid may leak through the interface under realistic contact [95], [96]. Considering fluid loss for a realistic joint geometry, experimental investigations that explore the effect of the interface are limited [97], [98]. Furthermore, connecting in vivo contact loads with contact stress, i.e. the driver of fluid exudation, has been relatively unreliable [99], [100]. The ability to predict contact stress and the resultant exudation characteristics have need to be addressed to understand how much fluid is lost during loading periods.

1.8 Cartilage fluid strain in the context of human movement

Considering large in vivo contact areas and in vivo contact loads, FLS could remain high (>90%) for hundreds to thousands of seconds [78], [84], [90], meaning that 90% of the load was supported by the fluid constituent. Since FLS is a reflection of cartilage function [21], [22], [79], a layer of cartilage could maintain its functionality for time scales longer than a single loading phase during a gait (<1

second). However considering bodyweight loads, a 20 minute walk with many gait cycles would reduce FLS to <50% [15], [90], making the tissue vulnerable to mechanical damage and biological dysregulation. Fortunately, studies show that cartilage establishes a ~5% dynamic equilibrium strain during movement [35], [37], [73], [101]–[104], which reflects sustained pressurization of the tissue. Therefore, loading does not necessarily lead to net time-dependent exudation and reduced FLS even though biphasic theory had predicted as such.

To reconcile this problem, Ateshian and Wang considered the migration of joint contact area during movement. They showed that exudation is effectively stopped if the speed of the contact area is faster than the exudative speed [12], [20]; i.e. the exudation process cannot occur if contact stress is always moving to a different location. Theory [16] and experiments [18], [83] have demonstrated that cartilage can maintain high FLS and low fluid strain for a migrating area [105]. The migrating contact area (MCA) paradigm explains that our joints maintain cartilage thickness and hydration throughout an entire day of loading [106], [107] because joint movements disrupt the exudation process.

If movement serves only to disrupt exudation, one should expect periods of exudation during static loading conditions followed by periods of zero net fluid loss during periods of joint movement. This ‘prevention of flow’ model for the MCA paradigm is illustrated by the black line in Figure 1-4 presents a significant problem: humans are mostly sedentary [108], even for habitually active people [109]. Assuming movement serves only to prevent flow, a person that is active 50% of the day will experience 50% of the exudation and strain of a completely inactive person. Based on the ‘prevention of flow’ model, one would expect large strains by the end of the day,

not the small 5% strains observed in practice. In-vivo data of static bodyweight loading demonstrates that cartilage can reach 50% strain within 100 minutes. Thus, the accumulated 5% diurnal strains **cannot** represent a monotonic exudation from morning to night (see grey line in Figure 1-4), but actually represent a dynamic competition between load induced exudation and movement induced rehydration (see colored lines in Figure 1-4).

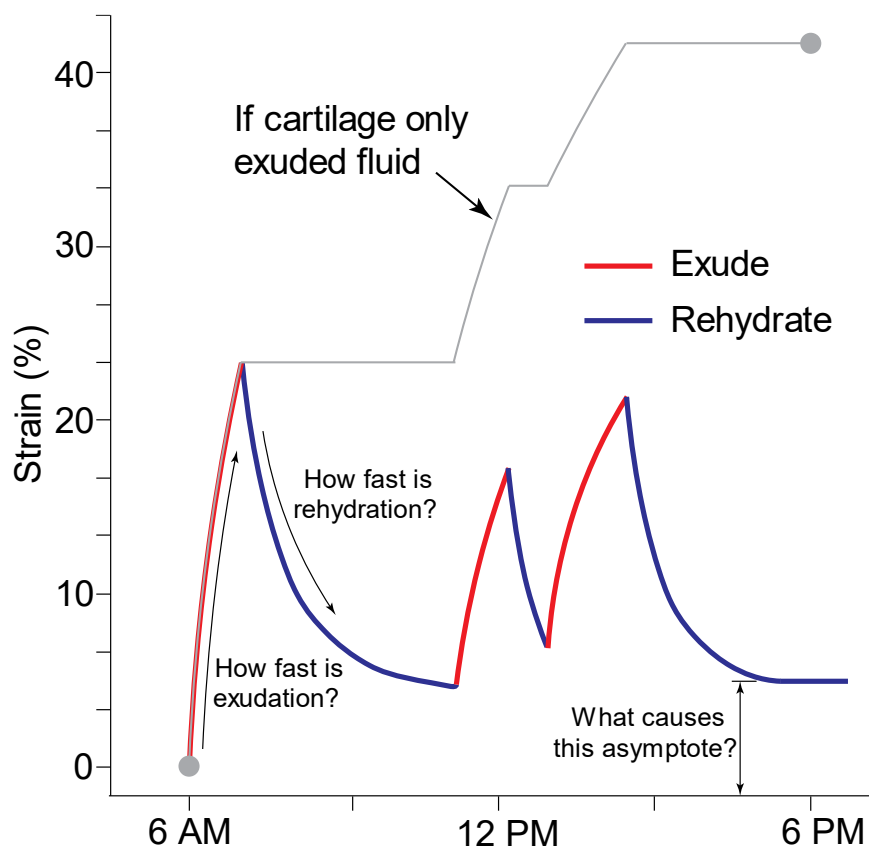


Figure 1-4: With the MCA paradigm, cartilage can only exude fluid throughout the day (shown in grey). However, this will equate to significant loading by the end of the day [102]. An alternative thought model includes the realistically high fluid loss (red), but exudation must be equally matched by rehydration (blue) if strains are kept low during movement and by the end of the day.

The dynamic competition between exudation and rehydration can be made clear by examining the contact excursion within an in vivo joint [110]–[114] (see tibiofemoral joint in Figure 1-5). One can see that contact will spend a considerable time under load, even in the MCA paradigm, and therefore will exude a significant amount of fluid. To maintain ~5% strain during movement, there would also need to be a competitive inflow to balance the exudative outflow. Considering that exudative flow rates slow with compaction of the tissue [115], any exposure of the contact area to the surrounding bath imbibe fluid much faster than the exudation rate, as originally postulated by Linn [73]. However, this does not account for buried stationary contacts on the tibial plateau. Fortunately, recent work from our group has demonstrated that physiological sliding speeds can incur hydrodynamic pressures to rehydrate buried contacts, even under loaded conditions [116]. Regardless of the contact configuration, exudation will persist during movement and must be combatted by either intermittent bath exposure or hydrodynamic pressures. However, the question remains if either of these rehydration mechanisms dominate the rehydration process. More importantly, it is unknown if these rehydration mechanisms persist in a variable load environment that joints experience during normal activities.

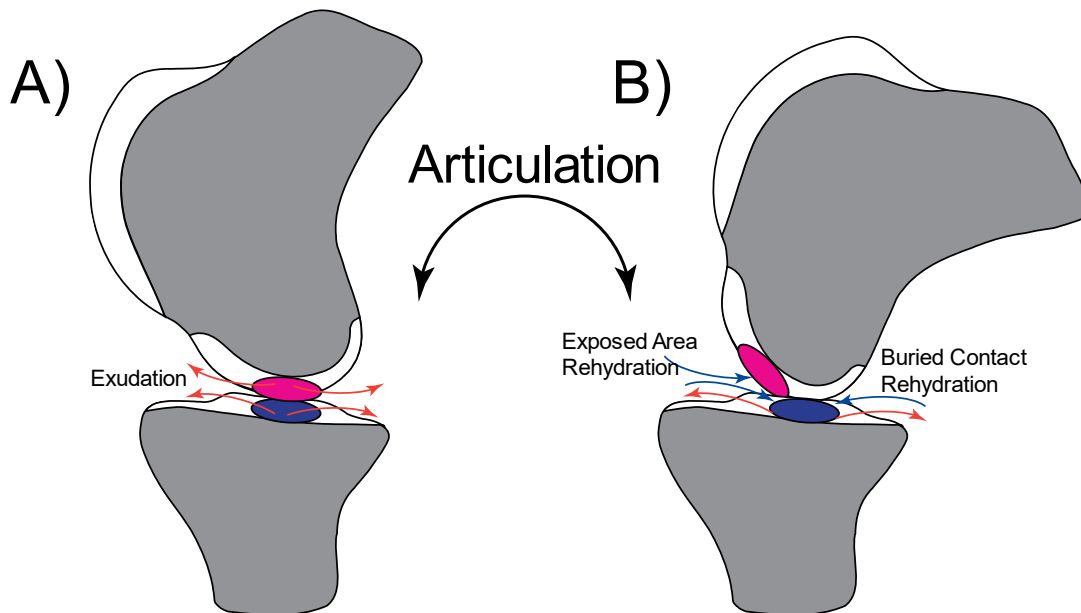


Figure 1-5: A) During static loading, contact areas under load will exude fluid. Upon articulation in B), contact areas are directly exposed to the bath for rehydration and hydrodynamics can rehydrate the contact via tribological rehydration [117]. However, due to the periodic motion of joints, joints will always incur some exudation when they return to original contact conditions shown in A). This suggests that cartilage is in a competitive framework of exudation and rehydration during movement.

1.9 Objectives

Overall, interstitial pressurization is important for cartilage function and longevity, which can only be achieved if there is regular competitive rehydration of the tissue. The correlation between sedentary behavior and OA rates the post-industrial age suggests that excessive inactivity has led to deficient levels of hydration and pressurization. Understanding the rate and magnitude of fluid inflow/outflow during articulation can uncover the required activity time to maintain cartilage function. Currently, researchers have developed foundational mechanics to describe cartilage outflow but have yet to apply it in a realistic loading situation with known

contact stresses. Furthermore, researchers know less of what drives fluid inflow and the conditions that can maintain high fluid content during extended periods of activity. If scientists, engineers, and clinicians need to predict cartilage functionality throughout the day and long-term tissue health, they must better understand the mechanics of this competition between fluid exudation and rehydration, particularly under realistic stresses. Thus, **this dissertation aims to elucidate the conditions that drive fluid loss, gain, and maintenance under an array of physiological conditions.** Refer to Figure 1-6 for a pictorial representation of the proposed dissertation aims.

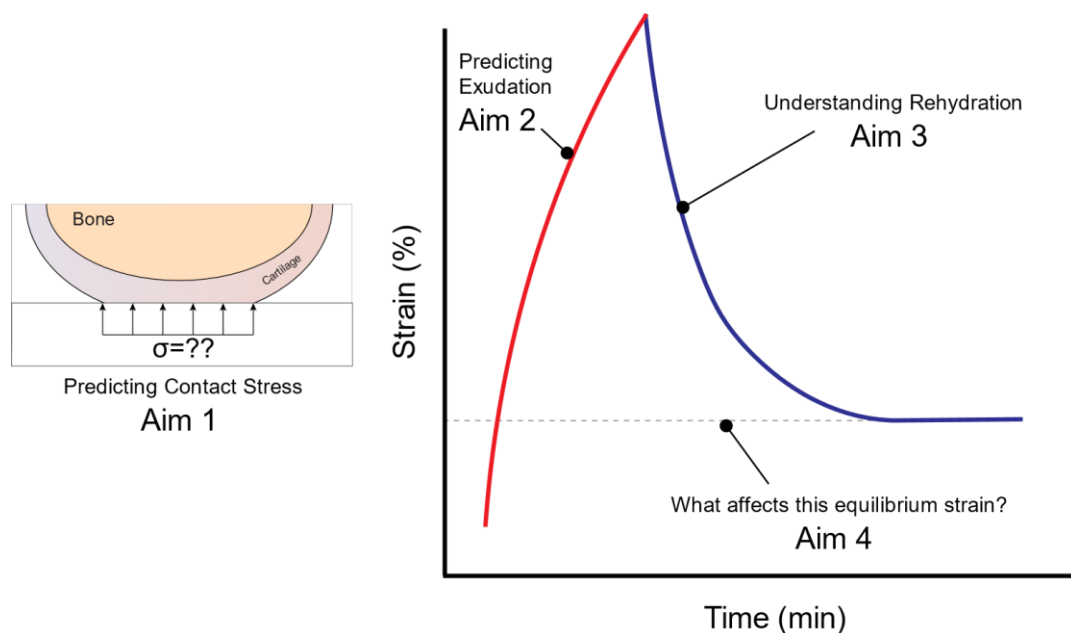


Figure 1-6: The pictorial outline of this dissertation. To understand exudation/rehydration, the contact stress must be predictable (**Aim 1**). The mechanics of inflow and out must be well understood to determine the strain on the tissue (**Aim 2 and 3**). The equilibrium strain defined the “operating conditions” of cartilage, and the physiological parameters that drive the equilibrium strain will be defined (**Aim 4**)

Since contact stress is the main driver of fluid exchange, **Aim 1** investigates the ability to predict contact stress using well-established models of contact. Numerous analytical [15], [118]–[122] and numerical models [80], [123]–[127] of cartilage contact have been developed, but validation of these contact models are limited. Specifically, there has been no serious attempt to validate model predictions about the effect of joint loads on contact stress. Thus, this aim models the contact mechanics of cartilage, predicts how contact stress varies as a function of load, and measures load-dependent stresses directly to test the model prediction under well-controlled experimental conditions.

Aim 2 measures cartilage exudation rates in realistic contacts that include roughness and curvature. Most exudation models have only included the permeability of cartilage tissue [11], [15], [128], however this has led to inaccurate results as compared to experiments [123]. Recent numerical studies have highlighted the inclusion of interface permeability in the exudation response [129], but experimental verification is lacking. For this aim, we test the effect of interfacial permeability on the overall exudation response with an experimentally derived model.

While Aim 2 addresses the realistic exudation response, **Aim 3** determines if activity can promote a faster recovery as compared to an unloading of the joint. Currently, recovery of fluid in-vivo has only been quantified for joint unloading [35], but it is unknown if activity can more quickly drive fluid into the tissue, and therefore repressurize the joint faster. Activity mediated rehydration recovery rates are quantified and contrasted with sedentary based rates of recovery.

After the tissue can recover fluid, cartilage maintains a mean ~5% strain during movement, but this value may increase or decrease by 100% based on the mechanical

environment [37]. This indicates that the loads and walking speeds may affect fluid loss, and therefore functionality, of the tissue during movement. **Aim 4** explores what physiological parameters affect the movement equilibrium strain as shown in Figure 1-6, specifically load and joint sliding speeds. Through the investigation, we quantify the joint speeds required to rehydrate the tissue and determine if an increase in joint loads reduce the function of the tissue.

In short, this dissertation elucidates the pertinent physiological parameters that drive fluid loss and recovery. At the end of this dissertation, you (the reader) will garner insight into realistic cartilage mechanics, specifically in the relation to maintaining hydration, and ultimately cartilage functionality and health.

Chapter 2

AIM 1—CAN A RANGE OF CONTACT STRESSES BE PREDICTED FOR A RANGE OF PHYSIOLOGICAL LOADS?

2.1 Introduction

Osteoarthritis (OA) is characterized by cartilage breakdown, which is associated with aberrant joint contact loads [130], [131]. These aberrant loads lead to aberrant stresses, which have a direct influence on joint disease and failure [1], [62], [132], [133]. Whereas joint loads can be measured in-vivo, contact stresses can only be determined through modeling, which is exceptionally difficult for cartilage and joints due to its biphasic structure, nonlinear elastic properties, extreme roughness, and irregular surface geometry among other factors. Consequently, attempts to appropriately model and quantify contact stresses during activities such as walking and running is an ongoing area of OA research [134].

Because quantifying contact stress in vivo is inherently difficult, joint contact models have been developed to predict contact stress [135]–[137]. Many contact models account for the intricate cartilage tissue structure to capture the viscoelastic and biphasic strain response, which increases model complexity and consequently reduces ease-of-use. Fortunately, the biphasic response can be considered negligible since human movement (i.e. the gait cycle) is on a much shorter time scale than the exudation time constant of cartilage [11], [12], [118], [121], [125], [138]–[142]. Therefore, cartilage can be assumed as purely elastic in a realistic loading condition—an assumption verified by Ateshian et al. [138]. Although the elastic assumption

simplifies the material response, applying an accurate and robust contact model is an ongoing research topic. The gold standard for modeling includes finite element (FE) methods [126], [137], [143]. Unfortunately, the FE modeling pipeline is time-consuming and prone to numerical instabilities, creating a cumbersome implementation that diminishes usability [100]. To improve ease of use, analytical models have also been explored, such as a modified Hertzian contact and Winkler foundation model [144]–[150].

Regardless of complexity, most models fail to predict important realities of the contact response of cartilage. Thus, regardless of the modeling approach taken, testing and validation are the two most important features of any modeling effort. Unfortunately, testing and validation is the area in which the current cartilage and joint modeling literature fall short. In many instances, a single material modulus is taken from literature and applied to the contact model [151]. The most obvious problem with this approach is that the reported values for the cartilage modulus vary by at least an order of magnitude and there is no obvious reason to choose one value over any other. In addition, these models are typically validated against an in vitro test with a single load and single specimen [152]. It will always be possible to find a defensible modulus from the literature, which, when used with the model, can nearly estimate an experimental result. Thus, whether or not it's the case, such results often have the appearance of calibration rather than validation.

This approach has other technical problems. First, articular cartilage exhibits heterogeneity in elastic modulus among different joints (e.g. knee vs hip) [153], joint surfaces (e.g. tibial plateau vs femoral condyles) [154], and even across the same joint surface [155], [156]. Second, cartilage stiffness increases with higher loads because

more collagen fibrils are being recruited [157]. Thus, the selection of any one modulus value may be unable to account for load-dependence, which is the primary purpose of contact modeling. This may be the reason why researchers report such a large range of material modulus (1-68 MPa) [151]. Ambiguity in input model values, like cartilage modulus, can result in a wide range of reported cartilage contact behavior [99], [100]. Testing and validating model **contact stress as a function of load** eliminates these problems.

This study is, to our knowledge, the first to predict, test, and validate the contact response of joint surfaces as a function of load. For the sake of simplicity, ease of use, and applicability to other studies, we develop and employ the simplest analytical model that can reasonably represent the contact response of joint surfaces. We used novel in-situ measurements of contact area to experimentally quantify contact stresses for real joint surfaces against a model plexiglass flat under a range of physiological loads. Finally, we used these results to determine the extent to which the model can predict the load-dependent stress response of cartilage.

2.2 Methods

Experimental Details

2.2.1 Sample Extraction

Adult bovine stifles were obtained from a local abattoir. Full thickness ϕ 19 mm osteochondral plugs (n=51) were extracted from the medial and femoral condyles from N =6 joints. Samples were then rinsed and stored in 1X phosphate buffered saline (PBS) containing protease 1X inhibitor solution (Sigma-Aldrich, P8340) at 4°C. The samples were CNC-milled for mounting into a custom loading-rig (Figure 2-1A).

All tests were completed within 4 days of extraction to minimize the risk of enzymatic digestion-induced changes in material properties.

2.2.2 Experimental Procedure

After sample extraction, two orthogonal profile images (see Figure 2-1Ci) were captured to define the principal radii of curvature (R_1 and R_2). Images were imported into an image processing software (ImageJ) and curvature across the surface of the sample was computed via an open-source curvature analysis plugin (Kappa). The mean and standard deviation of curvature were used in subsequent analyses.

Following orthogonal imaging, cartilage explants were clamped via the bone to a 1-DOF pressurized loading apparatus, as illustrated in Figure 2-1A, to allow for the cartilage to be loaded against a Plexiglas® plate. After mounting the sample in the apparatus, a tilt stage was used to ensure that contact areas were located near the center of the explant. Each explant was submerged in a 0.15 M PBS and allowed to equilibrate for 10 minutes prior to contact testing. India ink was then added to the solution to provide a discernable contact area when the cartilage was loaded against the plate.

After equilibration, cartilage explants were loaded against the plate for 0.2 seconds and the axial load was recorded via a custom 6-axis load cell. Because the loading time is relatively minimal to the exudation time constant, the cartilage material can be assumed an incompressible solid [11], [118], [138]. A camera (Dino-Lite Premier AD4113TL) captured the contact area image immediately after load was applied. Although exudation was expected to be negligible, the sample was unloaded and allowed to recover for 60 seconds while submerged in the PBS bath. This process

was repeated for each cartilage explant starting at 10N and ending at a maximum of 450 N.

After contact area measurements were completed, cartilage explants were sectioned near the centerline for layer thickness measurements. Depicted in Figure 2-1Cii, cartilage thickness equaled to the average of 3 distance measurements from outer edge of cartilage to the subchondral bone.

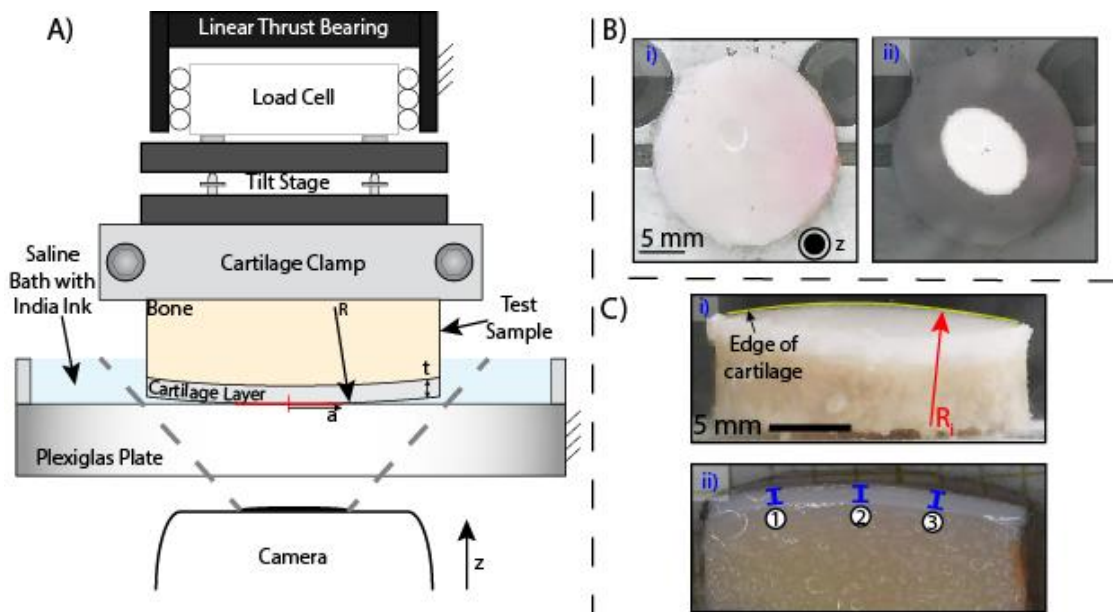


Figure 2-1: A) The uniaxial loading apparatus for loading cartilage. While the test sample was submerged in a 1x PBS, an air piston (not shown) loads the cartilage against the plexiglass plate while a camera records the resultant contact area and the load cell records the force. B) A view of the cartilage sample i) prior to loading and ii) a resultant contact area near maximum loading conditions. The contact radius (a) never exceeded the sample radius (9.5 mm). C) The geometrical parameters i) an orthogonal view of a cartilage sample was recorded to define the principal radius of curvature ii) after testing, cartilage samples were sectioned and the thickness was measured at three locations to yield a mean and standard deviation of each plug.

2.3 Data Analysis

2.3.1 Experimental Contact Mechanics

Contact area images were imported into image processing software (ImageJ), and the limits of contact area were manually segmented based on color threshold. An ICC (two-way mixed effects, absolute agreement, single rater) of 0.99 ($p < .01$) demonstrated a reliable method to measure the contact area. The average contact stress (σ_C) is the ratio of the measured load (F) and contact area (A); $\sigma_C = \frac{F}{A}$.

2.3.2 Theoretical Contact Mechanics Framework

We used a modified Hertzian contact model to determine how well the experimentally observed mechanics of cartilage contact agree with existing theory. As first proposed by Eberhardt et al., we neglect permeability and exudation since loading times (0.2 s) are negligible compared to the exudation time constant of cartilage [11], [118]. Assuming an effective elastic sphere on rigid flat, Hertzian contact mechanics gives Equation 4 as the expected relationship between the “effective” contact modulus (E_c'), the applied load (F), and the contact radius (a).

$$E_c' = \frac{3 R^* F}{4 a^3} \quad (4)$$

The effective contact radius is computed using the measured contact area (based on image analysis as described above) assuming a circular contact area (it is elliptical or irregular in reality), where $a = \sqrt{\frac{A}{\pi}}$. The measured major and minor radii are used to determine the effective radius of curvature, where $R = \frac{1}{R_1} + \frac{1}{R_2}$. In this manner, any combination of force and area for a given sample geometry gives a unique value for the effective contact modulus per Equation 4.

The effective contact modulus reflects the modulus of cartilage if and only if the cartilage is an infinite half space. In practice, because the cartilage is relatively soft and thin, it reflects a combined modulus of the cartilage-bone system. The modulus of the cartilage itself, E_c , can be isolated after correcting for the thickness effect using Equation 5 with the effective contact radius, a , and the measured thickness of the cartilage layer, t [158]; thickness correction factors have been extensively used in other studies of cartilage modulus [155], [159], [160]. Equations 4 and 5 can be combined to obtain a single expression relating the contact modulus of the cartilage layer to input force and experimental contact radius (Equation 6). To determine how much cartilage stiffens with increased load, we calculated the contact modulus at each experimental contact load and contact radius using Equation 6.

$$E_c = E'_c * \left(1 - 1.04 e^{-1.73 \left(\frac{t}{a} \right)^{0.734}} \right)^3 \quad (5)$$

$$E_c = \frac{3 R * F}{4 a^3} * \left(1 - 1.04 e^{-1.73 \left(\frac{t}{a} \right)^{0.734}} \right)^3 \quad (6)$$

Using Equation 4, it can be shown that the contact area and stress increase with load to the 1/2 and 2/3 powers, respectively, given a constant modulus. The Winkler or elastic foundation model, which is often used for thin, soft layers like cartilage, predicts 1/4 and 1/2, respectively. Additionally, the effective modulus of cartilage is likely to increase as the load increases due to the alignment and enhanced load carrying by the collagen. Thus, a major aim of this study is to experimentally elucidate how these outputs depend on load in practice. To obtain these relationships, we apply a power law fit to contact area versus load and contact stress versus load results:

$$A = C \cdot F^\alpha \quad (7)$$

$$\sigma = D \cdot F^\beta \quad (8)$$

Finally, we used Equation 6 to determine how well the modified Hertz model with a constant cartilage modulus can describe the experimentally observed load-stress relationship of cartilage. Thus, a best-fit contact modulus ($E_{c_{bestfit}}$) was calculated from the experimental range of loads and corresponding contact radii for each tested sample (using ‘lsqnonlin’ fitting algorithm in MATLAB). To calculate the theoretical contact stress with a constant modulus, a theoretical contact radius (a_{th}) was numerically computed with the best-fit modulus ($E_{c_{bestfit}}$) at each experimental load. Next, the average contact stress was calculated ($\sigma_{th} = \frac{F}{\pi a_{th}^2}$) for each load condition and compared with the experimentally observed value. The predictive capability of the model was then quantified with the root-mean-square-percent-error (RMSPE) between experimental and predicted contact stresses for a given sample.

2.4 Results

2.4.1 Experimental results

Contact area results are shown for a single representative sample at three loads in Figure 2-2A-C. As load increased, the contact area and stress increased, as expected. Figure 2-2D demonstrates the sublinear effect of load on contact area. As load increases, the rate of growth of the area decreases. The contact stress (Figure 2-2E) also increases sublinearly with load.

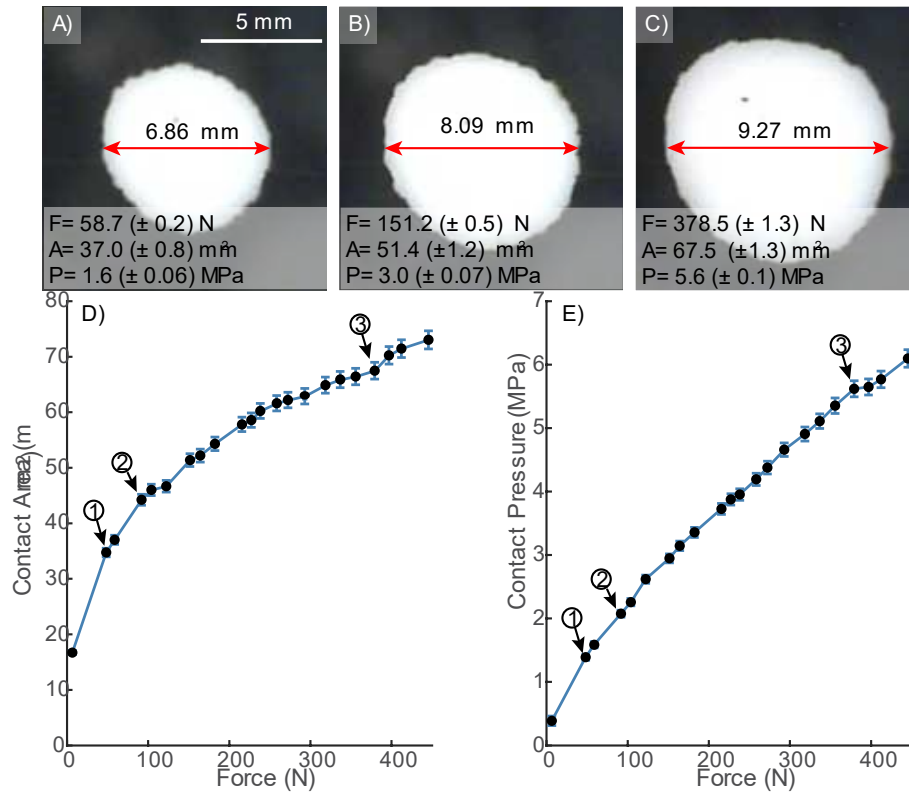


Figure 2-2: The contact mechanics of a representative sample of cartilage is visualized in A), B) and C). The measured force (F), contact area (A), and contact stress (P) are displayed with each of the images. The contact area data are shown in D) for the experimental range of loads (0-450 N). The resultant contact stress data are graphed in E). Errors in measurements were consistent across all samples.

Contact stress is plotted versus load for all samples in Figure 2-3G. The graphs in Figure 2-3A-F are used to isolate the results from each of the 6 joints tested in this study. Within each joint, we observed significant sample-to-sample variation in their stress response to load. This variation within joints was as or more significant than the variation between joints. At the maximum load of 450 N, the mean contact stress for

each joint was consistently near 5 MPa. At this maximum load, the lowest stress was 2.5 MPa and the highest stress was 9 MPa.

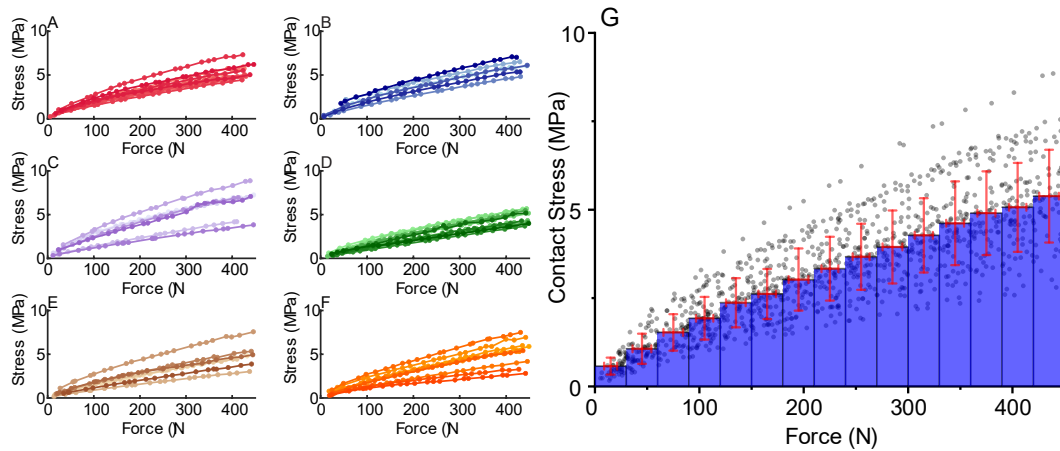


Figure 2-3: Resultant contact stress vs. input force is separated out for each joint in A) - E). Connected data points represent the response for a single sample. Aggregated results are displayed in G) including binned means (bin size =30 N) with +/- standard deviation lines.

The entire dataset is shown in Figure 2-3G, which includes the mean stress (+/- STD) at binned intervals across all samples. The standard deviation for contact stress within each bin increased linearly with load ($STD = 0.0024 * Force + 0.32, R^2 = .97$).

As illustrated in Figure 2-3, the samples did not increase their stress linearly with increased load. Fitting the contact stress to the power law function in Equation 8 (i.e. $\sigma = \alpha F^\beta$), The power-law exponent, β , followed a normal distribution (Shapiro-Wilk test) with a mean (SD) value of 0.7320 (0.0713). These values were used for comparison with the proposed Hertzian contact model defined in Section 2.3.2.

2.4.2 Contact Model Results

The contact modulus (Equation 6) is plotted versus load for all samples in Figure 2-4. The graphs in Figure 2-4A-F represent each of the 6 joints tested in the present study. An aggregate of all the moduli is shown in Figure 2-4G, which includes the mean modulus (± 1 STD) across all samples. As illustrated, the contact modulus increased with increasing load, indicating a stiffening effect from increasing contact loads.

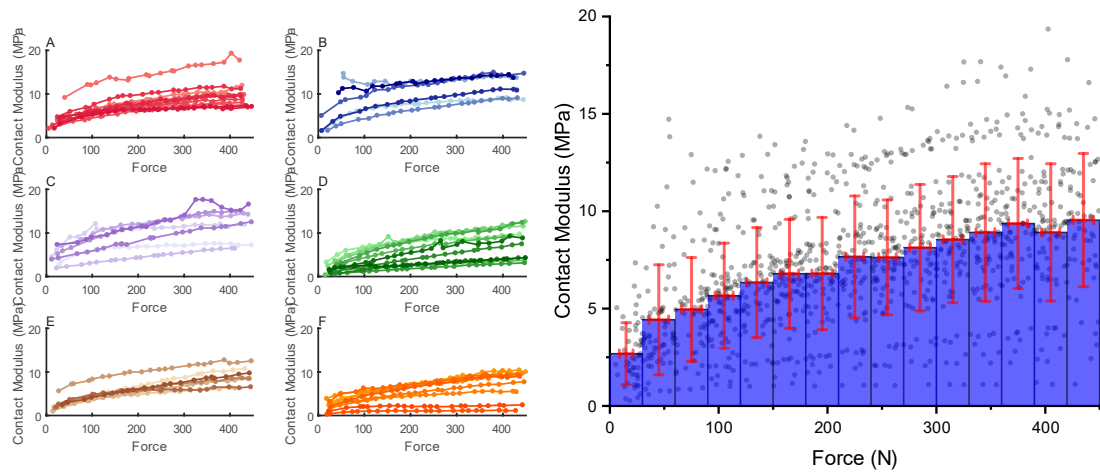


Figure 2-4: Theoretical Hertzian corrected contact Modulus vs. input force is separated out for each joint in A) - E). Connected data points represent the response for a single sample. Aggregated results are displayed in G) including binned means (bin size =30 N) with \pm standard deviation lines.

The best-fit modulus among all samples was 8.17 MPa with a standard deviation of 3.25 MPa. Figure 2-5 displays the best-fit modulus and corresponding confidence interval for all samples, separated by each tested joint. Figure 2-6A

demonstrates the predictability of contact model with a best-fit modulus. For all samples, the Hertzian layer corrected model over predicted the contact stress for lower loads, but under predicted at higher loads. To express the relative error between the model and the theoretical data, the RMS percent error (RMSPE) is displayed for each sample in Figure 2-6B. The mean RMSPE among all samples was 13.8%, with a maximum value of 22.5%.

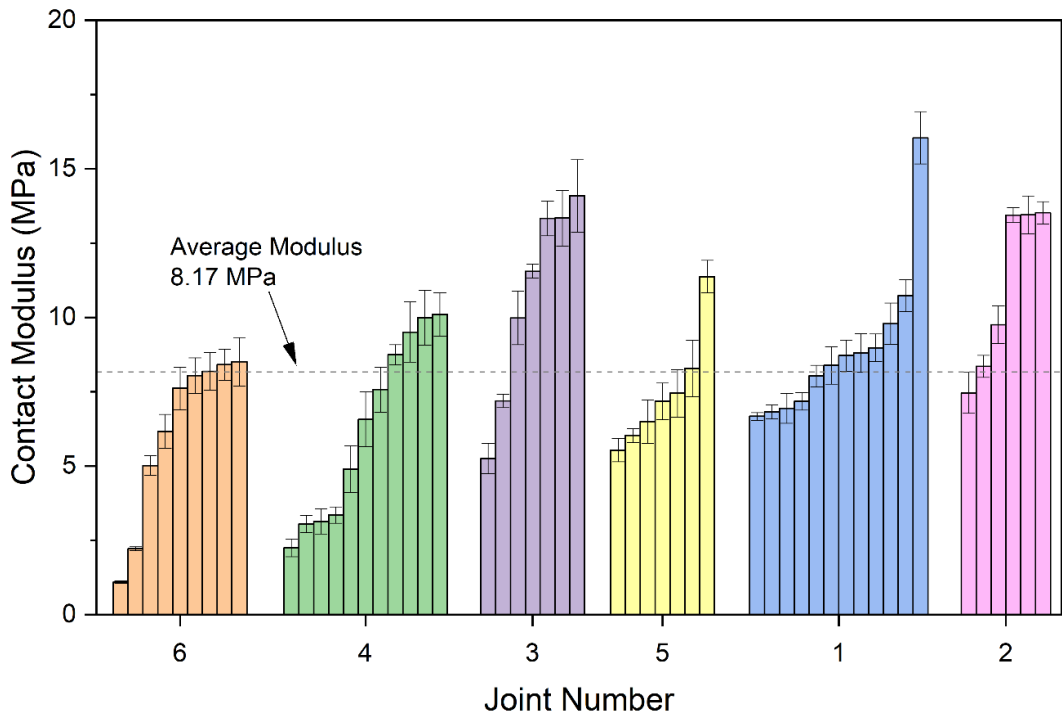


Figure 2-5: The mean Hertzian corrected contact modulus for each sample. Separating the data by joint illustrates the variability of modulus within a joint, and thus, constant modulus should not be assumed for a unique joint. The error bars represent the standard deviation of the modulus over the range of experimental loads.

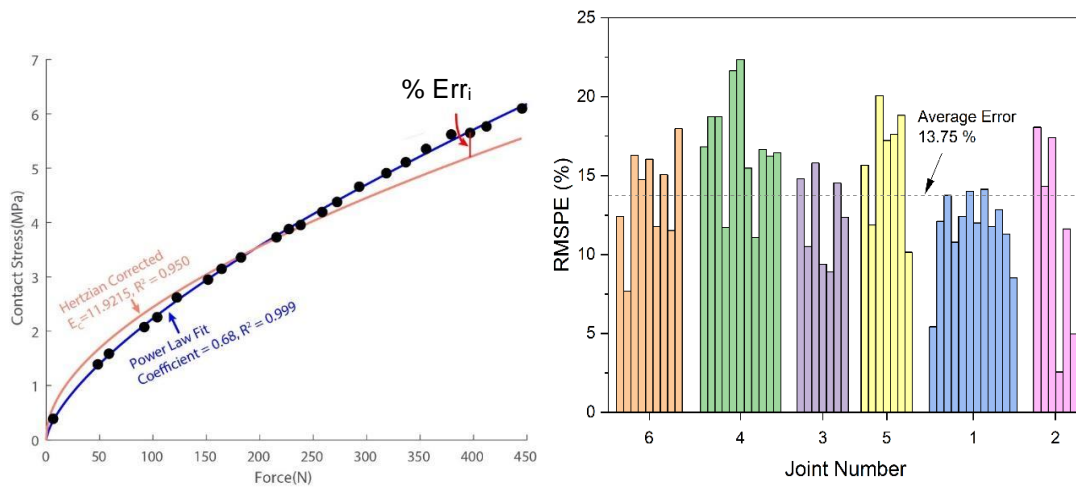


Figure 2-6: A) With the average contact modulus, the predicted Hertzian substrate corrected contact stress is plotted against experimental data for a representative sample. The power law fit is also provided. The percent error (% Err_i) was calculated at each data point to yield the RMSPE from the fit. B) The RMSPE for all samples separated by joints tested.

As a final analysis, a power law fit was applied to the generated theoretical Hertzian substrate corrected models to compare to the power law fits of experimental results (Figure 2-7). According to the popular Winkler model, stress increases with load to the 0.5 power. According to the Hertzian substrate corrected model (assuming constant modulus), stress increased with load to the 0.56 power on average (standard deviation of 1.8%). According to the experimental results, however, cartilage stress was more sensitive than expected to load, increasing with load to the 0.73 power (standard deviation of 9.7%).

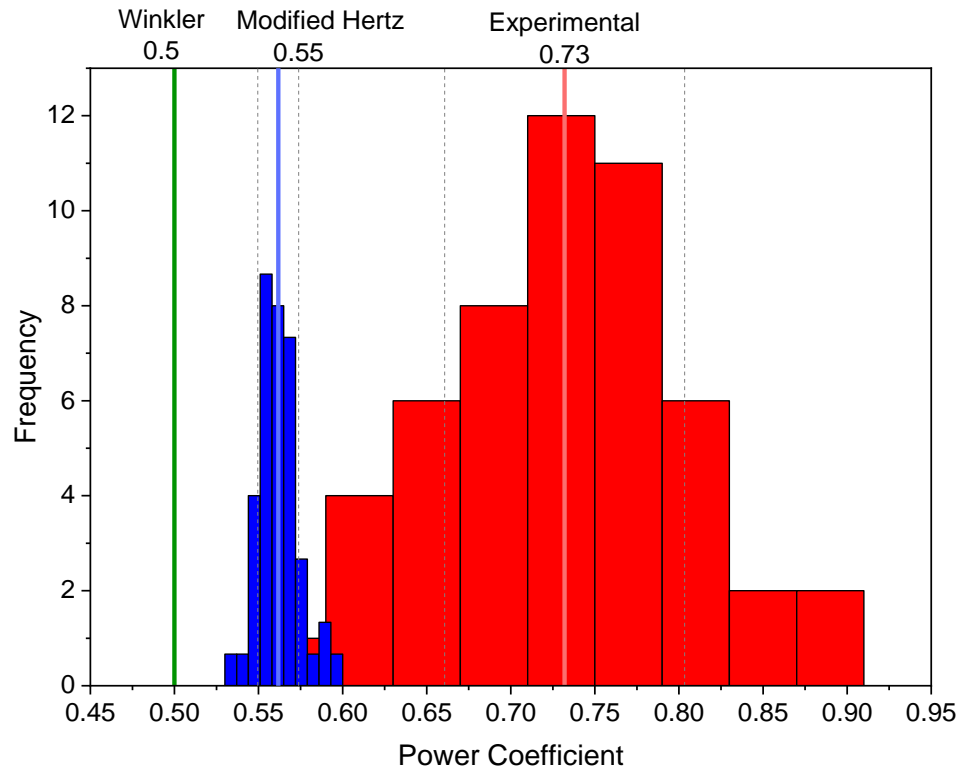


Figure 2-7: A histogram plot of the power law coefficients from the Hertzian corrected model and the experimental results. The larger range in the experimental power law coefficient (0.6-0.9) likely demonstrates that there are sample specific stiffening effects.

2.4.3 Discussion

To our knowledge, this is the first known study to measure and theoretically predict how cartilage contact stresses vary with load under a physiologically relevant range of load conditions. The experimentally reported contact stresses from this study are similar in magnitude as compared with articular joints [1], [161]. However, previously reported contact stresses also include native structures of articular joints, which modify cartilage contact loads. For the present study, our “ball-on-flat”

configuration removes any confounding factors from other structures (e.g. ligaments, meniscus) to elucidate the true cartilage contact mechanics, specifically how contact stress develops with increasing load.

A power law (Equation 8) well describes the contact stress for a range of loads ($R^2 > 0.99$ for all samples). However, the large range in the power coefficient of 0.73 ± 0.07 (see Figure 2-7) demonstrates that the cartilage contact behavior varies significantly based on the characteristics of the sample. Our proposed Hertzian corrected model, which assumed a constant elastic modulus for all loads, resulted in an average power coefficient of 0.56 with a much tighter range of ± 0.01 . This is comparable to the Winkler Foundation model power coefficient of 0.5. The discrepancy between the analytical models and experimental contact stress are likely due to the stiffening collagen fibers of cartilage (see Figure 2-7). The non-linear increase in elastic modulus agrees with previous literature, which found that cartilage stiffens with increasing strain [162]–[164], partly due to the non-linear behavior of the cartilage matrix [165]. However, Figure 2-4 also demonstrates that the relative increase in contact modulus is not consistent among each sample; some moduli remained at 2 MPa while others exceeded 10 MPa. Osmotic pressurization likely pre-stressed cartilage fibers of some samples, thus leading to a more significant increase in tissue stiffness [166]. Additionally, deep-zone cartilage fibers, which anchoring at the tide mark, can substantially increase tissue stiffness [167]. We can presume the wide ranging power coefficient is likely a factor of the 1) heterogeneity in fiber recruitment at the superficial layer and 2) fiber anchoring to the subchondral bone, which has been seen in other experimental studies[157], [168]. Future studies may need to probe the

material properties of each layer to capture the full stress characteristics of cartilage [121], [169]–[171].

Although it may be accurate to capture the true non-linear behavior of cartilage fibers, a load-varying modulus may not be feasible in practical applications. Our study demonstrates that a Hertzian-modified model with a single best-fit contact modulus can predict the contact stress with an expected mean error of 13.7%, which is comparable to the increase in contact stress in OA joints [134]. The Hertzian model requires only easily attained geometrical parameters, thickness and curvature, to extract the modulus of the tissue. Equation 6 can then be easily employed for a practical prediction for a range of physiological loads.¹ It should be again noted that this model was developed for fully-hydrated samples of cartilage. Because of its exudation characteristics, cartilage stiffness will significantly alter based on the fluid content of the tissue [17], [83], and the model should only be employed at similar fluid strains.

Beyond simplicity of the model, the proposed Hertzian corrected model is more reliable/robust than the Winkler model. For a “ball-on-flat” contact configuration proposed in this study, a Winkler “bed-of-springs” contact modulus can be calculated analytically ($E_c = \frac{4F \cdot R}{\pi a^4}$) [172]. Applying this model to data in Figure 2-6A would yield a Winkler contact modulus of 49.3 MPa. Problems in applying this model arise when accounting for the Poisson’s ratio of cartilage. Linear biphasic theory predicts an effective instantaneous Poisson’s ratio of 0.5 [173]; this would equate to a ~0 MPa

¹ It is suggested, though, that if the Hertzian-modified approach is practically implemented, that the modulus should be defined at the expected average load. For example, a modulus should be defined at 100N for an expected 0-200N load range.

elastic modulus according to an elastic foundation under plane strain. Conversely, using an elastic modulus from literature would equate to an infinite contact modulus. These numerical singularities have been avoided in literature by assuming a Poisson's ratio ranging from 0.40-0.49, which have been validated experimentally for nearly instantaneous loads [134], [174]–[176]. In a Winkler foundation model, this range corresponds to an 8x increase in contact modulus for a given elastic modulus and a 182% increase in contact stress for a given contact force. For the same range of Poisson's ratio, the Hertzian model predicts only a 10% increase in contact modulus and only a 6.5% increase in contact stress for a given force. Therefore, a Hertzian model is preferred over a Winkler foundation model because its potential error is reduced.

Most importantly, this study demonstrates that even simple models will incur significant error if the contact modulus is arbitrarily chosen from literature, instead of being measured for the sample being tested. For example, Figure 2-6A demonstrates that the best-fit modulus for that sample was 11.9 MPa. If, instead, a 5 MPa modulus was assumed [177]–[179], stresses would be underpredicted for all loads, resulting in a ~5x increase in RSMPE. This potentially large error has been highlighted in a critique of arbitrarily chosen contact modulus, which the authors conclude that more demographically relevant material properties (i.e. OA vs healthy) “can only improve comparisons between injured and diseased tissue...” [151], [180]. While the authors could not comment on the error from widespread use of material properties, this study clearly demonstrates that the large range of contact moduli chosen can have drastic effects on predicting contact stress.

Because of our simplified contact model approach, there are several limitations to this study. First, our derived contact modulus does not decouple the complex material interactions of the cartilage matrix. As stated, the contact modulus of cartilage increases with increased contact load based on the toe region [165]. Materials characterization of strain-stiffening properties that depend on fiber orientation would likely have improved our model, yet, at the expense of complexity. Second, our model assumed the attached bone to be a rigid substrate, but differences in bone modulus may have manifested as changes in cartilage modulus. A similar investigation found that the attached bone did not contribute to the overall deformation of the osteochondral specimen and could be considered rigid [167]. Still, a more comprehensive study considering the modulus of the bone may have provided insight into the cartilage modulus response.

Overall, this is the first known study to quantify and characterize the contact stress behavior of a curved cartilage layer. Secondly, it demonstrates that the heterogeneity of cartilage material properties can substantially alter the contact stress, even for a simple ball-on-flat loading configuration. However if the contact modulus is well defined, the proposed Hertzian model can predict stresses with confidence for studies ranging from benchtop testing [73], [116] to in-vivo joint contact [181]. Lastly, this study stresses the importance of empirically defining a contact modulus for a given sample, regardless of the contact model chosen.

Chapter 3

AIM 2—EXUDATION CHARACTERISTICS OF CARTILAGE IN PHYSIOLOGICAL CONDITIONS

3.1 Introduction

The functionality and long-term health of articular cartilage depends on its ability to regularly pressurize fluid within the tissue [182]. Because most of daily life is spent in sedentary behavior [108], [183], humans statically load articular joints, which drives interstitial fluid loss, decreases pressurization [36], and ultimately decreases tissue function [21].

Upon the instant of loading, interstitial fluid is initially conserved and the deformation response is effectively elastic [138]. Load is primarily supported by fluid pressure, which drives fluid outflow or exudation at the cartilage boundary [84]. As fluid exudes and the tissue compresses, fluid pressure and tissue permeability decrease, both of which slows the exudation rate [184], [185]. As the tissue compresses, the repulsion between fixed charges within the matrix increases leading to an increase in osmotic swelling pressure [85], [186]. Eventually, cartilage reaches a compressive equilibrium in which interstitial pressure and flow vanish and the contact pressure equals the osmotic swelling pressure [187].

This exudation response can be extremely fast or slow depending on what one assumes about the conditions of the contact interface. The interstitial pores of cartilage are nanoscale but the roughness of its surface is microscale. Under normal situations, contact between such rough surfaces can be expected to leave large interfacial gaps

with high permeability to fluid flow. According to McCutchen's "weeping lubrication" theory, pressurized interstitial fluid easily flows into these interfacial gaps and effectively lubricates the contact [22]. In this situation, pressurized fluid will take the shortest path into the contact interfaces and, as a result, the exudation rate will be independent of the contact area (or it will depend on the interfacial permeability rather than the cartilage permeability).

In practice, however, the exudation rate decreases with increased contact area in a manner consistent with an impermeable contact interface. Considering this result, Ateshian and colleagues applied biphasic theory to curved cartilage layers to calculate contact creep behavior [11], [15]. Their solution only accounted for creep behavior after a "squeeze film" was depleted (>10s) [188]. Additionally, their model supported "boosted lubrication" theory, which assumed that any fluid within the contact gap would follow a pressure gradient into cartilage [189]. Stolz et al. developed a theoretical model of a cartilage contact with realistic surface roughness and found that any trapped fluid is depleted within seconds or minutes as a result of flow into the cartilage [190]. Thus, most efforts to model cartilage contact now assume a no flow boundary at the contact interfaces to reflect perfect impermeability [11], [15].

These models often overpredict relaxation times of cartilage by $10X^2$ [191], [192]. Clearly, roughness does increase interfacial permeability and does impact contact and flow mechanics. To reconcile this problem, cartilage contact models with contact-dependent boundary conditions were developed [80], [193], [194], but these interfacial models were not based on experimentally derived permeabilities. Most

² Theoretical ~285 minutes [191] and experimental ~25 minutes[282]

importantly, these interfacial models could not compute the effect of the extremely rough cartilage surface [92], [93]. Wu and Ferguson used known roughness values of cartilage to show the intra-articular gap was at least an order of magnitude more permeable than the bulk tissue, allowing for an alternate flow path during exudation [94], [95]. However, it was unknown if the rapidly deforming surface asperities would quickly destroy the interface permeability such that the interface was practically impermeable. In response, Liao et al. developed a numerical poroelastic cartilage model which included the effect of surface asperities [129]. They found that the permeability of the gap was 1000X larger upon initial loading and remained 30X larger after 60 minutes of sustained load. This highly permeable interface provides a new drainage route normal to the contact interface and then is laterally transmitted through the contact gap to contribute to overall exudation [195]. The ‘weeping flow’ may speed up the consolidation time of the tissue, but the retention of pore pressure within interfacial gaps reduces the deformation stresses on individual asperities and extends the time over which the interface remains permeable.

Even with the permeable interface condition, however, the resultant relaxation time constant in Liao’s model was only reduced by a 21% [129]. While the developed poro-elastic model provides a useful framework that demonstrating the importance of asperities and the contact gap permeability in fluid exudation, the proof of concept only applied to a potentially non-realistic loading geometry with assumed material properties. In addition, the model does not account for any loading history, including the fact that joints remain in contact in unloaded conditions [196]–[198]. Even with light loads, soft asperities on the cartilage surface will significantly deform [199], which diminish the contact gap permeability such that the contact interface is

“functionally closed”[96]. It is unknown if upon higher loading situations, if the contact pressure can reopen the contact interface, thus re-establish the higher permeability interface, such that fluid flows into the gap rather than strictly through the tissue. Finally, exudation models that predict the contact area growth have excluded the presence of a permeable contact interface [11], [15], [128], which the Zhang group has shown to be a significant contributor to exudation characteristics and functionality of the cartilage contact gap, including potential weeping lubrication and sustained fluid pressurization [21], [22], [27], [129], [200], [201].

The rough surface, rough interface, interfacial permeability, and their effects on exudation mechanics are unaddressed experimentally, specifically with a realistic curved joint geometry. Tissue permeability properties from indentation may or may not be the most relevant measures of permeability in the context of physiological contact situations, i.e. curved cartilage surfaces. Because exudation defeats interstitial pressurization, there is a critical need to experimentally clarify the impact of interfacial permeability on the exudation mechanics of cartilage and joints. To address this need, we measured the time-dependent exudation and contact mechanics from osteochondral cores for a range of contact loads. To calculate the effect of the interface on exudation mechanics, we applied our data to an experimentally derived analytical cartilage contact model that accounts for both tissue and interfacial permeability (see Aim 2.1 in Figure 3-1A). Furthermore, we test if cartilage still can “weep” fluid into the interface, even when cartilage asperities have been significantly deformed and the interfacial permeability has substantially decreased (see Aim 2.2 in Figure 3-1 B).

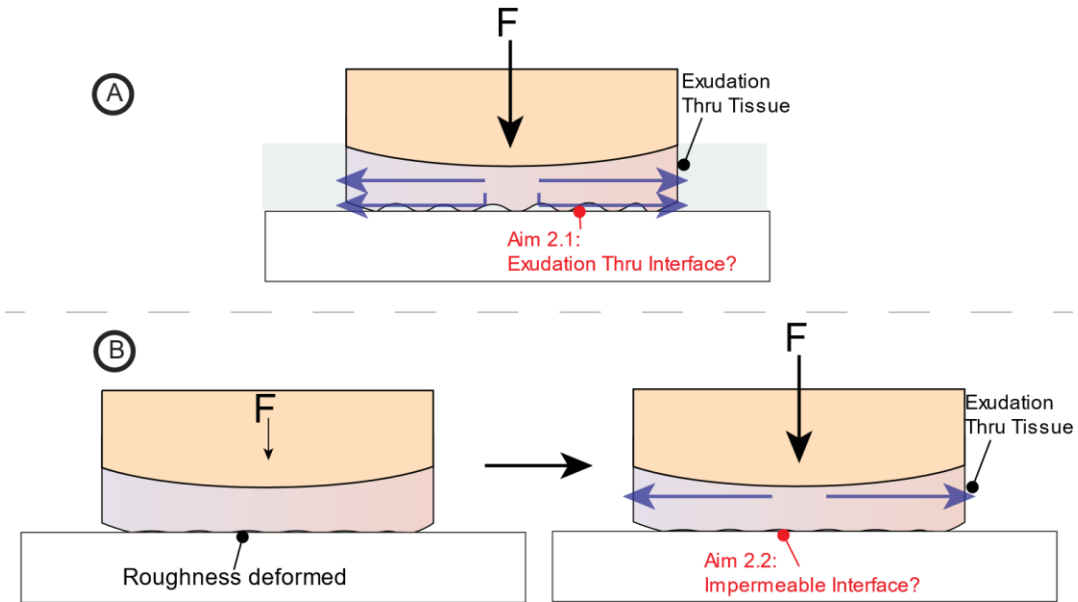


Figure 3-1: A) In Aim 2.1, we will determine the exudation characteristics of a fully hydrated cartilage sample. B) Aim 2.2 will address if interfacial permeability can be reestablished after a passive load

3.2 Methods

To capture the time-dependent exudation characteristics and contact stresses of cartilage, we subjected osteochondral cores to a constant loads against a flat plate while measuring the deformation and contact area (See sections 3.2.3 and 3.2.2). From these experimental values, we were able to derive a Darcy's flow model to calculate the effective permeability of cartilage during the exudation process (Section 3.2.4). We compared these experimentally derived permeabilities to previously known tissue permeabilities to determine if the interface permeability augmented the exudation response.

3.2.1 Materials and specimen preparation

This study used a total of $n = 3$ samples from 2 mature (> 18 -month-old steer) fresh bovine stifles acquired locally (Herman's Quality Meats, Newark, DE). A coring saw was used to extract 19 mm diameter osteochondral cores from the medial and lateral femoral condyles. Following extraction, samples were washed and then stored in DI water containing protease 1X inhibitor solution (Sigma-Aldrich, P8340) at 4 °C or dried under rough vacuum for 24 + hours to preserve the tissue. Previous studies have demonstrated tissue dehydration is an effective means of preserving cartilage mechanics [22], [116], [117], [202]. Testing on samples commenced within 4 days of DI water storage and were tested at 23 °C over a period of less than 35 h.

After commencement of all testing procedures, cartilage explants were sectioned near the centerline of cartilage for cartilage thickness measurements via image acquisition (see Figure 2-1C for more detail). The average cartilage thickness was used to calculate strain measurements in the proposed model.

3.2.2 Testing Instrument

Samples were clamped to a custom loading rig as illustrated in Figure 3-2 to quantify the contact area and deformation under a prescribed contact load. Normal loads were measured with a 6-channel load cell (ATI nano17, ± 10 mN) and controlled using a vertical nanopositioning stage (Q-545, Physik Instrumente) with force feedback. The displacements of this stage (± 10 nm) were used to maintain constant load conditions and to track cartilage deformation (δ) over the course of the test. Cartilage samples were submerged in deionized (DI) water with 10-15 ml of India Ink

(Winsor & Newton©) to provide contrast while imaging the contact area during testing³.

A dual-LED light source provided the necessary lighting for the camera (Teslong Inc.®) to capture the contact area image below the glass plate. NI Vision Acquisition software integrated into a LabView VI was used to capture the image data. The following image attributes were used to capture data: Contrast = 0.64 (maximum), Brightness = 64 (maximum), Exposure time <0.11 seconds, Gamma = 1, Saturation = 0 (minimum), and Gain < 25.

³ The inclusion of India Ink did not significantly change the exudation characteristics of cartilage samples. (See Figure B. 2 in Appendix A for analysis)

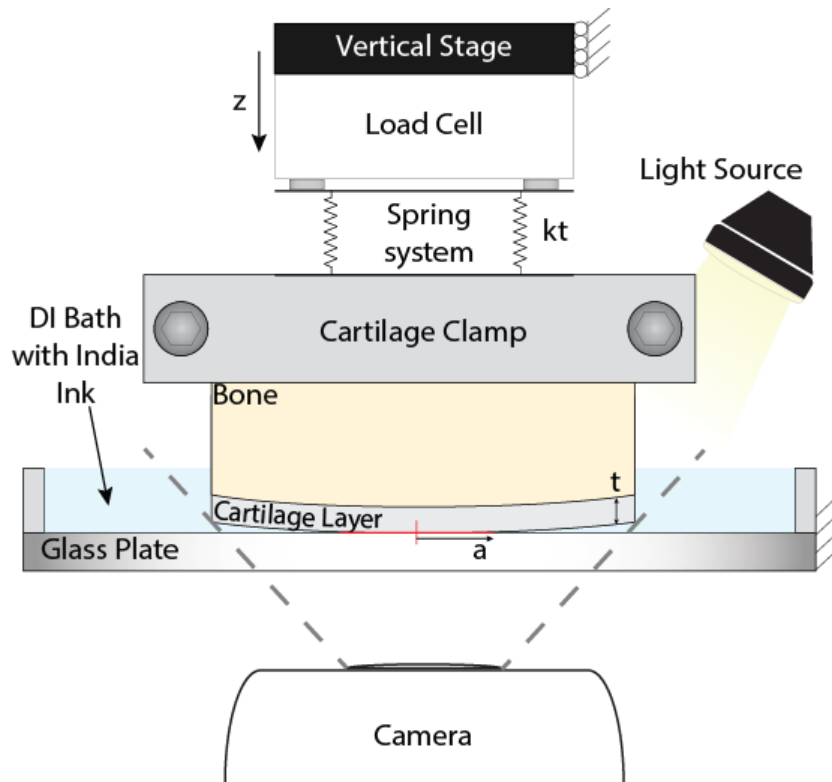


Figure 3-2: The experimental setup for exudation data collection. The deformation of cartilage could be tracked via the spring/vertical stage/load cell system [18], [28]. India ink infused in the DI bath provided the necessary contrast to discern the changing area of contact.

3.2.3 Exudation Testing Procedure and Data Curation

After cartilage samples were clamped to the testing rig, each sample underwent a preconditioning step prior to exudation testing as to normalize the free-swollen sample to the mechanical environment as described in [117]. Each sample was first loaded to 5 N (static) for 5 min, followed by free swelling at 0 N (static and out of contact) for 10 min. Cartilage samples then were positioned immediately above the glass plate ($<5\mu\text{m}$) prior to loading.

Samples were then loaded via the vertical stage (Figure 3-2) at either 2, 3, 4, or 5 N for 90 minutes or until a sample reached a deformational equilibrium. Samples were then unloaded at the original vertical testing position to allow for a free-swelling of the surface; samples remained in this position for 90 minutes to allow for full-tissue reswelling [203]. The 90 minute loading phase followed by the 90 minute recovery phase was repeated for the remaining four loads. The loading order was randomized.

A second series of experiments were conducted to determine how passive contact impacted asperity deformation, interface permeability, and exudation. In these experiments, samples first underwent a passive load (0.3 N) before loading at one of the aforementioned loads (2, 3, 4, or 5 N). Passive loads were imparted until cartilage reached an equilibrium deformation (~60 minutes of loading). Samples were then loaded for 90 minutes and allowed to free swell for 90 minutes after loading.

Deformational and force data were collected at 10 Hz. Load imparted on cartilage was controlled by a proportional controller updated at 10 Hz. During the loading phase, cartilage reached its target load in <1.5 s, and we treated deformations during the loading ramp as effectively elastic⁴. In the first 10 seconds of load, we collected image data at 10 Hz to measure contact area growth. After 10 seconds, image data were collected at 1 Hz since contact area did not rapidly increase after the early loading phase.

After all the time series data was collected, the contact area was extracted from image data via an adaptive color threshold in MATLAB image processing software. See Appendix A.3 for further explanation of contact area analysis. The elastic loading

⁴ Our biphasic model [83] with typical properties gives a mean flow rate of ~50 nm/s, which indicates that at most ~75nm of the ‘elastic’ deformation is attributable to flow

portion was removed prior to analysis; only data within 2% of the target load was considered. A 6th order Savitsky-golay filter with a 100 point window was used to filter the force, area, and deformation data and resampled at 1 Hz with a spline interpolation to fill in any missing time series data. Deformation rate data ($\dot{\delta}$) was then calculated via finite differencing methods and was smoothed via a 50-point moving mean filter. Next, any data after deformation equilibrium was removed; deformation reached equilibrium once the deformation rate was < 2.5 nm/s. The contact radius was considered the mean contact radius calculated from the area data ($a = \sqrt{\frac{A}{\pi}}$). Contact stress was calculated as the mean contact stress ($\sigma = \frac{F}{A}$). Experimental strain was calculated from the experimental deformation data ($\varepsilon = \frac{\delta}{thickness}$). Time constants for both the deformation (τ_{δ}) and contact radius (τ_a) were calculated as the time required for the response to reach 63.2% of its equilibrium value.

3.2.4 Model Development

With the experimental data, an exudation model was developed to include the effect of the permeable interface. The proposed model is similar to [98], where both interfacial and tissue exudation are considered. To simplify our model and remove any assumptions about the interface, the permeability of the interface and tissue were aggregated to determine the overall exudation response. The initial deformation of the cartilage tissue is calculated based on an initial Hertzian contact and subsequent exudation deformation is based on Darcy flow. The model assumes an isotropic, homogenous material with linear elasticity in tension and compression [154], [160].

Upon initial loading ($t=0+$), the initial contact deformation (δ_0) and strain (ε_0) was assumed to be Hertzian:

$$\varepsilon_0 = \frac{\delta_0}{t} = \frac{1}{t} \cdot \frac{3}{4} \frac{F_0}{a_0 \cdot E_0} \quad (9)$$

where F_0 is the imposed load, a_0 is the initial experimental contact radius, t is the thickness of the cartilage layer, and E_0 is the initial effective contact modulus of the cartilage layer.

Because the volume is conserved upon initial loading and Poisson's ratio can be assumed ~ 0 , the initial contact modulus (E_0) can be assumed as $(E_c' + E_t)$ [83], [154], [160], where E_c' layer corrected equilibrium compressive modulus, and E_t is the tensile modulus. The layer corrected equilibrium modulus can be calculated based on the thickness and area of the cartilage layer [158], which was introduced in Aim 1:

$$E_c' = \frac{E_c}{\left(1 - 1.04 e^{-1.73 \left(\frac{t}{a_0}\right)^{0.734}}\right)^3} \quad (10)$$

Equation 9 only considers a fully hydrated osteochondral plug. Because some of our experiments incur small preload (0.3 N) prior to imparting the larger load, F_0 , the strain accumulated fluid loss prior to loading (ε_{AF}) must be accounted for. Thus, ε_{AF} must be subtracted from the initial strain (ε_0) such that the Hertzian strain from a large contact load is not falsely inflated. Accounting for volume conservation upon loading and the accumulated fluid loss prior to loading, Equation 9 can now be rearranged as:

$$\varepsilon_0 = \frac{3}{4} \frac{F_0}{a_0 \cdot t \cdot (E_c' + E_t)} - \varepsilon_{AF} \quad (11)$$

In a fully hydrated state, $\varepsilon_{AF}=0$ but $\varepsilon_{AF} > 0$ if cartilage has a small preload prior to imparting the larger load, F_0 . Refer to Figure B. 1 in Appendix B.1 for calculations of ε_{AF} from a preload.

With the initial strain calculated, the strain in subsequent time steps (ε_{i+1}) could be calculated based on material properties that affect biphasic mechanics and

fluid load support. Upon loading, the initial fluid load support (FLS_0), which is the portion of load carried by the fluid, of the system can be calculated as:

$$FLS_0 = \frac{E^*}{E^*+1} \quad (12)$$

where E^* is the ratio of the tensile modulus to the compressive modulus ($E^* = E_t/E_c$) [83]. Per biphasic mechanics, the initial fluid pressure (P_0) and initial elastic stress ($\sigma_{0_{elastic}}$) can be calculated by the initial contact stress (σ_0) and FLS_0 as:

$$P_0 = \sigma_0 \cdot FLS_0 \quad (13)$$

$$\sigma_{0_{elastic}} = \sigma_0 \cdot (1 - FLS_0) \quad (14)$$

From the initial conditions, incremental increases in cartilage strain will be calculated based on fluid exudation and resultant deformation of the elastic phase. See illustration in Figure 3-3 for depiction of mechanics. Fluid strain or exudation is driven iteratively with a Darcy Flow at each time step (i):

$$\dot{\varepsilon}_i = \frac{9 \cdot k_i}{4 \cdot a_i^2} \cdot P_i \quad (15)$$

where $\dot{\varepsilon}_i$ is the strain rate and k_i is the strain dependent permeability of the system represented as:

$$k_i = k_0 \cdot e^{-M\varepsilon_i} \quad (16)$$

where k_0 and M are material constants [184]. Development of Equation 15 can be found in AppendixA.1.

Based on material properties, the strain at the next time step (ε_{i+1}) can then be calculated from the strain rate of the current time step:

$$\varepsilon_{i+1} = \varepsilon_i + \dot{\varepsilon}_i \cdot (t_{i+1} - t_i) \quad (17)$$

and the increase in elastic stress ($\sigma_{i+1_{elastic}}$) depends on the change in strain:

$$\sigma_{i+1_{elastic}} = \sigma_{i_{elastic}} + E_c \cdot (\varepsilon_{i+1} - \varepsilon_i) \quad (18)$$

Thus, the fluid pressure (P_{i+1}) can be calculated with the total contact stress (σ_{i+1}) and the elastic contact stress ($\sigma_{elastic_{i+1}}$) at the next time step:

$$P_{i+1} = \sigma_{i+1} - \sigma_{i+1_{elastic}} \quad (19)$$

Calculated values of P_{i+1} and ϵ_{i+1} are then used to determine the permeability and strain rate at the next time steps to drive the model forward in time. This exudation model was then applied to experimental deformation, area, and force data to compute the effective material properties of cartilage (E_t , E_c , k_0 and M) as detailed in Section 3.2.5. For a visual representation of model computations, please refer to the flowchart in Figure A. 3 in AppendixA.2.

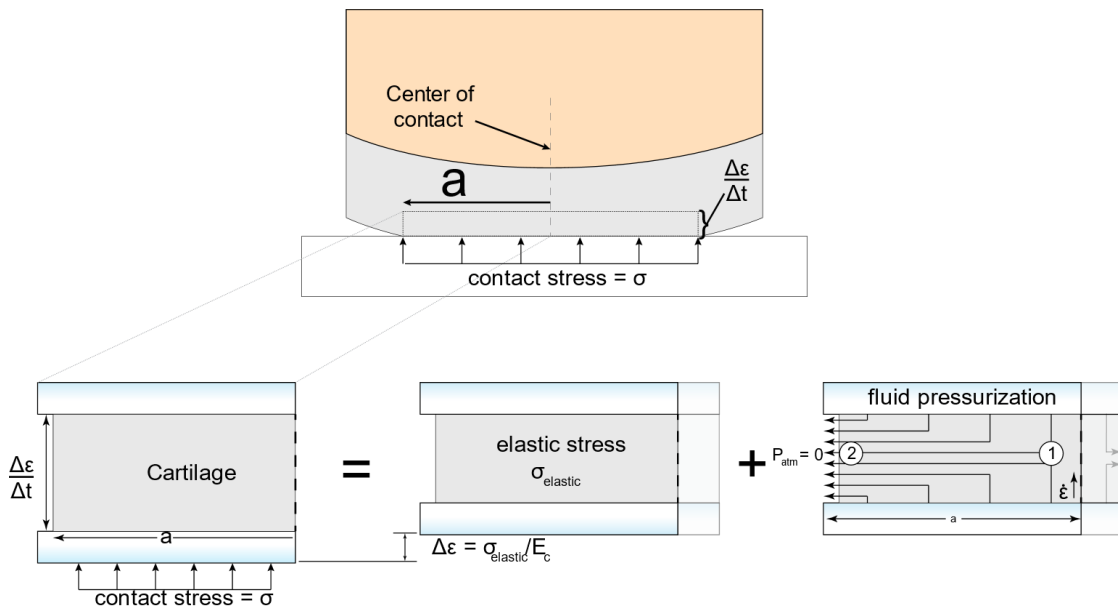


Figure 3-3: The biphasic model of contact and exudation. It was assumed that the fluid within the tissue and the gap laterally ejected through the tissue. Per Darcy's Law, the pressure in the system was calculated based on streamlines from 1 to 2. See Appendix A for model development. Based on a given contact stress (σ) and change in deformation ($\Delta\epsilon$), the elastic stress ($\sigma_{elastic}$), could be calculated. Thus, the resultant fluid pressure could be calculated at future time steps according to Equation 19.

3.2.5 Data Analysis

The curated data set was then fit to the exudation model from Section 3.2.4. With time series experimental data of strain, contact radius, and contact stress, the 4 unknown material properties (E_c , E_t , k_0 , and M) were computed with the ‘fgoalattain’ function (MATLAB®), which attempts to optimize several objective functions during fitting. The objective functions during optimization were 1) minimize the sum-squared-error (SSE) between the experimental strain and model strain and 2) minimize the SSE between the experimental strain rates and model strain rates:

$$\text{minimize } f(E_c, E_t, k_0, M) = \text{minimize} \begin{cases} \sum_i^n (\varepsilon_i - \varepsilon_{i_{model}})^2 \\ \sum_i^n (\dot{\varepsilon}_i - \dot{\varepsilon}_{i_{model}})^2 \end{cases} \quad (20)$$

The first 5 seconds within the loading response were weighted in the strain SSE equation ($\varepsilon_1 \dots \varepsilon_5$) by 10X since initial points in the model are very sensitive to changes in material properties. Additionally, the last 100 data points were weighted in the strain rate SEE equation ($\dot{\varepsilon}_{end-100} \dots \dot{\varepsilon}_{end}$) by 10X to ensure the model response reaches equilibrium. The material properties were bounded as such:

$$\begin{aligned} 0 &\leq E_c \leq \infty \\ E_c &\leq E_t \leq \infty \\ 0.00001 &\leq k_0 \leq 10 \\ .5 &\leq M \leq 200 \end{aligned} \quad (21)$$

Initial guesses for the material properties were based on methods from [160], which assumed a Hertzian contact. Because the model fit uses numerical optimization and is prone to finding multiple local minimums, a ‘multistart’ framework [204] was applied to determine the stability of model solutions (n = 10 simulations, within $\pm 50\%$ change in original guess). From the 10 simulations, the mean and standard deviation of each material property are reported.

The material properties for each load (k_0 , M , E_c , and E_t) were all fit to linear mixed models with load and preload as independent variables. Load was coded as a continuous variable from 2-5 N, and preload was coded as categorical (1 = preload and 0 = no preload). The inclusion of preload in the model tested if the apparent material properties changed when the interface was fully depressurized. All statistical analyses were used an a priori significance of $p=0.05$. All analyses were completed on MATLAB 2019.

3.3 Results

A representative measured deformation and contact radius plot are shown in Figure 3-4. As expected, larger loads resulted in both larger deformations and contact radii at both initial loading and equilibrium. As depicted in Figure 3-4, the contact radius time constant (τ_a) was substantially faster than the deformation time constant (τ_δ); the ratio of $\tau_a:\tau_\delta$ was 4.55, 3.17, and 3.55 for the three samples tested. This demonstrates that the contact interface relaxed 3-4x faster than the bulk tissue.

The proposed exudation model fit well to the experimental data with all $R^2 > 0.99$. Figure 3-5 demonstrates the goodness-of-fit for a single sample for a single contact load. Among all samples, the mean error between the data and the fit was $0.0255 \mu\text{m}$, based on generated deviations from the multistart approach. Because this error is within the noise floor of experiments, the multistart simulations demonstrated the robustness of the model to find the true behavior and apparent material properties at each load.

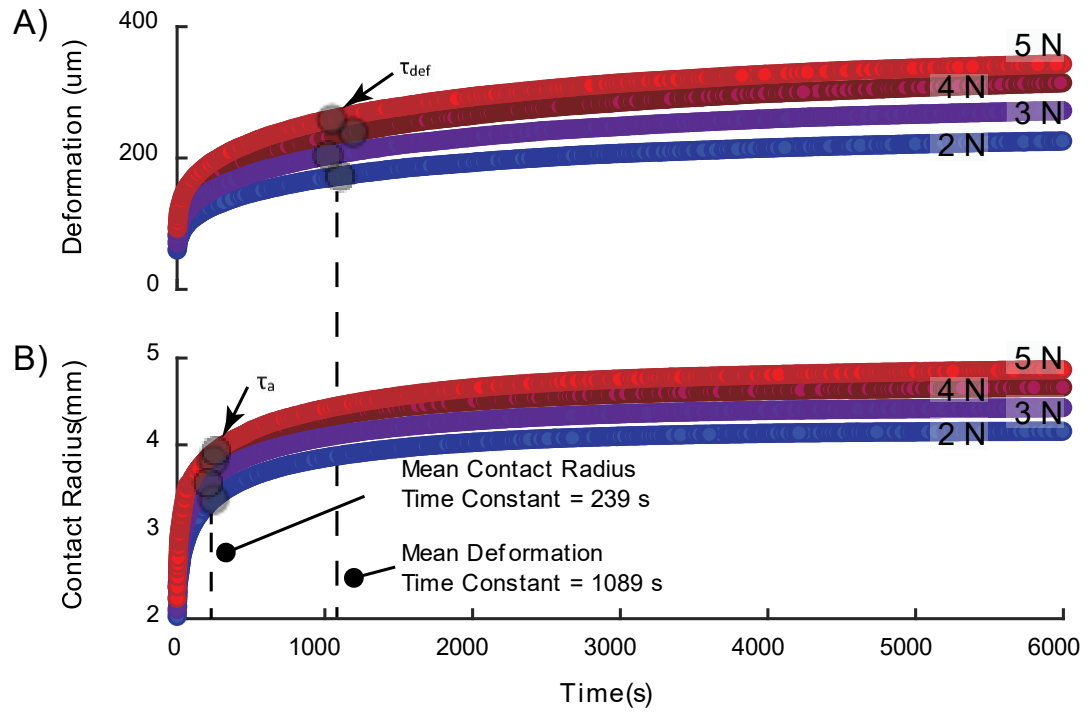


Figure 3-4: The measured deformation (A) and contact radius (B) is plotted vs. time for a single sample and multiple loads. The respective time constants (τ) are shown in light gray circles. For this sample, the average τ_a was 4.6 times larger than average τ_δ .

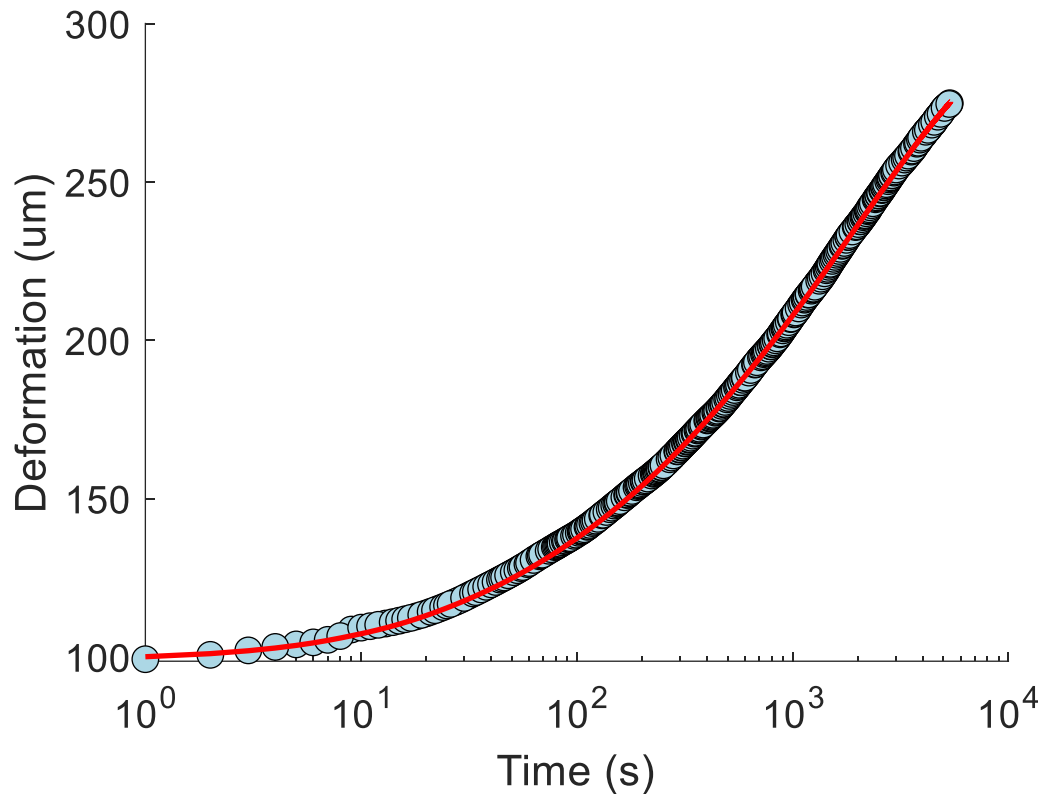


Figure 3-5: A representative fit for a single load shown in red. The first data point (~100 um) was considered the initial elastic deformation. All subsequent deformation accounted for the exudation response. Although this sample did not reach equilibrium within 90 minutes, the model was able to well predict the exudation response. The standard deviation between all simulated fits is non-discernable from the fit shown in red.

3.3.1 Effect of load and preload

For each sample, the apparent permeability increased as a function of load. The model permeability from the representative data from Figure 3-5 is shown in Figure 3-6. Corresponding FLS curves are generated for each load for the representative in Figure 3-7. As expected, the FLS support started above 80% for all samples, which is similar to other experimental results [21], [83], [206]. The applied

linear mixed models demonstrated that the calculated intrinsic permeability ($p=0.001$) and tensile modulus ($p=0.002$) all increased linearly with load, while the equilibrium modulus decreased with load ($p=0.03$). The permeability decay constant did not significantly change with increased load ($p=0.49$).

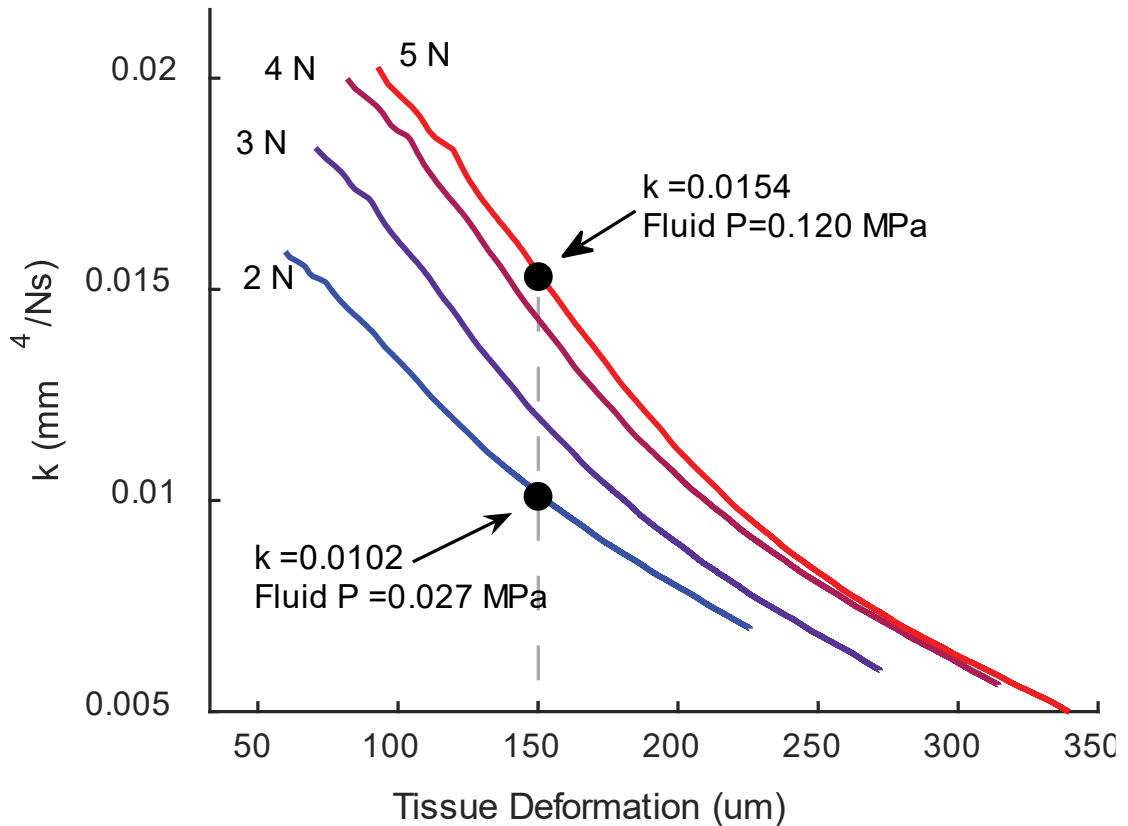


Figure 3-6: The predicted permeability curves vs. tissue deformation for the range of tested loads. The permeability at a given tissue deformation was systematically higher for higher loads. For example, at $150 \mu\text{m}$, the apparent permeability was 50% higher when comparing 5N to 2N, but also had a ~4X increase in fluid pressure, resulting in a 6X quicker exudation rate at the same deformation.

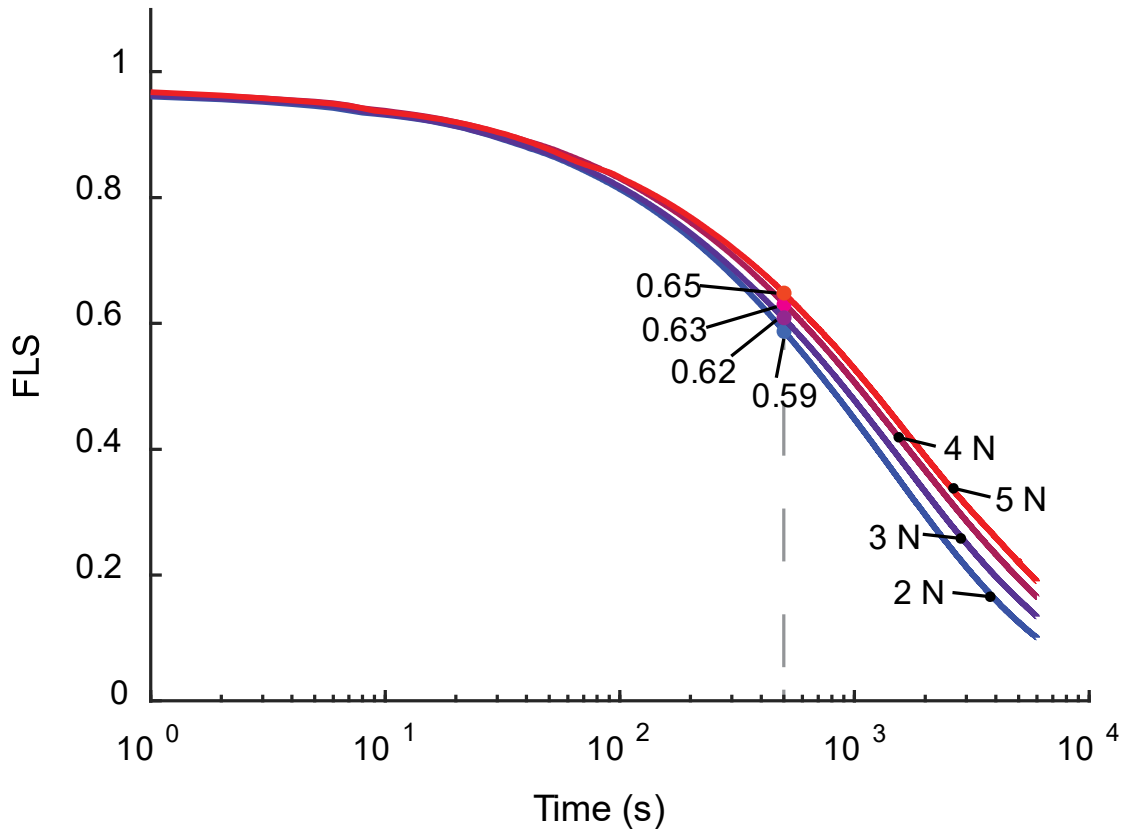


Figure 3-7: The generated FLS curves for a representative sample. In this sample, the FLS started at ~96% at initial loading, which is expected since fluid exudation ≈ 0 . The FLS dropped to below 20% after ~5000 seconds. Increased load maintained FLS for a longer period.

The 0.3 N preload increased the initial deformation of the cartilage by a mean 14 μm , which can be attributed to asperity deformation and fluid exudation prior to the larger induced load (2-5 N). However, beyond 100 seconds, the exudation and contact area curves were characteristically comparable, as seen in a representative sample in Figure 3-8. As expected, the equilibrium modulus (E_c) did not significantly vary

between preload and no-preload ($p = 0.5$). This was expected since the equilibrium cartilage deformation was equal between the two conditions. The tensile modulus (E_t) was significantly lower in the preload case ($p < 0.001$), likely due to fact that a preload exuded some fluid and the superficial fibers could not produce substantial tension upon a larger load. This also caused the initial fluid load support to decrease. Surprisingly, preload did not significantly change the intrinsic permeability of the system ($p=0.81$), indicating that the interface was not effectively “shut off” from the preload. Lastly, the permeability decay constant was not significantly affected by preload ($p=0.83$). This again indicated that permeability characteristics were preserved even when a passive load depressurized had initially depressurized and reduced the permeability of the interface. To compare the effect of preload on the experimentally derived material properties, Table 1 reports E_c , E_t , k_0 , and M for all the samples in the current study.

Table 1: The predicted model material properties separated by sample and preload. For each sample and preload condition, mean and standard deviation of E_c , E_t , k_0 and M are reported for imparted loads 2,3,4, and 5 N. Although an increase in load yielded a statistical change in material properties, these data demonstrate a more substantial sample-based effect on material properties. Additionally, the effect of preload only significantly reduces the tensile modulus of the tissue, while the remaining tissue properties remain indistinguishable.

Sample #	Preload?	$E_c \pm \text{STD}$ (MPa)	$E_t \pm \text{STD}$ (MPa)	$k_0 \pm \text{STD}$ (mm⁴/Ns)	$M \pm \text{STD}$ (unitless)
1	No	0.776±0.051	9.193 ±1.133	0.0072 ±0.0032	2.5 ±1.9
	Yes	0.819±0.088	7.327 ±1.105	0.0070 ±0.0022	2.7 ±1.7
2	No	0.223±0.009	13.761 ±2.152	0.0291 ±0.0058	6.8 ±0.4
	Yes	0.249±0.009	6.545 ±1.686	0.0315 ±0.0052	7.6 ±0.3
3	No	0.270±0.024	12.240 ±2.198	0.0165 ±0.0064	6.0 ±1.6
	Yes	0.290±0.017	9.645 ±2.307	0.0138 ±0.0042	4.8 ±1.7

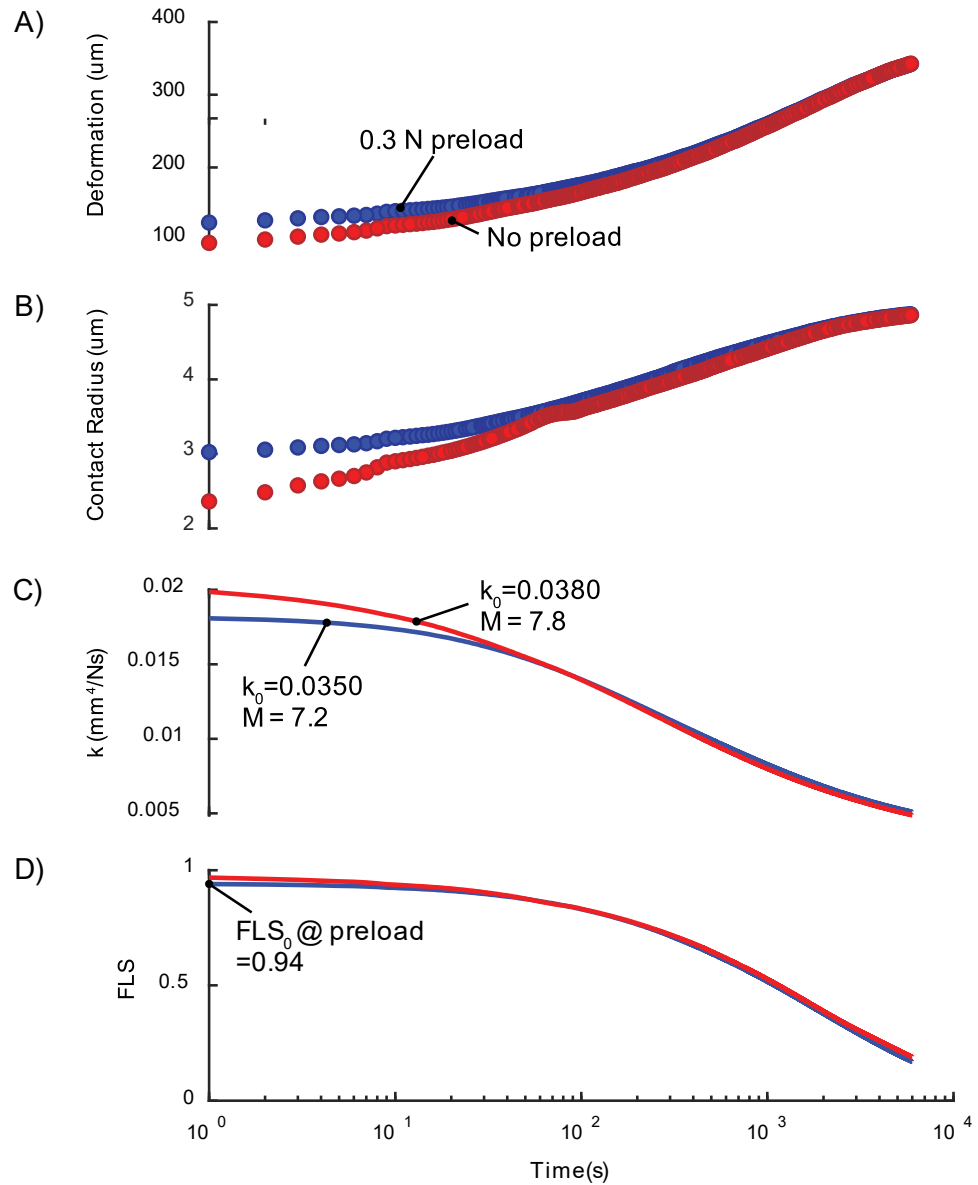


Figure 3-8: Comparing the effect of a 60-minute 0.3 N preload on the response of A) deformation, B) contact radius, and generated C) permeability and D) FLS curves for a 5 N contact load. Both the initial deformation and contact area were greater in the preload case, likely due to prior exudation from the 0.3 N load. By 100 seconds, the response was visually indistinguishable, indicating the interface likely repressurized with fluid. Consequently, the permeability characteristics (k_0 and M) were also indistinguishable in this loading case. However, compaction of the interface had limited effect on the fluid pressurization, as depicted in similar FLS curves in D)

3.3.2 Simulating the effect of indentation-based permeability

To demonstrate the effect of the interface on exudation, we employed our exudation model based on intrinsic permeability properties from literature [205]. We used the best-fit values for E_c and E_t from Table 1, Sample 3 to maintain the stiffness properties of cartilage. However, k_0 and M were set to $0.00171 \text{ mm}^4/\text{Ns}$ and 4.3 , respectively, to match previous experimental work [205]. For the representative sample, predicted exudation curves and FLS curves are shown in Figure 3-9A and Figure 3-9B, respectively. The simulated low permeability exudation required 9.5-10.5X longer time to reach the similar strains from the experimental data.

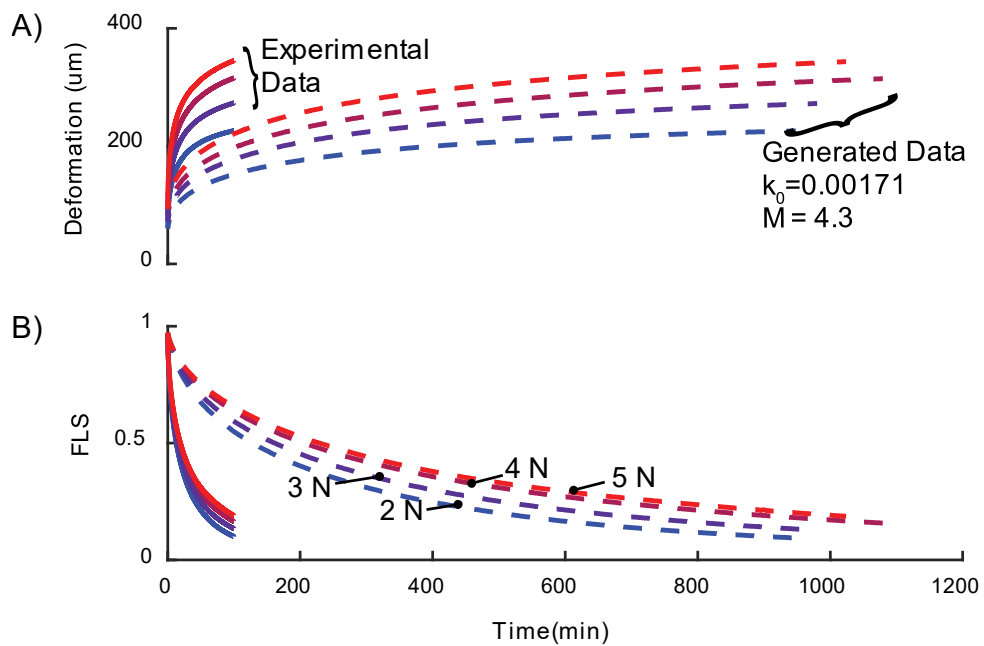


Figure 3-9: A) The experimental exudation curves (solid lines) are contrasted with the generated exudation curves (dashed lines) with permeability values from literature ($k_0 = 0.00171 \text{ mm}^4/\text{Ns}$, $M = 4.3$). Because the intrinsic permeability is reduced by $\sim 10\text{X}$, the generated exudation curves take $\sim 10\text{X}$ longer to reach the same strains. B) Using the reduced permeability from literature result in an extended FLS decay time. Again, FLS requires 10X the time to reach low FLS.

3.4 Discussion

In this study, we measured the exudation response of cartilage explants using both strain and contact area in an effort to investigate the potential role of interface permeability. These are, to our knowledge, the first direct measurements of exudation from the perspective of contact area. The deformation-based exudation response was about 10x faster than expected based on reported properties. This result implies that permeability was about 10x larger than reported in the literature or obtained by us using direct indentation measurements. Interestingly, the contact area relaxed about 4x faster than thickness. Our interpretation of these results is that the effective permeability is much larger than expected due to the presence of interfacial gaps of relatively high permeability. These gaps provide a lower resistance path than the tissue, which increases overall permeability. This gradient of permeability, biased toward the surface, explains why the contact area relaxed much faster than the bulk.

The proposed model is based on standard elastic and mixture theories but its details and implementation are unique to our knowledge. This model successfully captured the creep behavior of curved cartilage contact as all model fits yielded $R^2 > 0.99$. Prior analyses of cartilage contact creep and exudation only considered uniform loading [11], [12], [15], [207], which significantly simplified the modeling approaches. While these models were developed to estimate stresses in cartilage, there has been no experimental verification of cartilage contact area or the overall exudation response under more realistic nonconformal contact situations. Furthermore, our constitutive model is relatively simple and easily implementable based on the flowchart shown in Figure A. 3 in Appendix A.2.

The corrected Hertzian contact model, introduced in Aim 1, works well for an instantaneously loaded contact, where the response is an equivalent elastic solid [138].

Through Equation 11 and Equation 12, the model can capture the behavior of compressive (E_c) and tensile modulus (E_t) working in concert to increase initial FLS to greater than 90%. For a standard linear elastic material with $E^* = E_t/E_c=1$, cartilage FLS is limited to 50%, as demonstrated in previous investigations [83], [105].

As expected, our model indicates intrinsic permeability values up to 20X higher than previously reported permeability of cartilage [78], [105], [154], [160], [185], [210]–[212]. The 5X range in the effective permeability calculated in this study ($0.007 - 0.034 \text{ mm}^4/\text{Ns}$) is not unexpected as indentation tests have demonstrated nearly an order of magnitude difference in intrinsic permeability [154], [160]. Furthermore, the effective permeability of the interface is strongly dependent on the height of the gap ($k \propto \frac{1}{\text{gap height}^3}$), which is determined by the surface roughness [96], [98]. The large variance in cartilage surface roughness [92], [93]⁵ combined with the large variance in tissue permeability likely contributed to the apparent variance in our experiments.

Still, the evidence that intrinsic permeability increases with contact load, while being unaffected by a preload implies that the interface is a substantial contributor to the exudation response. First, intrinsic permeability, which is an innate material property of cartilage, should not vary with increased loads, only with deformation. In the current study, however, intrinsic permeability increases with contact load which implies increases in fluid pressurization opens interface for an alternate fluid exudation pathway. The characteristic increase in permeability agrees with a previous numerical study from Liao et al. They calculated that ~4X increase in fluid pressure

⁵ Some roughness RMS measurements of the hip can even exceed up to $70 \mu\text{m}$ [97]!

(see Figure 3-6) equates to a ~15X increase in gap permeability [96]. This increase in gap permeability likely led to an 3X increase in apparent permeability when comparing the 2 and 5 N load in Figure 3-6. Interestingly however, the authors also predicted that the interface is “functionally” closed if fluid pressure drops below 0.5 MPa; i.e. the gap permeability of the system equates to the tissue permeability [96]. However, the fluid pressures incurred in this study never reached 0.5 MPa, but the impact of the interface was still apparent on the scale of exudation.

When Liao et al. simulated the effect of a permeable interface, they calculated that the exudation time only decreases 25% as compared to an impermeable interface [129], which is still significantly lower than the 10x reduction in time constants calculated from this study. Our results demonstrate the leaky interface substantially alters the exudative time as compared to numerical measurements. One explanation of this difference may be attributed to the asperity stiffness [129], [201]. Liao et al. had as simulated the effect of increased asperity stiffness and found the interfacial gap fluid pressure would fall quicker as compared to softer asperities, thus reducing the time constant of cartilage [129]. Because the current experimental time constants are 10X quicker as compared to an impermeable interface, one may assume that the asperities are as stiff as the bulk tissue to promote a stronger outflow. However, it is known, qualitatively, that surface asperities are generally softer than tissue [199]. This warrants a rigorous investigation of asperity stiffness and gap height *during loading conditions* to accurately model the exudation process. This is important because fluid flow from tissue into contact gap increases the duration of hydrodynamic lubrication [195]. Faster weeping into the gap will complement more hydrodynamic lubrication initially, but will hasten onset of boundary lubrication [97], [98], [195].

Aside from asperity stiffness, surface roughness characteristics can significantly alter the gap permeability, which is known to change in osteoarthritic tissue. With OA, defibrillation of surface fibers can increase the roughness height >200% [94], [214], [215] and reduce the surface correlation wavelengths are reduced [200], [216]. Although increases in roughness increase the gap permeability, a numerical study of OA surface roughness demonstrated that the reductions in correlation lengths actually tissue reduced gap permeability [200]. In addition, asperity stiffness is known to decrease in OA joints [217], which would further reduce gap permeability. Furthermore, permeability of the bulk cartilage tissue [218], [219] and the osteochondral junction [220] also increase in OA joints. The resistance of flow through the gap may be preferentially redirected through the tissue and the osteochondral junction, more quickly dehydrating the surface, decrease interfacial pressurization, and incur higher friction forces. To examine this effect, future investigations should measure “start-up” friction after different durations of static load in osteoarthritic osteochondral tissue.

The passive loading case was intended to preferentially deform very soft asperities and reduce interfacial permeability. Our hypothesis was that an ‘untouched’ surface would have an artificially large roughness and that interface permeability would also be unnaturally large relative to joint surfaces, which are more or less always in contact under small loads. Interestingly, the passive load had only a small initial effect on exudation. As Figure 3-8 demonstrates, the exudation response was essentially identical with and without passive loading by 40 seconds. It should be noted that increasing from 0.3N preload to the experimental contact load (2-5 N), increased the contact area by only 25% to 30%. If the asperities were extremely soft,

then even small passive equilibrium loads would compress them and eliminate high permeability pathways within the interface, thus providing much slow exudation and permeabilities close to those of the tissue itself. The lack of sensitivity of exudation to prior passive loading is consistent with: 1) the effective stiffness of the asperities is close to that of the tissue itself; or 2) interfacial gaps and permeability are restored by repressurization of the subsurface and interfacial fluid. While we do not have any direct evidence of one over the other, we favor the second option. First, there is evidence that the surface is much softer, perhaps orders of magnitude so. Second, the observation that aggregate permeability (tissue and interface) tends toward tissue permeability at equilibrium suggests that the asperities effectively collapse over time. Finally, repressurization must occur and when it does, that will reduce load support by the asperities along with their strain. However, this is only possible if there is enough fluid in the bulk tissue, or “reservoir”, to drain into the interface. This phenomenon well agrees with the concept of cartilage tissue as a “source” term for exudation into the cartilage contact gap [195], which is illustrated in Figure 3-10.

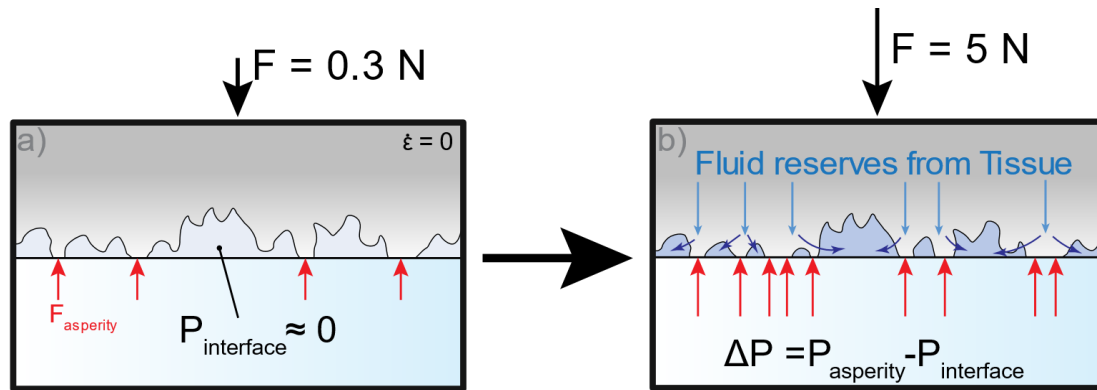


Figure 3-10: a) Applying passive load of 0.3N to equilibrium equates to ~ 0 pressure within the interfacial gaps and all of the load is supported by the asperities. b) Once a higher load is introduced, asperities experience more contact pressure as other asperities come into contact, resulting in pressurized fluid into the cartilage gap, thus reopening for the interface for flow.

The only comparable contact creep model of cartilage-on-flat was from Kelkar and Ateshian, who applied linear biphasic theory [15]. However, through linear biphasic theory, cartilage cannot achieve high FLS [17], [83]. Still, the authors calculated FLS time constants of 1950 – 2300 seconds for loads ranging from ~ 3 -15 N, which are comparable to the time constants from this study (~ 1200 to 1600 seconds). However, the authors assumed joint radii of curvature ranging from 200-2000 mm, which are 10-100X larger than actual radii of curvature [210], [221]–[224]. This leads to an increased conformability of contact, which is known to increase FLS time constants due to a longer fluid flow paths [195]. With a realistic radius of curvature and inclusion of a permeable interface, the linear biphasic theory would predict FLS time constants in the order of 10s of seconds (based on the gel diffusion equation, $\tau \propto \frac{A}{E_c \cdot k}$). With the inclusion of tension-compression non-linearity from our model, cartilage can create and sustain high FLS, despite having a leaky interface. In

this manner, cartilage can supply fluid to the interface for potential reductions in friction, while also maintaining functional levels of FLS within thousands of seconds of static loading.

Because of our simplified model and well controlled experimental configuration, some limitations should be noted. First, the exudation model is extremely sensitive to initial deformation responses since minimal fluid loss is assumed. However, the loads were applied within 1.5 seconds, leading to a non-infinitesimal fluid loss. Regardless, we consistently achieved $FLS > .8$ when comparing load cases (2N vs 5 N), reflecting intraload reliability.

Second, we did not measure tissue permeability via indentation measurements for a direct comparison to our exudation model. While indentation derived permeability may be correlated with total fluid loss [210], values may not be directly applicable to predict fluid loss in larger scale exudation models where the interface plays a significant role. Other studies have demonstrated that indentation permeability measurements may not actually capture the realistic permeability of the system [225], [226].

Third, the use of DI water in our investigation does not replicate the viscosity or osmotic swelling potentials of the true joint. We chose DI water over 1X PBS (0.15 M NaCl) because maintaining osmolarity of the solution is inherently difficult, even when being tracked using an osmometer [212]. With the use of DI water, we simulated an increase in GAG content and stiffened the tissue through osmotic pressure. Increases in osmotic potential has been shown, numerically, to decrease volume of exudate into the contact gap, reduce gap closure, and encourage gap fluid loss [201]. Using 1X PBS in our study, would equate to more overall exudation, but since the

interface would collapse faster, we predict increased time constants. We intend to test this model with increasing hypotonic solutions to determine the effect on the exudation rate and permeability of the interface/tissue. Lastly, synovial fluid viscosity is known to be 3-10X more viscous than DI water based on the shear rates it experiences [227]. This may increase the resistance to flow at the interface [98], but also extend the gap consolidation time [129]. Preliminary evidence suggests that the addition of viscous mediums, like hyaluronic acid, do not significantly affect the exudation response of cartilage [117], [227]. Still, future investigations should explore the effect of viscous substances on exudation to confidently predict fluid loss in vivo.

Lastly, the proposed exudation model simplifies cartilage tissue into a homogenous porous layer with the inclusion of a rough surface that augments the exudation response, like previous studies [129], [228]. In reality, permeability is the greatest near the surface of cartilage and decreases with depth [3], [211]. Furthermore, the tangential orientation of superficial zone (SZ) collagen fibers reduces the radial permeability at the surface of cartilage, which promotes preferential flow normal to the cartilage surface [229], [230]. Because of the high permeable superficial layer, one may suppose that the fast exudation times in this study were a direct result of SZ compression instead of a leaky interface. Further support for this conclusion is shown in Figure 3-4, where the contact area creeps faster than the bulk tissue, indicating a much faster relaxation near the surface of the tissue. However, under compressive load, the SZ is also known to strain much faster than the remainder of the tissue, quickly diminishing the permeability of the superficial zone, restricting exudation to the interface [231]–[234]. With the removal of the SZ in experimental [234], [235] and numerical studies [236], the permeability of cartilage *increases* two

fold, indicating that the SZ compression actually *slows* fluid loss. Unfortunately, most of these experiments leveraged a porous indenter, practically eliminating the effect of the interfacial permeability. To decouple the effect of interfacial permeability and superficial layer permeability on the overall exudation response, future studies should use the current exudation model for experiments with SZ removed while preserving the surface roughness of the tissue.

Despite these limitations, this is the first experimental evidence that the contact interface is permeable, that interfacial flows are significant, and that rates of interstitial fluid loss exceed those predicted based on the standard assumption of interfacial impermeability. As expected, as cartilage contacts are being scaled to the joint level, the effect of the interface can no longer be ignored when predicting exudation. For example, Macirowski et al. investigated the interfacial exudation at the hip and calculated that FLS is still > 0.9 after 20 minutes of physiological loading [97]. However, the authors predict a sharp decrease in gap conductance after a short loading time of joints because they assumed that fluid pools remained trapped and sealed within the cartilage interface. Our results demonstrate that these pressurized pools may appear sealed on a macro scale, but will eventually be defeated based on the smaller deformation undulation. To fully capture time scales pressurized fluid at the interface, we propose that future research includes all scales of trapped fluid in order to predict the function of a joint after a static load.

Chapter 4

AIM 3—THE MODES AND COMPETING RATES OF CARTILAGE FLUID LOSS AND RECOVERY

(Portions of this chapter are published in—Voinier, Moore, Benson, Price, and Burris, Acta Biomaterialia, 2022)

4.1 Introduction

Cartilage, the multiphasic tissue responsible for the load bearing and lubrication of joints, normally comprises about 75% interstitial fluid [237]. Under fully hydrated conditions, interstitial pressure preferentially supports the load, which reduces tissue strain and friction [19], [21], [211], [237]. While interstitial pressure performs key functional roles, it is also responsible for fluid exudation, a process that defeats interstitial hydration, pressure, and lubrication [21]. Indeed, experimental studies with cartilage explants have shown that tissue strains and friction coefficients approach 50% and 0.3, respectively, as fluid is lost over time [19], [20], [22], [27], [28].

The mechanics of fluid exudation are well understood, predictable, and observable even at the joint level [12], [17], [37], [77], [78]. Loading experiments with cadaveric human knees have shown that joint strains can reach 50% within 2 hours of static loading [238]. Fortunately, this exudation process is arrested during physical activity. In one study, MRI measurements during repeated sets of knee bends showed no time-dependent joint space thinning following an initial strain of only ~5% [35]. Theoretical work from Ateshian and Wang showed that exudation effectively stops

during articulation because the contact area migrates across the cartilage surface faster than the interstitial fluid can respond [21]. Interestingly, Coleman et al. showed that joint space thickness in the human knee is quite effectively preserved, thinning only by 1-5%, throughout the day [106]. Given that the average American is physically inactive or sedentary for most of the average day [108], such findings suggest that joint space thicknesses reflect a dynamic competition between load-induced exudation and movement-induced fluid recovery rather than the absolute absence of fluid flow.

The mechanics of fluid recovery by cartilage has received disproportionately less research attention than the mechanics of fluid loss. Eckstein et al. showed that the human knee thickened during rest following exercise at an average rate of $0.03 \mu\text{m/s}$ [35]. This recovery rate was uncompetitive with the loaded exudation rates observed at similar strains [238], which raises questions about the nature of the surfaces and interface during the recovery process. The authors attributed this slow recovery process to low permeability of the consolidated surface but another possibility is that the interface itself resisted inflow.

The nature of this surface/interface boundary is arguably the most important characteristic of exudation mechanics [84]; the two limiting cases are confined and unconfined compression [78]. In confined compression, the surface boundary is defined by zero pressure and the characteristic deformation time constant is independent of contact area; unconfined compression is instead defined by a zero flow surface boundary condition and its characteristic time constant is proportional to the contact area [78]. The same distinctions must be made for fluid recovery. In this study, free swelling is the limiting case of fluid recovery by an exposed surface with a zero-pressure boundary condition at the surface; passive swelling is the limiting case of

fluid recovery within an unloaded contact area with a the zero-flow boundary condition at the surface. While it is reasonable to assume that cartilage surfaces separate during/following unloading, experimental evidence indicating that contact areas remain following unloading [196], [197]and even persist under tension [193]refute this assumption. To date, however, the nature of these unloaded interfaces and their implications for fluid recovery dynamics remain largely unstudied.

We recently discovered another distinct mode of fluid recovery, which we call tribological rehydration, using convergent stationary contact area (cSCA) sliding experiments designed to activate hydrodynamic pressurization [116]. In the case of the cSCA, sliding caused interstitial fluid recovery within the shielded contact area without any change in the applied load. Our studies of tribological rehydration consistently suggest that hydrodynamic pressures are responsible for pushing entrained fluid into the loaded contact area [116], [117], [208]. Unlike free swelling, which only rehydrates surfaces outside the contact area, tribological rehydration rehydrates surfaces within the contact area (e.g., the femoral condyle and tibial plateau contact patch). Unlike passive swelling, which requires reductions in applied loads, tribological rehydration occurs at constant loads. While the phenomenon of articulation-induced fluid recovery has been widely attributed to free swelling at exposed surfaces [73], [211], tribological rehydration may also represent an important contributor. However, because these modes have yet to be isolated and quantified, their potential contributions to fluid recovery within joints remain uncertain.

The preservation of joint space during physical activity is often attributed to the absence of flow [20] [6], but we propose that the constant strains observed within articulating joints [37][102] [13, 28] represent a dynamic equilibrium between

competing rates of fluid loss and fluid recovery. This distinction between competing flows and the absence of flow at equilibrium [20] [12] [6, 10] may be extremely important physiologically and biomechanically given that local flows mediate solute transport, biochemistry, mechanobiology, non-equilibrium biomechanics, and other flow-dependent processes [37], [211], [237], [239]. Furthermore, it implies that the cartilage strain behaviors typically observed during activity [35], [37], [73], [106], [116] fundamentally depend on a competition between rates of fluid loss and fluid recovery. This paper isolates and quantifies these rates for the first time using controlled cartilage explant testing under physiologically relevant stresses, strains, and sliding speeds. The results show that free swelling and tribological rehydration are disproportionately fast compared to passive swelling and suggest that periodic joint movements may represent a critical mechanism for preserving and even restoring cartilage hydration and joint space throughout a mostly sedentary typical day.

4.2 Methods

4.2.1 Materials

This study used nine mature (>18-month-old steer) bovine stifles acquired through two local sources (Herman's Quality Meats, Newark, DE and Bowman's Butcher Shop, Churchville, MD). Following thawing and joint dissection, a coring saw was used to extract 19 mm diameter osteochondral cores from the medial and lateral femoral condyles. Each sample was stored and hydrated in phosphate buffered saline (0.15 M) containing protease inhibitor (P2714, Sigma Aldrich); we refer to this solution as PBS from here on. Samples were stored at 4°C for less than 4 days prior to testing and they were tested at 23°C over a period of less than 12 hours.

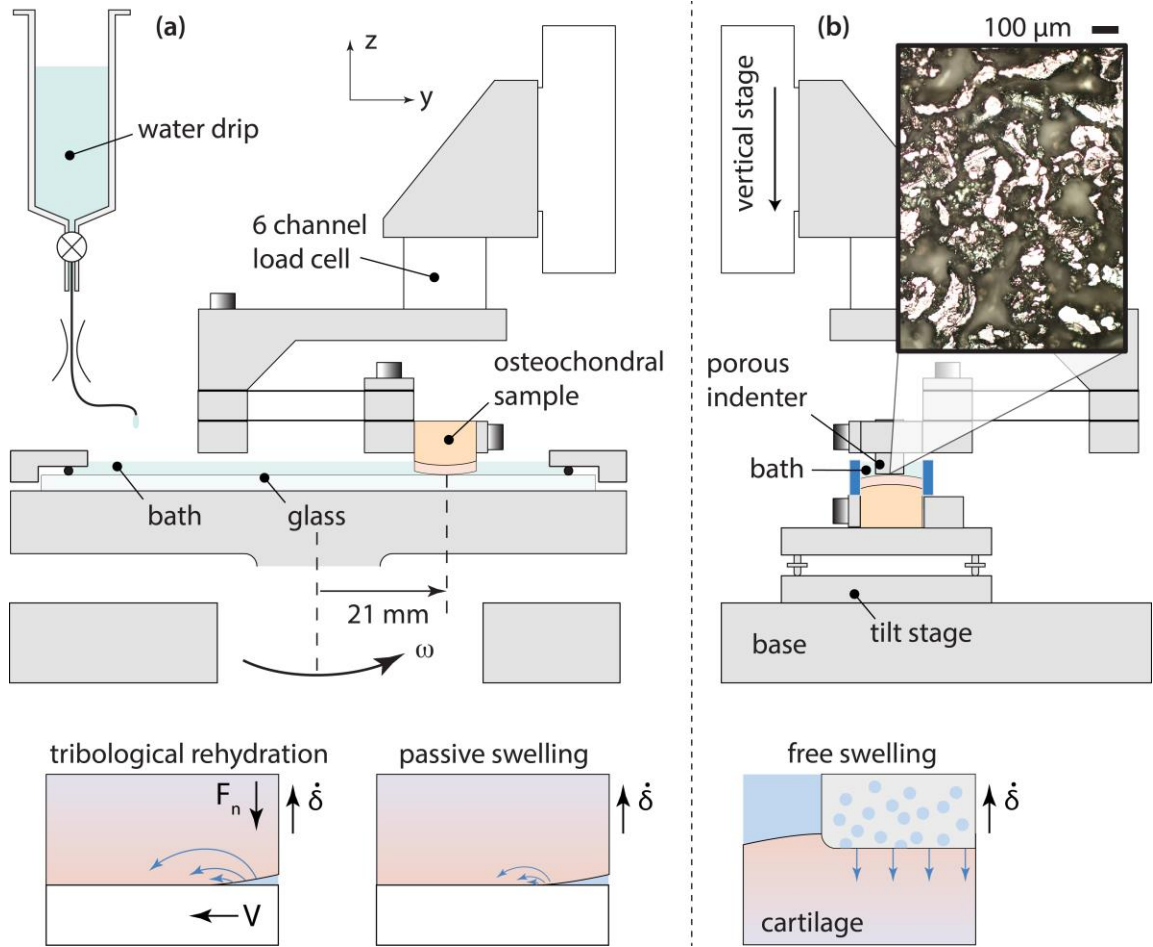


Figure 4-1 Schematic of the experimental apparatus. (a) The cartilage-on-flat configuration (which generates a convergent stationary contact area, cSCA) was used for passive swelling and tribological rehydration tests. The sample was clamped via the subchondral bone and the convex cartilage surface was loaded against a glass disc 21 mm from a rotary spindle. A calibrated water drip added DI water at the same rate as evaporation to maintain osmolarity. (b) The indenter-on-cartilage configuration was used with a porous (60 μm pores, 60% solid, permeability (k) $\sim 2500 \text{ mm}^4/\text{Ns}$) plane-ended stainless-steel indenter (ϕ 6 mm) for free swelling tests. The sample was mounted to a 2-axis tilt stage to align it with the indenter. Schematic sketches of tribological rehydration, passive swelling, and free swelling are shown for reference.

4.2.2 Instrument and Measurements

The custom pin-on-disc tribometer shown in Figure 4-1 was used to quantify fluid loss and recovery by measuring sample compression in real time under varying experimental conditions (loaded or nominally unloaded, static or sliding). Normal loads (F_n) were measured with a 6-channel load cell (ATI nano17, ± 10 mN) and controlled using a vertical nanopositioning stage (Q-545, Physik Instrumente) with force feedback. The displacements of this stage (± 10 nm) were used to maintain constant load conditions and to track cartilage compressions (δ) and compression rates ($\dot{\delta}$) in situ (i.e., cartilage thickness). The load head assumed either of two orientations. The ‘cartilage-on-flat’ mode (Figure 4-1a) was used for passive swelling and tribological rehydration characterization. In this configuration, large diameter convex osteochondral samples were mated against an impermeable glass counterface that was fixed or rotated ($\omega = 0$ or 4.8 rad/s, respectively) depending on the experiment. The ‘indenter-on-cartilage’ mode (Figure 4-1b) was used for free swelling measurements. In this configuration, a cylindrical porous plane-ended indenter with effectively infinite permeability was used to load and nominally unload cartilage (to a tare load) without inhibiting fluid flow out of or into the compressed surface. The cartilage surface was aligned normal to the indenter’s axis of rotational symmetry using a two-axis tilt stage. Both the cartilage surface and indenter were bathed in PBS.

4.2.3 Fluid Recovery Measurements

A total of 21 osteochondral cores were used to quantify free swelling (N=7 samples), passive swelling (N=7), or tribological rehydration (N=7) rates following varying periods of fluid exudation. These recovery modes are depicted in Figure 4-1. We used static recovery of cartilage under a nominal 0.1 N tare load against a porous

indenter to represent free swelling; this experiment tracks recovery without obstructing fluid recovery through the ‘contacting’ surface [240], [241]. We used static recovery of cartilage in contact under a nominal 0.1 N tare load against impermeable glass to represent passive swelling; this fixed-boundary experiment is well-controlled yet mimics the cartilage-on-cartilage passive recovery response as shown in Figure B. 3, Appendix B.2.1. In-situ contact area measurements showed that the contact pressure during passive swelling is ~1-10 kPa (Figure B. 4, Appendix B.2.2). We used recovery of cartilage under a maintained 5 N load against an impermeable glass surface sliding at a mean speed (V) of 100 mm/s to represent tribological rehydration. The measured contact pressures were ~0.1-0.2 MPa (Appendix B.2.2); for context, this is consistent with the contact pressures observed during static body weight loading of the human knee in-vivo (~0.2 MPa)[242]. The 100mm/s sliding speed was selected as it falls in the middle of the range cited for the human knee during gait[243], [244]. The superficial layer fiber direction was not recorded during extraction and was randomly oriented with respect to the sliding direction; a previous study testing this effect detected no significance [117]. To start each test, samples were loaded at 1 N/s to a target of 5 ± 0.05 N. We neglected flow during each loading and unloading ramp and treated deformations during loading and unloading as effectively elastic⁶. At the target load, the sample lost fluid over time until reaching a randomized compression target between 100 and 500 μm ; these targets correspond approximately to the compressions reported for the human knee after 10 to 100 minutes of static loading [238]. Following this point,

⁶ Our biphasic model [83] with typical properties gives a mean flow rate of ~50 nm/s, which indicates that ~0.25% of the ‘elastic’ deformation is attributable to flow

passive and free swelling were initiated by reducing the load to 0.1 ± 0.05 N at 1 N/s. The fluid recovery rate (passive swelling and free swelling) was quantified as a function of time (after reaching the target) using the time derivative of compression measurements; we used a zero-phase filter with a five-point moving average to mitigate the effect of measurement noise on the derivative. These loss and recovery rates are based on changes in cartilage thickness ($\mu\text{m/s}$) and they are equivalent to the rate of volumetric recovery per unit contact area. We then averaged these results from the first 100 seconds of recovery to quantify a representative mean rate for each sample; we chose this time to i) capture temporal changes, ii) represent a physiologically relevant time scale (e.g., a walk to the water cooler), and iii) avoid excessive weighting by the decay toward zero near equilibrium.

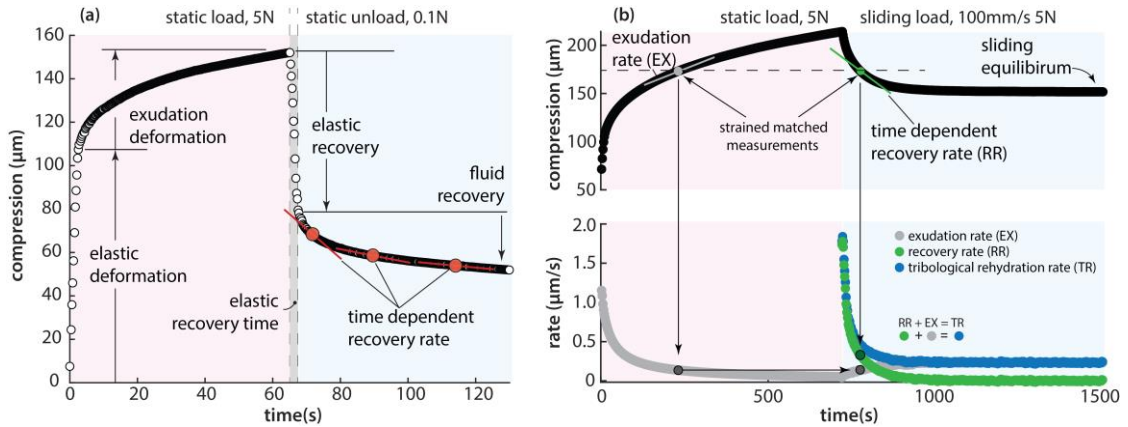


Figure 4-2: (a) Methods used to quantify passive and free-swelling rates (δ), which are defined here as the rate of change in thickness or the rate of volume change per unit contact area. Following static exudation at 5 N to a target compression, load was decreased to a tare load of 0.1 N. Time-dependent passive and free swelling rates were quantified using the instantaneous slope of recovery data taken just after reaching the 0.1 N tare load. The term ‘elastic’ denotes active loading and unloading phases where fluid volume is approximately conserved. (b) Methods used to quantify tribological rehydration and exudation rates, also defined based on the change in thickness per unit time. Following static exudation at 5 N to a target compression, fluid recovery accompanied the onset of sliding at 100 mm/s under the constant 5 N load. The time-dependent exudation and recovery rates were quantified using the instantaneous slopes of the exudation and recovery curves as shown. The tribological rehydration (total fluid gained, blue points) rate is the sum of the strain-matched exudation (fluid lost, grey) and recovery (net fluid gained, green) rates as shown.

Following exudation, tribological rehydration was initiated by sliding the disk at 100 mm/s while maintaining a constant 5 N load. The magnitudes of fluid exudation and recovery rates were quantified before and during sliding, respectively, by taking the time derivative of filtered compression data as described above. In this case, the applied load was maintained so there was no elastic recovery component. Given prior experimental evidence that exudation to be approximately independent of sliding [19],

net fluid recovery, which is measured, represents the difference between tribological rehydration (fluid gained) and exudation (fluid lost). To quantify the tribological rehydration rate at a given time, we added the measured recovery rate and the exudation rate for the same compression as shown for an arbitrary time point in Figure 4-2b.

While there may be considerable uncertainty in the exudation rate during sliding, the confounding effect on tribological rehydration rates is minimal when recovery rates are positive; as Figure 4-2b illustrates, the tribological rehydration rate only deviates significantly from the measured recovery rate due to exudation when the recovery rate approached zero. These uncertainties can become dominant when the majority of the recover signal comes from exudation. To avoid this potentially confounding effect, we only quantified tribological rehydration rates when net recovery rates were positive. An example of net exudation can be found in Figure 4-2a.

4.2.4 Data Analysis

The primary objectives of the study were to quantify mean rates of cartilage compression recovery due to passive swelling, free swelling, and tribological rehydration and identify any significant differences between these recovery modes. To detect statistical differences between average rates, we utilized one-way ANOVAs with Tukey's HSD multiple comparisons tests; the threshold for establishing statistical significance was defined as a multiplicity adjusted p-value of $p < 0.05$. A secondary aim was to determine if recovery rates characterized by a given mode depended on the initial exudation. These relationships were assessed using Pearson's correlation

coefficients (r), with the equation of the linear fit of this data being provided to assist interpretation. All data analyses were performed using MATLAB 2019b.

4.3 Results

Passive swelling results are shown in Figure 4-3a (green data points) for a single representative sample subjected to varying compression targets. The last 15 seconds of exudation (dark background) under static loading (5N) and the elastic recovery response (light background) during unloading (to 0.1N) are shown for reference. Figures 4-3c and 4-3d show that passive swelling rates slowed monotonically as cartilage recovered fluid (i.e., decompression) over time; in this case, passive swelling rates decreased from an initial range of 0.10-0.25 $\mu\text{m/s}$ to a range of 0.01-0.10 $\mu\text{m/s}$ after 150 s.

Free swelling results are shown in Figure 4-3b for a second representative sample subjected to varying compression targets (yellow data). The elastic recovery was about 50 μm for both sets of experiments regardless of the initial exudation. Figures 4-3c and 4-3d show that free swelling had a first-order character similar to that of passive swelling but with faster rates; free swelling rates decreased from an initial range of 0.9 to 1.3 $\mu\text{m/s}$ to a range of 0.2 to 0.4 $\mu\text{m/s}$ after 150 s.

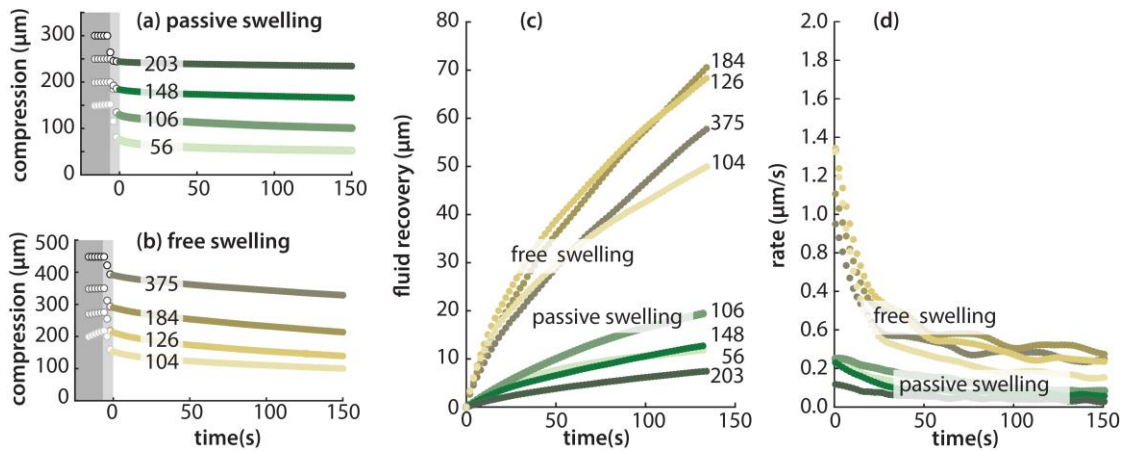


Figure 4-3: Results of passive and free swelling experiments. (a) Raw end-of-compression and start-of-recovery results from passive swelling measurements for a single representative sample subjected to varying tissue compression; each experiment is labeled with its initial exudation in microns. (b) Raw compression and recovery results from free swelling measurements for a different representative sample with varying tissue compression. The exudation and elastic recovery portions of the curve are highlighted in dark and light grey zones, respectively. (c) Fluid recovery (in microns) for passive and free swelling versus time from the same two representative samples. (d) Passive and free swelling rates (in microns per second) versus time for the same two representative samples.

Tribological rehydration results are shown in Figure 4-4a for a third representative sample subjected to varying compression targets followed by loaded high-speed sliding. The load was fixed at 5 N and the compression measurement comprised an initial elastic component (~ 100 μm on average) and an initial exudation component (indicated). Regardless of the initial exudation condition, this sample approached the same dynamic equilibrium (~ 175 μm) during sliding. The sample recovered fluid during sliding when the compression exceeded the dynamic equilibrium and it lost fluid when sliding was initiated below this target (*e.g.*, the 98 μm initial exudation case). These observations are consistent with our hypothesis that

the absence of net flow at the dynamic equilibrium reflects a competitive balance between tribological rehydration (input) and exudation (output) rather than the absence of flow in an absolute sense. The amount of net fluid recovered by the sample increased with initial exudation as shown in Figure 4-4b. In each of the four ‘net recovery’ cases⁷, tribological rehydration rates were 1-2 $\mu\text{m/s}$ initially and decreased over time to a final value of $\sim 0.2 \mu\text{m/s}$ at the dynamic equilibrium (Figure 4-4c). As Figure 4-4c illustrates, the dynamic equilibrium represents the compression/strain for which the tribological rehydration rates equal the exudation rates. Across all samples and conditions, the mean and standard deviation for the dynamic equilibrium compression and the dynamic equilibrium inflow/outflow rates were $181 \pm 64 \mu\text{m}$ ($82 \mu\text{m}$ from outflow after accounting for $99 \mu\text{m}$ of elastic compression due to loading) and $0.22 \pm 0.07 \mu\text{m/s}$, respectively.

⁷ We excluded the $98 \mu\text{m}$ initial exudation case from our analysis because it experienced ‘net exudation’ during sliding. While it is possible to quantify tribological rehydration rates despite net exudation, the measurement signal is dominated by exudation and sensitive to the uncertainty in the exudation rate.

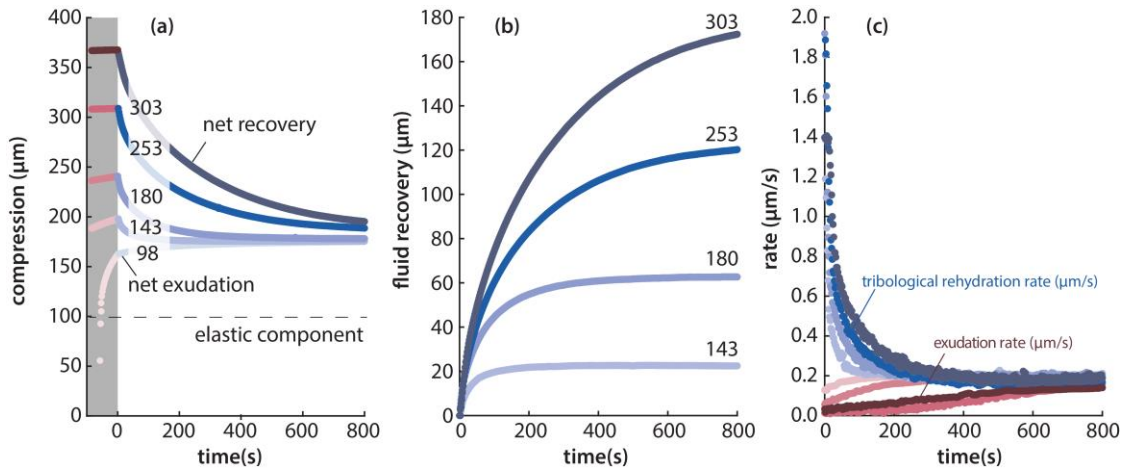


Figure 4-4: Results of tribological rehydration experiments conducted with varying tissue compressions for a single representative sample. (a) Raw compression and recovery results from tribological rehydration measurements for a single representative sample subjected to different initial compressions; each experiment is labeled with the initial compression at the onset of sliding minus the elastic compression. (b) Net measured fluid recovery starting from the onset of sliding as a function of time for the same experiments. (c) Tribological rehydration rates and exudation rates for the same experiments as a function of time. The system reached a dynamic equilibrium of zero net flow when exudation (outflow) balanced tribological rehydration (inflow) at $\sim 0.2 \mu\text{m/s}$ each.

Figure 4-5a shows how the mean flow rates (all samples, all conditions) vary as a function of time for the first 100 seconds of each recovery experiment; the shaded regions represent 95% confidence intervals for these mean values. All three modes slowed as the system approached full recovery over time. Free swelling and tribological rehydration were consistently an order of magnitude faster than passive swelling. Interestingly, free swelling and tribological rehydration exhibited overlapping confidence intervals over the entire range with both rates decreasing from initial rates of $>1 \mu\text{m/s}$ to $0.3 \mu\text{m/s}$ after 100 s of sliding (rehydration time).

The average inflow rate over the first 100 seconds of recovery is plotted for each sample as a function of compression due to exudation in Figure 4-5b. For this range of testing conditions, the rates (mean \pm the standard deviation) of free swelling, tribological rehydration, and passive swelling were 0.71 ± 0.15 , 0.63 ± 0.22 $\mu\text{m/s}$, and 0.11 ± 0.04 , $\mu\text{m/s}$, respectively. The shaded regions represent the overall means and their 95% confidence intervals. A one-way ANOVA detected significant differences among these rates. Post-hoc testing showed that free swelling and tribological rehydration rates were significantly faster than passive swelling ($p < 0.0001$); it revealed no significant difference between free swelling and tribological rehydration rates ($p = 0.16$). On average, free swelling and tribological rehydration rates were ~6 to 7-fold faster than passive swelling. We detected no significant correlation between the compression due to exudation and the tribological rehydration rate ($r = 0.11$, $p = 0.34$). However, the free swelling rate increased with compression due to exudation ($r = 0.53$, $p = 0.007$) and the passive swelling rate decreased with compression due to exudation ($r = -0.51$, $p = 0.003$).

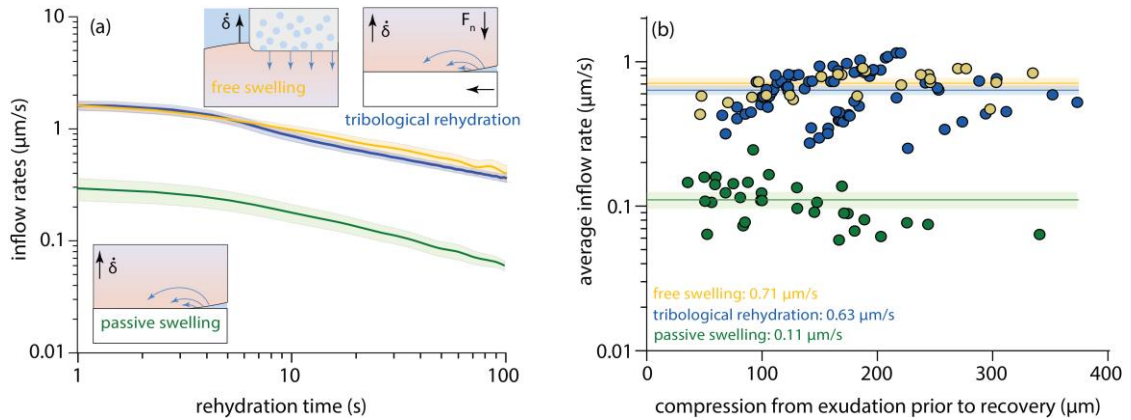


Figure 4-5: Summary of fluid recovery rates for all samples. (a) Mean inflow rates from all measurements for passive swelling (green), free swelling (yellow), and tribological rehydration (blue) as a function of time for the first 100 seconds of recovery (shaded regions represent the 95% confidence intervals for these mean values). All three recovery rates decreased with time but tribological rehydration and free swelling rates were approximately an order of magnitude higher than passive swelling over the entire time course. (b) Average inflow rates for the first 100 seconds of recovery versus compression from exudation prior to recovery for all tested samples. Shaded regions represent the overall means and their 95% confidence intervals.

4.4 Discussion

This paper defined, isolated, and quantified three distinct modes of competitive fluid recovery that cartilage has access to: passive swelling in nominally unloaded contact areas, free swelling at exposed surfaces, and tribological rehydration within loaded tribological contact areas. To our knowledge, these are the first direct measurements to quantify the fluid recovery rates associated with each mode. Tribological rehydration rates (0.63 $\mu\text{m/s}$) and free swelling rates (0.71 $\mu\text{m/s}$) were significantly faster than passive swelling rates (0.11 $\mu\text{m/s}$) over the first 100 seconds of recovery. In addition, this 7-fold difference in recovery rate was generally sustained at longer timepoints. More importantly, tribological rehydration and free swelling

rates were at least an order of magnitude faster than the exudation rates observed during static loading just prior to sliding ($0.06 \mu\text{m/s}$). This competitive asymmetry between fluid recovery and exudation helps explain why articulation reversed fluid loss so quickly in prior studies[73], [116], [243].

The specific rates reported here are, of course, limited to the conditions of the study. These rates are likely to change with sample size, load, sliding speed, and lubricant presence, among other variables[117], [208], [245], [246]. Nonetheless, their agreement with results from more clinically relevant studies is noteworthy. Following 14 minutes of static loading, the mean exudation rate from intact human patellofemoral (PT) joints was $0.03 \mu\text{m/s}$ [238]. The mean passive swelling rate observed for knees of live human subjects[35] was 2 to 6-fold slower than those observed here (0.05 and $0.2 \mu\text{m/s}$) and these differences are consistent with 2 to 6-fold larger contact areas in the PT joint [78]. Importantly, these observations are consistent with the hypotheses that joints maintain cartilage-on-cartilage contact following unloading, the contact interface is a significant impediment to fluid recovery, and the impediment increases with increased strain and contact area/path length. Additionally, following load-driven fluid exudation/compression within canine ankles, loaded articulation led to net fluid recovery at an estimated rate of $\sim 1 \mu\text{m/s}$ [73], which agrees well with the free swelling and tribological rehydration rates observed here. This preliminary agreement between our results and those of more clinically relevant studies suggests that our selection of stresses, strains, and sliding speeds provide a strong degree of physiological relevance while promoting experimental control. Perhaps even more interestingly, the dynamic equilibrium strain response during tribological rehydration ($\sim 5\%$ from fluid flow) was consistent with that observed in

the knees of mobile human subjects[37], [106]. Whether this consistency was fortuitous or the results of a more fundamental biomechanical response by cartilage remains to be seen. Subsequent work will aim to clarify how controllable experimental variables such as load, stress, and sliding speed influence the recovery process and dynamic equilibrium response.

The observation that joints maintain interstitial hydration and pressure during activity has been explained previously by the idea that the contact area migrates across the cartilage surface faster than the interstitial fluid can respond [12], [21]. This absence-of-flow paradigm is useful, particularly under equilibrium conditions, but it fails to provide insight into non-equilibrium dynamics. For example, it cannot explain the observation that cartilage in the human knee gradually thins toward a dynamic equilibrium during the first 30 min of walking[37]. To resolve this outstanding issue, we propose the competitive rates paradigm illustrated by Figure 4-6. During static loading, our observations and those of from the human patellofemoral (PF) joint[238] suggest exudation rates on the order of $0.05 \mu\text{m/s}$ (Figure 4-6c). Unloading the joint statically leads to comparable passive swelling rates of $0.03 \mu\text{m/s}$ according to measurements with living human subjects[35] (Figure 4-6b). During joint articulation, however, our results suggest that recovery rates are much faster due to the combined effects of tribological rehydration inside the contact ($0.63 \mu\text{m/s}$) and free swelling ($0.71 \mu\text{m/s}$) at free surfaces outside the contact (Figure 4-6c). Linn's measurements of exudation during static loading and joint space thickening during loaded and unloaded articulation are consistent with this paradigm and the rates measured here[73].

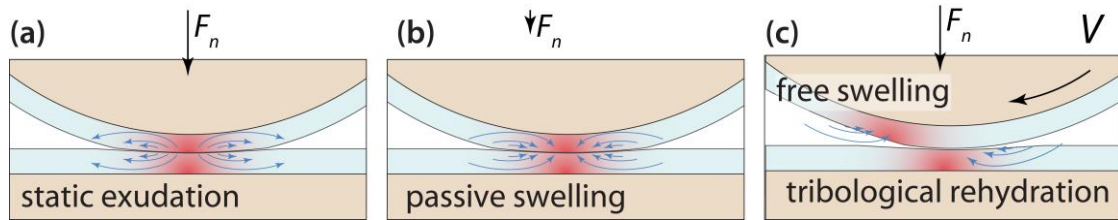


Figure 4-6: An illustration of the competing rates paradigm for describing cartilage fluid retention in the joint. (a) Exudation occurs during loading and the rates of fluid loss decrease with increasing contact area [9]. (b) Passive swelling occurs during static conditions within the contact area. (c) Free swelling and tribological rehydration occur during articulation outside and inside the contact area, respectively.

Our competitive-rates paradigm helps explain why Paranjape et al. [37] observed overall fluid exudation despite contact migration during walking. Walking from a fully hydrated state (the intended initial condition of the study), where the initial strain is assumed to be 0%, requires net exudation. As net exudation occurs, however, exudation rates decrease and recovery rates increase until meeting at the dynamic equilibrium (~5% strain is typical [35], [37], [73], [106]). In general, one can expect net fluid loss whenever strains are below their dynamic equilibria and net fluid recovery otherwise. Linn showed this effect directly. He observed either net fluid loss or net fluid recovery to the same dynamic equilibrium when he articulated canine ankles from a fully recovered state or from a consolidated state, respectively [73]. The same effect is evident in Figure 4-4; depending on the initial exudation, the sample exhibited either net exudation or net recovery during sliding, as appropriate, until reaching a consistent sample-dependent dynamic equilibrium compression. An important and unstudied practical question is whether and how quickly joint space is restored during walking following static loading (e.g. an hour at a standing desk). Our observations suggest that as little as a few minutes of walking might restore joint

space following an hour or more of continuous static loading. This hypothesis can be tested with existing methods and the results may have significant clinical and occupational implications.

Beyond clinical implications, these results help answer long-standing questions about the conditions of the contact interface following nominal unloading. Biphasic analysis assumes that the cartilage contact area is effectively impermeable[12] but this neglects the possibility that cartilage absorbs fluid from the interfacial gaps created by its unusually rough surfaces[189]. The latest theoretical studies support the impermeable interface assumption [95], [96], [129], [200]. In particular, a study by Liao et al. showed that exudation rates in realistically rough cartilage contacts were only slightly greater than those of an impermeable interface because compression of individual asperities reduces surface roughness, the size of interfacial gaps, and the interfacial permeability[129]. Using only basic contact mechanics arguments, Klein previously reached a similar conclusion that ‘under the pressures of living joints, the surfaces of the sliding articular cartilage are expected to conform smoothly and uniformly to each other, presumably down to separations of order nanometres’ [247]. Because both arguments are based on load-induced deformation, it is reasonable to expect asperity decompression, increased interface permeability, and high recovery rates following nominal unloading. However, our results are inconsistent with this expectation; the observation that passive swelling rates were only ~17% the free swelling rates suggests that the nominally unloaded (0.1 N tare load) contact area remained resistant to fluid inflow and that the unloaded asperities remain highly compressed. The low interfacial permeability (coupled with long fluid path lengths) following joint unloading helps explain the otherwise surprising fact that cartilage

contact areas remain large following unloading[196], [197] (see Figure B. 5) and even persist under tension [193].

Extremely thin interfacial gaps can be expected to slow exudation and passive swelling while amplifying hydrodynamic pressures and promoting tribological rehydration. Thus, it appears that movement-induced recovery is favored by design over static recovery. Interestingly, a recent theoretical study [248] showed that tribological rehydration is driven by hydrodynamic pressures and actually anticipated the rehydration rates observed here. Given its hydrodynamic origins, we were surprised that tribological rehydration rates at loaded low permeability interfaces were comparable to and even statistically indistinguishable from free swelling rates. One potential explanation is that hydrodynamic pressures only serve to push fluid into the low permeability interface[34], [117] and that osmotic swelling pressures ultimately regulate fluid uptake rates (as they do for free swelling). This hypothesis suggests that tribological rehydration rates will be limited by the lesser of the hydrodynamic transport rate (to the interface) or the free swelling rate. In the future, we will vary sliding speed (the driver of hydrodynamic transport) and contact stress and/or osmolarity (a driver of free swelling) to test this hypothesis more directly.

This study has several important limitations. While the conditions of this study were selected for their physiological relevance, no single set of conditions can represent the diversity of conditions in-vivo [161]; in particular, the effects of load, speed, and material properties remain untested. The only effects we tested here were those of time and strain. Free swelling rates increased with strain due, presumably, to increased osmotic pressure (Figure 4-5b). Passive swelling rates slowed with increased strain; in this case, the favorable effect of increased osmotic pressure appears to have

been offset by the competing effects of increased contact area/path length, increased asperity compression, and decreased interface permeability. Lastly, we used a smooth glass surface or a porous steel indenter as the mating surface depending on the experiment. Clearly, neither surface approximates the native cartilage surface. While migration makes tribological rehydration impossible to isolate in cartilage-cartilage contacts, we were able to test unloaded (passive) recovery of cartilage-on-cartilage contacts. The results in Figure B. 3 show that passive swelling occurred at about the same rate whether cartilage was mated against glass or another cartilage surface; thus, cartilage appears to be approximately impermeable from the passive swelling point of view, which explains the slow recovery during static unloading in-vivo[35]. We will study this effect in detail in a future study. In addition, the porous indenter is a concern due to the stress concentrator and may affect results if it damages the surface. We repeated passive swelling measurements after porous indentation and observed no effect from indentation (Figure B.). Additionally, we found no difference in the free swelling rates based on measurements with a porous indenter and a porous flat disc (not shown).

In summary, this study provides several important joint biomechanics insights. First, it provides evidence that dynamic compression/strain equilibria in cartilage reflect a balance between fluid loss and recovery rather than the absence of fluid flow. Second, it shows that movement-induced fluid recovery rates (due to direct surface exposure and tribological rehydration within the contact) are 7-fold those of passive swelling (due to nominal unloading) at the tested conditions. Third, it demonstrates that interfacial permeability is extremely low, even in nominally unloaded contacts, and suggests that low interface permeability may be the key feature underlying

competitive asymmetry between movement-induced fluid recovery and load-induced fluid loss (exudation would be far faster without significant resistance to interfacial flow). Fourth, it presents a new competitive rates paradigm with which to interpret these empirical results. In a recent study, for example, we used this competing rates paradigm with strain measurements from small range-of-motion MCA experiments to deduce that free swelling rates were likely $\sim 1 \mu\text{m/s}$ [105]; this study validates that deduction. This paradigm also provides a theoretical basis for anticipating dynamic equilibrium strains and loss or recovery rates during walking[37] and other activities. Finally, and most importantly, it suggests that brief but regular physical activity may be the most effective way to maintain maximum joint space thickness and cartilage function throughout an otherwise sedentary day.

Chapter 5

AIM 4—HYDRODYNAMIC DRIVEN REHYDRATION: HOW TO REACH FUNCTIONAL EQUILIBRIUM

5.1 Introduction

Articular cartilage transfers load between bones with minimal friction. When healthy, the tissue maintains this function throughout life. Cartilage remains healthy when chondrocytes achieve homeostasis and damaging stresses are limited. To achieve these goals, cartilage must regularly pressurize its interstitial fluid [39], [239], [249], which is generally achievable during load-bearing activities like walking [16], [250], [251]. However, some joint loading patterns may defeat fluid pressurization and predispose cartilage to a harmful environment leading to OA [131], [252].

Fortunately, cartilage maintains ~5% strain throughout the day, on average [106], [107], which reflects minimal fluid loss and high fluid pressure. Because static loading of the joint can yield ~50% strain within hours [238], low diurnal strains do not reflect an absence of exudation, but rather a play between load induced exudation and rehydration [243]. In the previous chapter, we demonstrated that movement mediated rehydration rates are ~10x faster as compared to passive swelling [198]; movement-based rehydration substantially outcompetes exudation rates to permit efficient rehydration. Thus, cartilage can establish a consistent ~5% strain during movement [35], [37], [73], [101]–[104], even though articular joints withstand forces much greater than body weight [253].

The asymptotic 5% strain – which is deemed the “dynamic equilibrium” — is where fluid inflow and outflow are equal, and represents the operating conditions of cartilage during movement [37]. One explanation of this low strain depends on the migration of the cartilage contact area during movement. With this migrating contact area (MCA) paradigm, dehydrated portions of cartilage are intermittently exposed to surrounding fluid for relatively quick rehydration [73], [75]. A recent paper out of our group demonstrated that cartilage maintains low strain and relatively high fluid pressure even when only a small portion (<10%) of the contact patch is periodically exposed to the bath [105]. The MCA paradigm, however, cannot be applied to situations where joint contact remains relatively buried during movement (e.g. tibial plateau).

Tribological rehydration, which was introduced in Chapter 4, is a substantial contributor when rehydrating buried contacts [198], even under constant load. Our current experimental evidence suggest that hydrodynamic pressurization promotes tribological rehydration when sliding occurs at high joint sliding speeds (>50mm/s) [116], [117], [208]. During the dynamic equilibrium, exudation continues due to a sustained contact, but hydrodynamic pressure restores fluid at the same rate. In a recent modeling study of dynamic equilibrium, de Boer, et al. confirmed that load induced exudation rates and hydrodynamic induced rehydration rates must equate [254]. Furthermore, they determined that cartilage inflow was primarily driven by a pressurized front at the leading edge of contact, which helps fluid advect through the dehydrated tissue [254], [255]; our previous experimental data have also suggested this phenomenon [116], [117], [208], [256], [257]. However, the authors treated the cartilage contact as two nominally flat surfaces in motion that could allow for

development of a fluid film. When the film thickness is zero, no rehydration exists in the contacting region because no flow can occur between a non-existent gap. This fact disallows any interfacial flow during mixed-mode lubrication. The cartilage tribology community, however, have generally accepted that articular joints experience mixed-mode lubrication during gait [195], [258], [259], since the roughness of cartilage, which is on the order of 1-10 μm [92], is much larger than any developed fluid film, which is on the order of nm [116].

In response, Putignano et al. developed a hydrodynamic model, which included the roughness parameters of cartilage, to investigate how sliding drives fluid into cartilage upon movement initiation [248]. Prior to moving, prolonged static loading substantially deforms the soft surface asperities, which essentially seals the interface from any more fluid flow [96]. Upon movement, a pressurized wedge (see Figure 5-1), ‘peels’ the leading edge of cartilage, effectively opening interface for fluid flow. The roughness of cartilage in Putignano’s model allowed for a percolated network of fluid flow within the interface [248]. In this model, the rehydration rate was linearly dependent on sliding speed of cartilage, but independent of load. Additionally, this model only analyzed the onset of sliding (i.e. movement initiation) and not the dynamic equilibrium (i.e. continual movement).

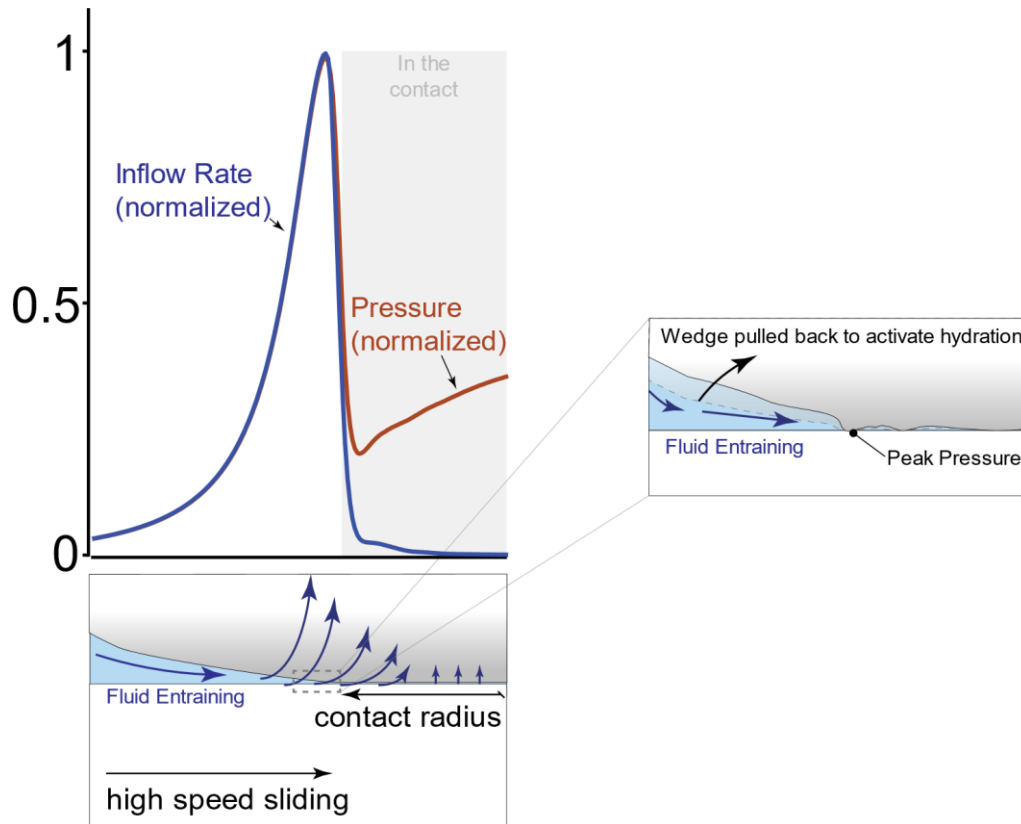


Figure 5-1: Activation of the hydration mechanism is dependent on the available wedge based on the curvature of cartilage. Pressure is increased as the fluid is entrained into the wedge and allows fluid to enter the semipermeable membrane. Most of the inflow rate into cartilage is within the pressured wedge, as predicted by hydrodynamics. The pressure and inflow rate data is modified from [248].

While initial rehydration rates scale with sliding speed, it is unknown how sliding speed and load will affect hydrodynamics at the dynamic equilibrium. Addressing this knowledge gap can illuminate the specific parameters that drive dynamic equilibrium strains witnessed in vivo, and consequently help scientists and engineers understand what biomechanical conditions promote cartilage function. Thus, we experimentally varied sliding speeds and contact loads while quantifying the

deformation and rehydration rates at dynamic equilibrium. Because increases in sliding speed drive up hydrodynamic pressure [116], [117], [208], [245], [248], [257], [260], we hypothesized that an increase in physiologically relevant sliding speeds would increase the rehydration rate and overall tissue thickness. Furthermore, we hypothesized that an increase in load would defeat interstitial pressure [17], [21], [206], and thus lead to a lower rehydration rate at higher loads. Accordingly, we calculated the fluid load support (FLS)—which represents the portion of load carried by interstitial pressure—as a function of load. Outcomes from this study will determine the crucial mechanical variables that predict the dynamic equilibrium, while also elucidating the role of hydrodynamics on tribological rehydration.

5.2 Methods

5.2.1 Materials and specimen preparation

This study used mature (> 18-month-old steer) fresh bovine stifles acquired locally (Herman's Quality Meats, Newark, DE). A coring saw was used to extract 19 mm diameter osteochondral cores from the medial and lateral femoral condyles for a total of n=17 samples. Following extraction, samples were then washed and stored in DI water containing protease 1X inhibitor solution at 4 °C or dried under rough vacuum for 24 + hours to preserve the tissue. Previous studies have demonstrated tissue dehydration is an effective means of preserving cartilage mechanics [22], [116], [117], [202]. Dehydrated samples were rehydrated overnight before testing the next day (12+ hours of rehydration). Testing on samples commenced within 4 days of DI water storage and were tested at 23 °C over a period of less than 12 hours. A previous investigation demonstrated that tribological rehydration characteristics are

reproducible within 96 hours of initial testing [245]. Immediately prior to testing, all samples underwent a preconditioning cycle of 5 minutes of static loading at 5 N, 5 minutes of sliding loading at 5 N, and 10 minutes of free swelling [117].

5.2.2 Instrument and Measurements

The custom pin-on-disc tribometer shown in Figure 4-1 from Chapter 4 was used to quantify the sample-specific dynamic equilibrium magnitudes by measuring tissue compression in real time. Normal loads (F_n) were measured with a 6-channel load cell (ATI nano17, ± 10 mN) and controlled using a vertical nanopositioning stage (Q-545, Physik Instrumente) with force feedback. The displacements of this stage (± 10 nm) were used to maintain constant load conditions and to track cartilage deformation (δ) and deformation rates ($\dot{\delta}$) in situ. The osteochondral samples were mated against an impermeable glass counterface 28 mm from the center of contact. The disc was rotated at varying rotational speeds to induce an array of sliding speeds. Rotational positions were tracked via an encoder (MA3, U.S. Digital) attached to the spindle. A dual-LED light source provided the necessary lighting for the camera (Teslong Inc.®) to capture the contact area during FLS measurements.

Because of the nature of the pin-on-disc tribometer and varying location of contact on the cartilage sample, the mean sliding speed may incur $\pm 30\%$ error [261]. A preliminary measurement of cartilage contact demonstrated that the center of contact only deviated by a maximum of 9.7% with a mean deviation of 4.5%; thus, reported sliding speeds varied a maximum of 9.7% based on sample variation. The cartilage surface was bathed in DI water containing protease 1X inhibitor solution during all testing.

5.2.3 Measuring the Dynamic Equilibrium with varying Sliding Speeds and Load

A total of $n = 7$ osteochondral cores were used to quantify the deformation and rehydration rates of cartilage at the dynamic equilibrium for 1,2,3,4 and 5 N loads for varying physiological sliding speeds of 200, 100, and 50 mm/s. These sliding speeds represent the maximum, average, and minimum sliding speeds, respectively, of the human tibiofemoral joint during swing phase [244]. For each load, samples were statically loaded for 20 minutes to develop the exudation rate profile needed during tribological rehydration [198]. After the static load, samples were then slid at 200mm/s at the same load to recover fluid until the dynamic equilibrium was reached (see Figure 5-2A). Because of the eccentricity of the spindle, 0.25 to 0.30 N of runout was expected within each rotation. Thus, the average desired load was maintained and updated after every rotation of the spindle.

Dynamic equilibrium was established when the rate of recovery maintained $< 0.075 \Delta\mu\text{m/rotation}^8$. After establishing dynamic equilibrium at 200 mm/s, the speed was reduced to 100 mm/s until dynamic equilibrium, and subsequently reduced to 50mm/s until dynamic equilibrium. Establishment of the dynamic equilibrium was repeated twice more at each speed to determine the repeatability of measurements. (see Figure 5-2B). The dynamic equilibrium process was repeated for all loads. Cartilage samples were allowed to free swell in DI water for 60 minutes between each tested load.

⁸ A first order Savitsky-golay filter with a 15 point window was used to filter the change in deformation data. Deformation rates were computed from filtered data.

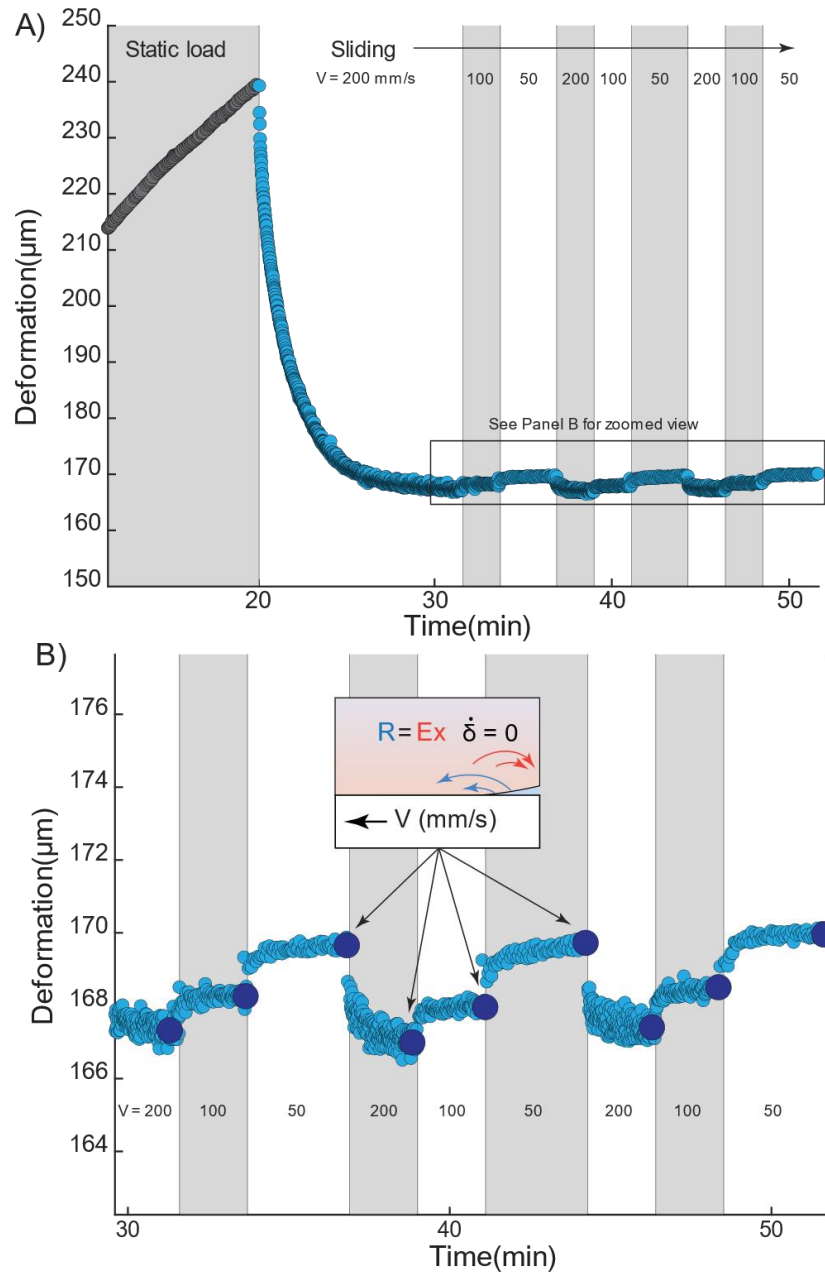


Figure 5-2: The measurements of dynamic equilibrium for a single load. A) After a static load, the load is maintained and slid at 200mm/s until equilibrium. The load was then reduced to 100mm/s and then 50 mm/s. Speeds were repeated 2X per load. B) The dynamic equilibrium is noted in dark blue circles for each sliding speed.

Because the rehydration flow equates to exudative flow, the rehydration rate at equilibrium was considered the strain matched exudation rate from the exudation curve (see Figure 4-2b for tribological rehydration rate analysis). Total deformation, fluid deformation, and rehydration rate were fit to separate linear mixed effects models with load and sliding speed as independent variables, and sample as the random variable ($\alpha = 0.05$ for significance).

5.2.4 Measuring the Fluid Load Support at Dynamic Equilibrium

Eight ($n= 8$) osteochondral cores were used to quantify FLS at dynamic equilibrium for 1,2,3,4 and 5 N loads for a single physiological sliding speed. Samples submerged in DI water and 10 ml of India Ink were statically loaded at a single load for 5 minutes to exude fluid (Figure 5-3A). Loaded samples were then slid at 100 mm/s to recover to sliding equilibrium (Figure 5-3B). Holding the equilibrium deformation constant, the sliding speed was set to 0 mm/s, while allowing the force on the cartilage to subside to an equilibrium value (Figure 5-3C). A camera captured contact area images at sliding-equilibrium contact pressure (σ) and force-relaxation-equilibrium contact pressure (σ_S). See Figure B. 6 in the Appendix for calculations of the contact area during sliding experiments. Per biphasic theory, the FLS was then calculated with the following equation:

$$FLS = \frac{P_{Fluid}}{\sigma} = \frac{\sigma - \sigma_S}{\sigma} \quad (22)$$

This process was repeated for each load for each sample. A linear mixed effects model was fit to FLS as a function of load to compare load dependency among samples ($\alpha = 0.05$ for significance).

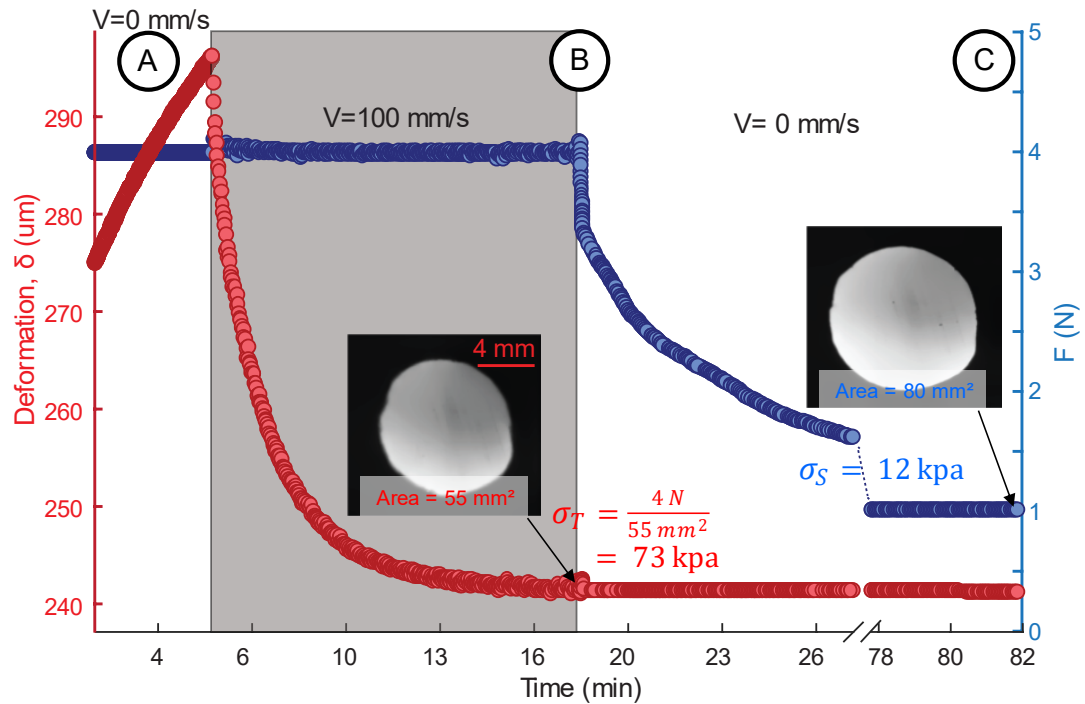


Figure 5-3: A representative test (4N) for cartilage FLS measurements. The force is maintained in part (A) to exude fluid. Cartilage was then slid to recover fluid and achieve equilibrium in part (B). Afterward, sliding ceased and deformation was held constant until force relaxation equilibrium (C). The FLS for cartilage was calculated at dynamic equilibrium deformation (B).

5.2.5 Measuring the Dynamic Equilibrium at Sub-physiological Sliding Speeds

To determine if hydrodynamics contributes to inflow at slower sliding speeds, dynamic equilibrium rehydration rates were computed for speeds under 50 mm/s for n=2 separate osteochondral samples. Loads of 3 and 5 N were used for this test.

Samples were statically loaded for 90 minutes to develop the exudation rate profile needed during tribological rehydration. After the static load, samples were then slid at

200 mm/s at the same load until dynamic equilibrium. After reaching equilibrium, samples were then slid at progressively smaller velocities until equilibrium (100, 50, 30, 25, 22, 20, 18, 16, 14, 12, 10, 8, and 6 mm/s). To minimize testing time, maximum of 30 minutes of sliding per speed was allowed.⁹ If equilibrium was not reached within 30 minutes, the data were fit to the first-order function $\delta(t) = A + Be^{-Ct}$ and the dynamic equilibrium deformation is, by definition, equal to A.

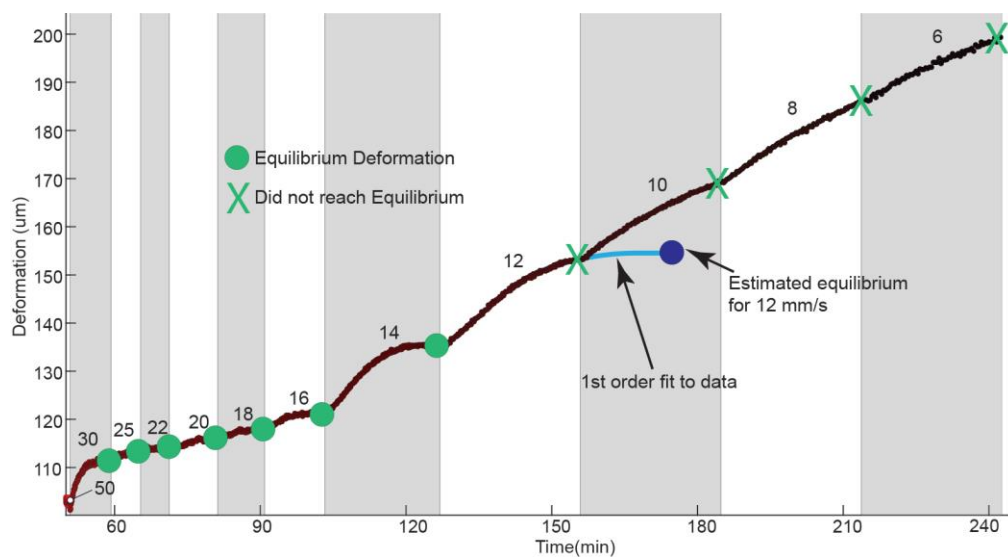


Figure 5-4: A representative test of slow speed testing for a single load. For this test, speeds 30 to 14 mm/s reached equilibrium within 30 minutes. The first order equation was applied for speeds 12 to 6 mm/s to estimate the dynamic equilibrium values.

⁹ Because of the slower rotational rate of the spindle, the lower sliding velocities would take longer to rehydrate to equilibrium and may not have reached an equilibrium value within a 30 minute sliding timeframe. This was to minimize wear from the increasing friction.

5.3 Results

5.3.1 Dynamic Equilibrium with varying Sliding Speeds and Load

The dynamic equilibrium deformation as a function of load and sliding speed for a representative cartilage sample is displayed in Figure 5-5. For each combination of load and speed, measures of the dynamic equilibrium were consistent, as standard deviations did not exceed 3% of mean values. This indicates that establishing the dynamic equilibrium is repeatable, regardless of the previous testing conditions.

The linear mixed model for total deformation ($R^2=0.91$) indicated sliding speed was not related to the dynamic equilibrium deformation ($p=0.80$), but that load was positively related to the dynamic equilibrium deformation ($p<0.001$). The model including dynamic equilibrium fluid deformation ($R^2=0.91$) indicated similar findings— it was positively related to input load ($p<0.001$), but was almost significant with sliding speed ($p = 0.056$). The linear model including rehydration rates ($R^2=0.70$) indicated the sliding speed significantly increased rehydration rate at equilibrium ($p<0.001$) while contact load significantly decreased the rehydration rate ($p<0.001$). The data for a representative sample is shown in Figure 5-6. As shown, the dynamic equilibrium is solely dependent on the normal force (Figure 5-6A), while the hydrodynamic effect is more apparent with decreased fluid equilibrium values and increased rehydration rates (Figure 5-6 B and C, respectively).

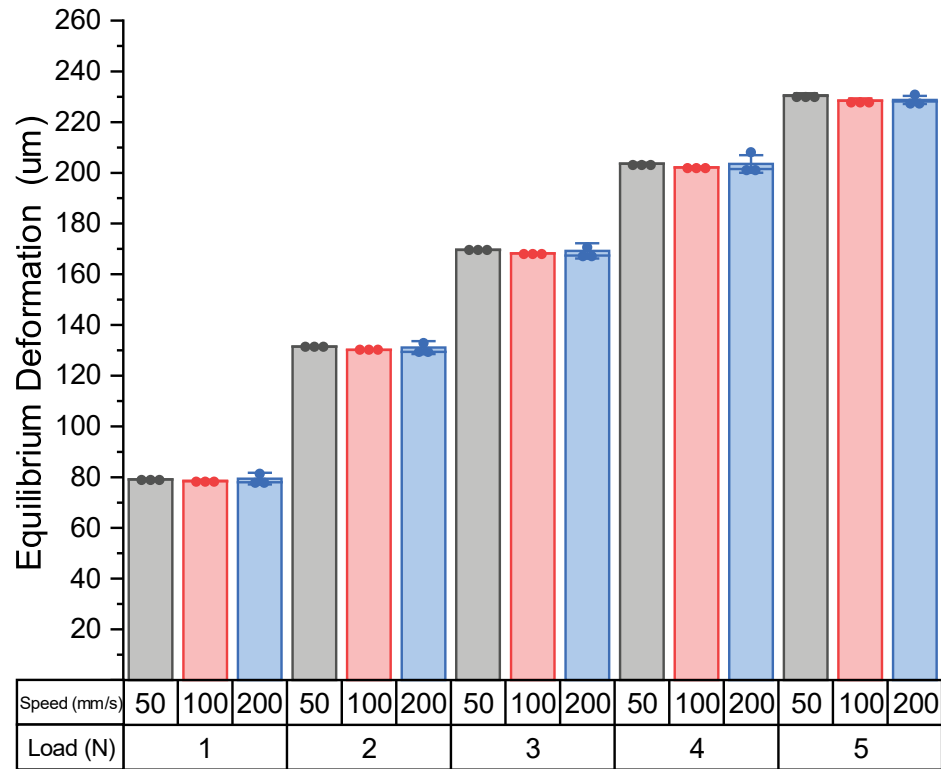


Figure 5-5 The dynamic equilibrium deformation as a function of load and sliding speed is shown for a single representative sample. The 3 data points displayed in each bar indicate the repeatability of the dynamic equilibrium to conditions. Error bars, albeit small, indicate 1 standard deviation.

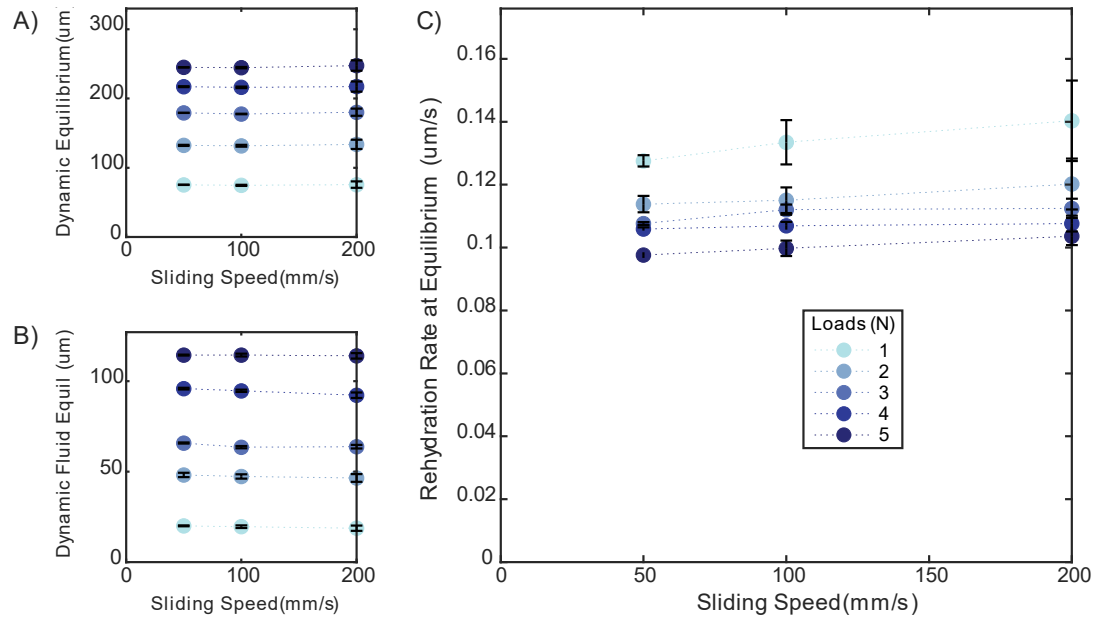


Figure 5-6: Representative sample data for A) the dynamic equilibrium, B) dynamic fluid equilibrium, and C) the rehydration rate at the dynamic equilibrium. Error bars shown indicate ± 1 standard deviation.

5.3.2 Fluid Load Support at Dynamic Equilibrium

The FLS vs. load at the dynamic equilibrium is shown in Figure 5-7 for all samples. The mean FLS ranged from 0.84 to 0.62 analyzed on a per sample basis. The linear mixed model demonstrates that force does not significantly affect FLS ($p=0.62$) among all samples analyzed.

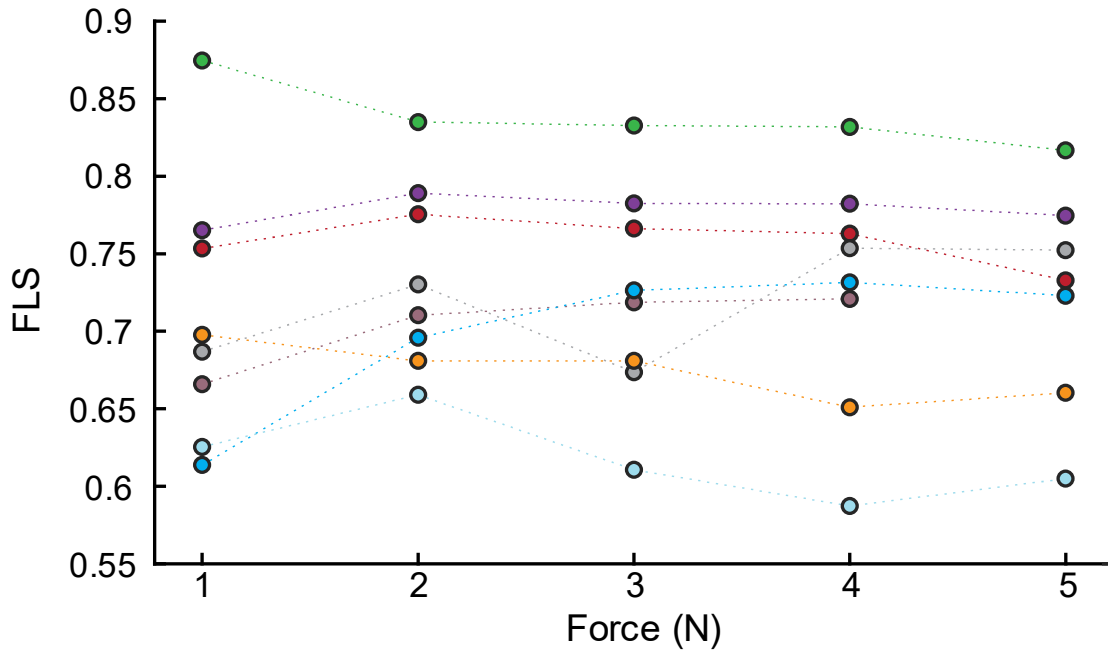


Figure 5-7: The FLS as a function of load. Different colors represent unique samples. The circles represent experimental data.

5.3.3 Dynamic Equilibrium at Low Sliding Speeds

The dynamic equilibrium rehydration rate as a function of load and sliding speed for two representative cartilage samples are displayed in Figure 5-8. At lower speeds (6-20 mm/s), rehydration rate increased with a very shallow slope. From speeds ranging from 20 to 100 mm/s, the rehydration rate rapidly increased 10 to 20-fold. The effect of increasing velocity on rehydration rate visually reaches an asymptote above 100 mm/s of sliding speed. While rehydration rates did increase above 100 mm/s as seen in section 5.3.1, the relative increase in rehydration rates were insignificant as compared to the increases from 20 to 100 mm/s. The implications of this behavior will be discussed.

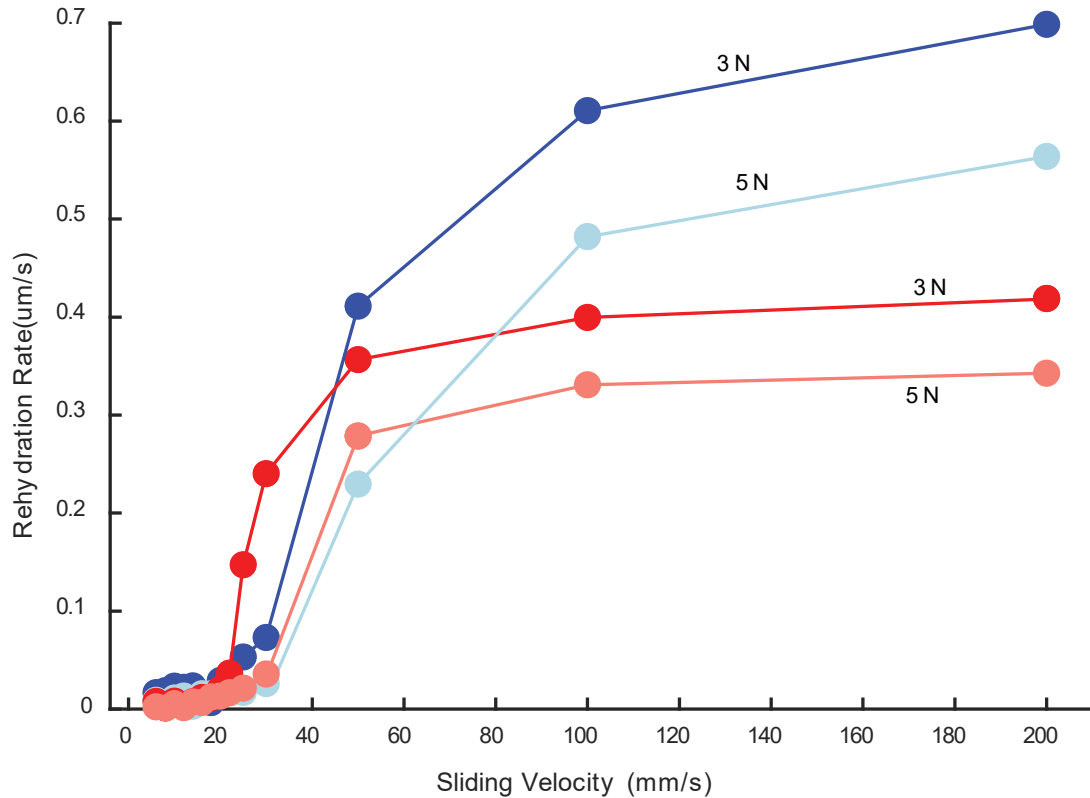


Figure 5-8: Rehydration rate vs sliding speed at 3N and 5N loads. The two base colors (red and blue) represent the two different samples. The rehydration <0.05 from 0-20 mm/s and rapidly increases from 20-100 mm/s. Each sample tends to have a different characteristic curve.

5.4 Discussion

This study uncovered the effects of physiological sliding speeds and loads that drive the deformations, rehydration, and fluid load support during tribological rehydration. As hypothesized, our results show that increasing load leads to increased dynamic equilibrium strain and decreased tribological rehydration rates. Increased sliding speeds had very little effect on the dynamic equilibrium strain or the tribological rehydration rate under a physiologically relevant range of speeds from 50 to 200 mm/s.

Interestingly, the observed effects of load and sliding speed on the tribological rehydration of cartilage appear to conflict with our previous theoretical predictions that tribological rehydration is proportional to speed and independent of load [247]. However, that study by Putignano et al. considered only the hydrodynamic rehydration upon start of sliding, after the interface had been depressurized from static loading. Because cartilage is dehydrated and depressurized, any entrained fluid entering the interface will be preferentially driven into the tissue. Thus, it is effectively a prediction of entrainment into the contact interface rather than a prediction of cartilage absorption [247]. In this case, the interface is pressurized at the dynamic equilibrium and the driving force for fluid absorption is radically diminished compared to static equilibrium. Thus, in the case of high fluid load support, the amount of fluid absorbed by the cartilage (tribological rehydration rate) is much less than the amount of fluid entrained into the contact (refer to Figure 5-9 for descriptive illustration). At high-speed sliding dynamic equilibrium, we presume that the flow supplied to the interface is shared between flow *into* the tissue and flow *through* the interface.

With this in mind, the two important questions to ask are: What regulates the rehydration rate and how does it change at higher loads and lower speeds? The key finding is our observation that fluid load support is independent of load. Increasing load by 5x increased the dynamic equilibrium strain proportionally, but it had no effect on fluid load support, which remained constant for each sample. In other words, when load increased, the stress supported by the matrix increased but the fluid pressure increased by the same amount. Thus, cartilage behaves such that strain and friction are proportional to load as would be expected based on Hooke's and Amonton's laws, respectively. It has been well-demonstrated that fluid load support is

fixed at some value that depends on the material properties of the sample during indentation, instantaneous loading, and sliding in the migrating contact area. This study demonstrates the same self-regulation effect on fluid load support in the convergent stationary contact area.

Thus, the generalized takeaway is that cartilage regulates fluid load support when sliding supplies the interface with sufficient fluid. Naturally, the dynamic equilibrium strain will increase proportionally with load as observed. This observation also provides an expectation for the effect of load on the tribological rehydration rate, which is equal to the exudation rate at the dynamic equilibrium strain. We can anticipate the effect of load on the tribological rehydration rate by considering biphasic theory. The exudation rate at a given strain increases with load, but the relevant strain (dynamic equilibrium) also increases. Thus, according to theory, the tribological rehydration rate is insensitive to load (other variables being equal) because the effect of increased load on the strain rate is offset by the competing effect of strain. The fact that we observe some effect of load can be explained by changes in other variables such as changes in interface permeability.

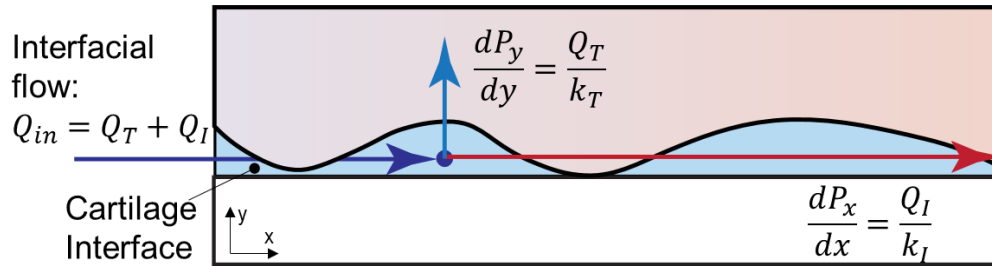


Figure 5-9: Illustration of the rehydration hypothesis at the dynamic equilibrium. After opening of the wedge, the flow into the cartilage interface (Q_{in}) is the sum of the flow into the tissue (Q_T) and through the interface (Q_I). P_y equals the sum of interstitial pressure and osmotic pressure. P_x is the lubricating pressure hydrodynamic pressure. After static loading, initial sliding will cause $\frac{dP_y}{dy} \gg \frac{dP_x}{dx}$, since interstitial pressures have dropped, and flow will preferentially drive into the tissue. At high-speed sliding, interstitial fluid pressure is restored and $\frac{dP_y}{dy} \approx \frac{dP_x}{dx}$, such that the flow into the tissue (Q_T) will now compete with flow through the interface (Q_I). An increase in sliding speed will increase $\frac{dP_y}{dy}$, but also increase $\frac{dP_x}{dx}$ and decrease k_T [185] such that hydrodynamic inflow is limited.

Lastly, the investigation into rehydration rates for a range of high and low sliding speeds (Figure 5-8) provides further insight into the hydrodynamic triggering mechanism of tribological rehydration. As expected, the rehydration rate is capped at high physiological sliding speeds and decreases with contact load. However, the rapid decrease in rehydration rates below ~ 50 mm/s demonstrates that hydrodynamic rehydration effects are rapidly blunted. From ~ 20 -6 mm/s, rehydration rates still scale with sliding speed, but are inconsequential as compared to physiological sliding speeds. Therefore, the rehydration characteristic of the tissue can be thought of three distinct behaviors, as illustrated in Figure 5-10. From 0 to 20 mm/s, hydrodynamics likely pressurizes fluid at the wedge, which is indicative of the non-trivial increase in rehydration rate with increased sliding speeds (see illustration in Figure 5-10 A). This

agrees with previous experimental investigations [117], [263]. Beyond 20 mm/s, elasto-hydrodynamics (EHD), ‘peels’ open the interface through fluid pressurization, and creates a preferential channel for fluid to enter the interface [116], [265], [266]. This pressurized fluid now can directly rehydrate the contact interface, instead of only the convergent wedge, leading to a >10X increase in rehydration rate (compare 20 to 50 mm/s in Figure 5-10 B). This “transition” speed to higher rehydration rates is consistent with previous data [117], [263]. In region B of Figure 5-10, increasing sliding speed will increase hydrodynamic pressure to push more fluid into the interface. Within this region, the fluid is still preferentially absorbed by the tissue.

Around 50 mm/s, the rehydration rate of the system begins to saturate, and some of the interfacial fluid is not absorbed and passes through the contact, as shown in Figure 5-10 C. The transition to rehydration saturation seems to be, pictorially, determined by sample uniqueness as the “red” sample in Figure 5-8 reached rehydration saturation faster than the “blue” sample. While previous studies demonstrated that higher loads require higher transition speeds [117], Figure 5-8 implies that cartilage characteristics, like radius of curvature and intrinsic permeability, also determine the rehydration saturation. Future studies will investigate the effect of geometrical parameters and material properties on the saturation speed. Nevertheless, these results indicate that once the contact interface has been opened with hydrodynamic pressure, exposure of the contact area overwhelmingly contributes to the rehydration rates.

Current cartilage models of hydrodynamic rehydration rely on a large ‘rehydration front’ at the wedge contact, with limited fluid flux in the contact area [248], [254], [255]; this departs from the current experimental findings. De Boer et al.

demonstrated that with a developed fluid film, fluid could enter the center of contact, but would also require an equivalent exudation at the trailing edge of contact [255]. An increase in contact load in their model decreased the fluid gap height, but increased the fluid inflow by ~10x due to the increase in film pressure; again, this contradicts the current experimental findings. Putignano et al. included the roughness of cartilage in their hydrodynamic model to allow for rehydration flux in the contact interface, but was extremely limited as compared to the convergent wedge rehydration rate [248].

Beyond the current experimental results, two other studies suggest that the contact interface is the main contributor to tribological rehydration: 1) Low friction coefficients are established much faster than the dynamic equilibrium deformation, indicating that lubricating fluid preferential rehydrates the contact surface prior the deep tissue [116]. And 2) fluorescence studies demonstrated that more solutes accumulate in the contact area as compared to the convergent wedge, indicating a preferential flow into the interface [260]. The current results and previous studies warrant a numerical investigation that focuses on high hydration rates from interfacial flow [129], [200].

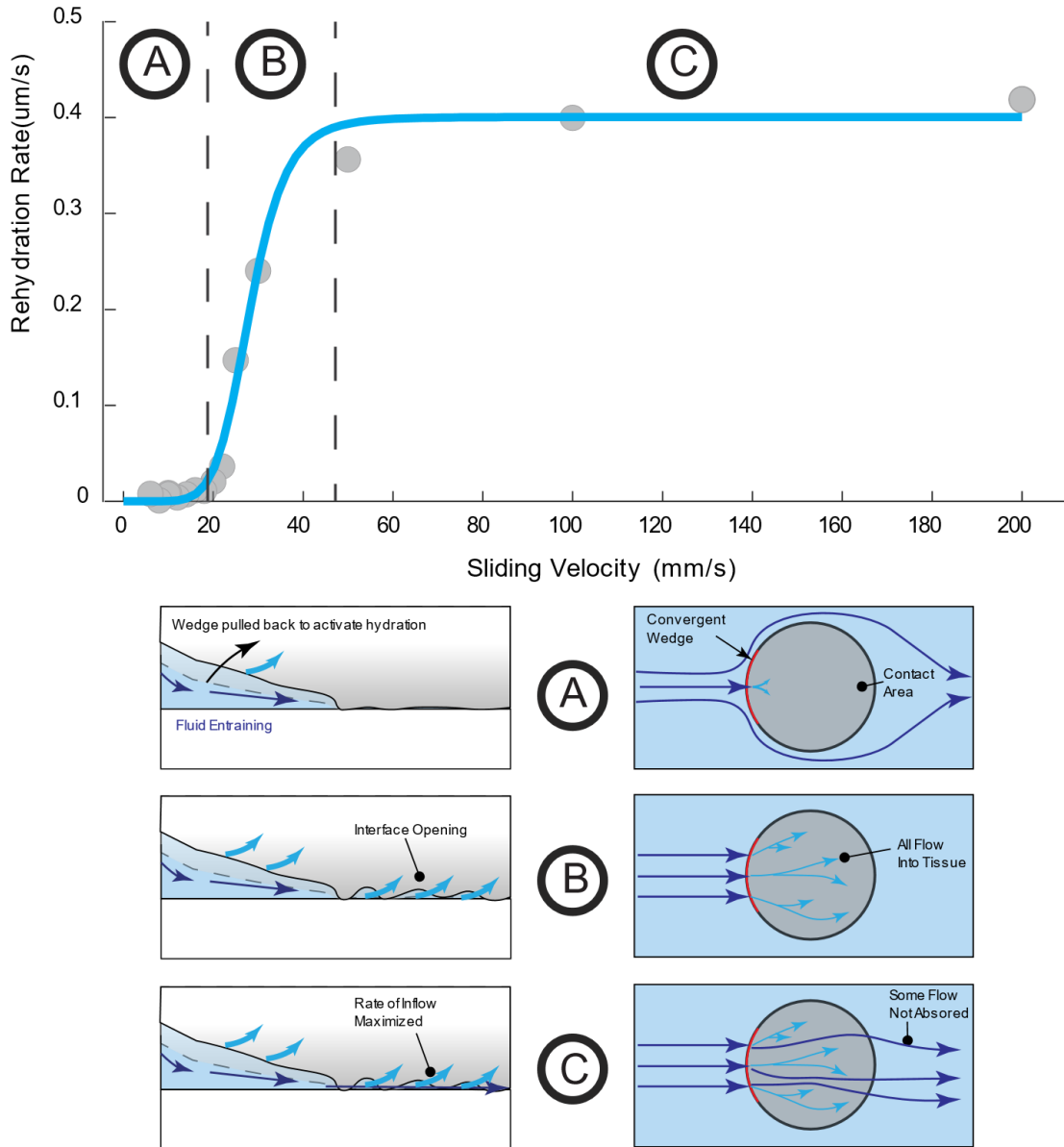


Figure 5-10: Thought model of tribological rehydration. A) The interface is effectively impermeable when speed is slow, an rehydration is insignificant B)The interface becomes permeable. Hydrodynamic pressures at higher speeds begin to push fluid into interfacial gaps, which expand to increase interface permeability. The rehydration rate increases with the rate of flow into the interface. C) The rehydration rate saturates due to tissue absorption limits or because the inflow rate is limited by the tissues ability to absorb fluid.

Lastly, these results offer important insights into the rehydration of synovial joints like the hip and knee. That is, we observed that the stationary contact area serves as an important source of rehydration at the joint surface with preferred rehydration in the interface, as depicted in Figure 5-11. From a physiological standpoint, it is unsurprising that cartilage preferentially rehydrates the surface given that lubrication is paramount to its function [267]. The stationary contact area mechanism/paradigm likely works in concert with the migrating contact area paradigm, which intermittently exposes cartilage contacts for rehydration [20], [83], [105]. Together, these paradigms allow cartilage to restore interstitial fluid to provide a lubricative and pressurization reservoir [195] for future static loading.

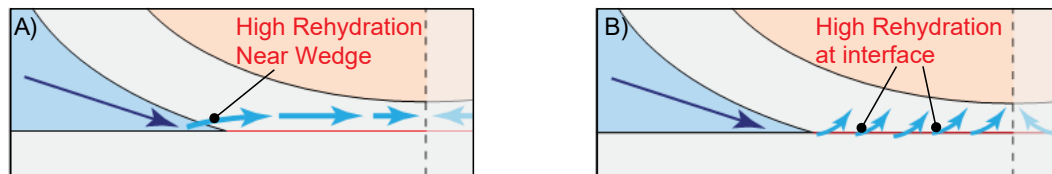


Figure 5-11: A) Current models predict a large rehydration front near the convergent wedge. B) The current results demonstrate that the rehydration occurs directly at the interface at physiological sliding speeds

Further, our results suggest that cartilage can maintain fluid load support at elevated loads in the convergent stationary contact area given a sufficient supply of interfacial fluid. Thus, slight increases in the dynamic equilibrium strain responses measured in vivo [37], [38], [102], [106] may not defeat interstitial fluid pressurization. Nonetheless, sustained fluid load support does not imply favorable conditions for long-term survivability. Even if cartilage can maintain FLS, increased

loads in vivo cause increased shear stresses, contact stresses [1], [62], [132]–[134], [268]–[270] and tissue strains [9], [107], [271], [272], each of which is well-correlated with increased OA risk due to some combination of structural degradation of the tissue[273]–[275], cellular apoptosis/necrosis[9], [276], and catabolic inflammation responses [23], [277].

Several limitations of the current study are worth noting, specifically our limited ability to simulate in vivo mechanics of the joint. The limited load capabilities of the experiment yielded contact pressures ranging 0.05-0.30 MPa, which is substantially lower than contact pressures measured in vivo [1]. Hydrodynamics may not be able to ‘peel’ the interface open with in vivo stress and prohibit interfacial rehydration. While peak contact stresses range from 1-8 MPa depending on the joint [1], the contact stresses during actual sliding (i.e. swing phase) are much less than peak contact stresses [161], [179]. For instance, the measured contact stress during swing phase is approximated 0.70 MPa for the tibiofemoral joint. While our experimental contact stresses reached an average peak pressure of 0.30 MPa at a 5N load¹⁰, the doubling in contact stress may not defeat tribological rehydration. Future studies will need to increase the stress of the experimental setup to determine if the dynamic equilibrium can be established through tribological rehydration, and ultimately sustain FLS at physiological joint contact stresses. Additionally, data was collected on a unidirectional pin-on-disc tribometer, while the true nature of the joint is reciprocal. Regardless of the direction of flow, the in vivo sliding speeds incurring hydrodynamic pressures require to open the interface for inflow. However,

¹⁰ Assuming a Herztian contact

tribological rehydration is likely only available to the joint during the swing phase of both the hip and the tibiofemoral joint, as those are associated with the highest joint sliding speeds [244].

In closing, this investigation into the dynamic equilibrium of cartilage indicates that 1) increases in load decreased the rehydration rate likely because the effective permeability of the system reduced under higher fluid pressure, 2) hydrodynamics seems to exist as the primary driver to tribological rehydration, but may be “capped” at higher speeds as the fluid passes through the interface, and 3) the FLS remains relatively unchanged with significant increases in load, indicating that cartilage exhibits a “pressure regulating” system to maintain its function. These results indicate that the cartilage interface plays a much larger role in rehydration than previously modeled, especially for a mixed mode lubrication setting.

Chapter 6

DISCUSSION AND CLOSING REMARKS

6.1 Summary of Aims

Aim 1 revealed that contact stress is highly varied, even in a simplified test bed (i.e. cartilage-on-flat with an instantaneous load), which can be attributed to highly variable material properties. Changes in modulus, specifically, can substantially affect the contact stress of cartilage and, thus, should be accurately defined based on its loading environment. For the cartilage-on-flat testbed, the proposed Hertzian model can well-estimate (~13% error) contact stresses **if** the contact modulus is well defined. Because of the simplicity of the model and the low error rate, the model can be easily implemented in benchtop testing of cartilage explants to predict contact stress with confidence.

With Aim 2, we developed an experimentally derived analytical model to predict exudation characteristics of cartilage based on the inclusion of the interface. While previous experimentalists and models debated the role of the interface, our experiments demonstrate that fluid pressurization in the contact gap keeps the gap open for an alternate exudation path, reducing the consolidation time constants of cartilage. While this equates to a quicker subsiding of FLS, the “open” interface allows for consistent fluid flow to minimize friction. Future research should ensure the interface is properly measured and modeled to appropriately predict exudation rates.

While Aim 2 explored the consequence of the interface on exudation of cartilage, **Aim 3** demonstrated that activity mediated rehydration pumps fluid into the tissue much faster than a strict unloading of the tissue, due to the compromised interface. While unloading unloads asperities, osmotic swelling is not able to adequately open the interface, resulting in slow rehydration rates. The variable permeability interface helps cartilage quickly exude from the tissue and rehydrate the during movement, but at a cost of functionally closing of the interface when cartilage is unloaded and needs to recover fluid. Most importantly, this study shows that joint articulation reverses fluid loss following static loading at > 10-fold the preceding exudation rate. These competitive recovery rates suggest that joint space and function may be best maintained throughout an otherwise sedentary day using brief but regular physical activity. Future studies should expand to joint level or person level to determine what the relative contributions of activity-based rehydration mechanisms (free swelling vs tribological rehydration) and how they may be defeated in high-risk populations for OA.

Lastly in Aim 4, we uncovered the physiological parameters that drive asymptotic equilibrium that is depicted in in-vivo strain measurement[36], [37]. As expected, the rehydration rate of cartilage is diminished as loads are increase, but unexpectedly, did not increase at higher sliding speeds. We propose that the rehydration rate is limited at higher speeds due to preferential flow through the interface vs into the tissue at dynamic equilibrium. Once the “reservoir” fluid has been restored in the tissue, any remaining flow can aid in surface lubrication. Furthermore, the loss in rehydration rates did not affect the protective fluid pressurization of the tissue, but in fact increased pressurization to maintain FLS.

Again, the variable permeability of the tissue and interface seems to be a design feature to maintain the pressure in the tissue. Because this study was completed at sub-physiological loads, we intend to complete future studies to determine if a critical physiological joint contact stresses shuts of hydrodynamics effects of sliding, and thus destroying interfacial rehydration.

Collectively, these aims demonstrate that the innate material properties of cartilage may not fully explain the complex mechanics of this system, specifically because the interface may play a much more active role than originally thought. During static loading, the permeable cartilage interface results in a much faster exudation time as compared to an impermeable interface, but this may be advantageous for two reasons: 1) it ensures that waste products across the entire cartilage surface can be exchanged with the surrounding synovium, and 2) it provides better lubrication through the “weeping” lubrication paradigm. However, this faster exudation time also means that the function of cartilage will deteriorate faster.

During movement, this same permeable interface promotes fluid flow through and into the tissue. This allows cartilage to rehydrate more quickly during movement (i.e., faster than a passive unload), and in turn, restores lubricative function and counteracts potentially damaging shear forces. In sum, the permeable interface plays a more integral role in fluid exchange than was originally thought. All of the studies in this dissertation did not decouple interfacial flow and bulk tissue flow in terms of gross fluid rehydration/exudation of cartilage and assumed that the permeability of the interface was the sole contributor to faster exudation and rehydration rates. However, the anisotropic structure of cartilage, particularly the high permeability, yet soft, superficial layer [3], [211], [229]–[234], may be a significant contributor to fluid

exchange. To determine the true effect of the interface, the superficial zone may need to be included as a separate layer in models or removed for experimental comparison. Regardless, this dissertation indicates that interfacial flow must be considered in any future studies that examine the fluid loss/gain, function, and longevity of articular cartilage [200].

6.2 How can this dissertation inform activity recommendations?

Recently, Andriacchi et al. proposed that healthy cartilage is a result of “play” between the biology, structure, and mechanics of articular joints and modulated by the “activity” the joint experiences (see Figure 6-1 A for illustration)[278], [279]. Each of these systems must be kept in a normal range to ensure cartilage can maintain its healthy state. Once one of these systems is exposed to an abnormal input outside the normal range, disease initiation can occur. This potentially diseased state then can adversely affect the other two systems, causing a negative feedback loop that further accelerates OA development (see Figure 6-1 B). While biology, structure, and/or mechanics systems may be difficult or even impossible to change, **modulation of activity may be more feasible.**

Outcomes from this dissertation can guide studies aiming to determine the effects of activity on cartilage health. Furthermore, we can start to address the issue that “today, [experimentally demonstrated] health advice on how to maintain healthy synovial joints is notably absent”[195]. We still have limited understanding how cartilage can maintain its daily functionality and, therefore, clinicians have difficulty prescribing adequate activity protocols to promote cartilage health. Combating OA with activity as a means of therapy is still far from understood and implemented; standard operating procedures on activity dosing are still in development [280].

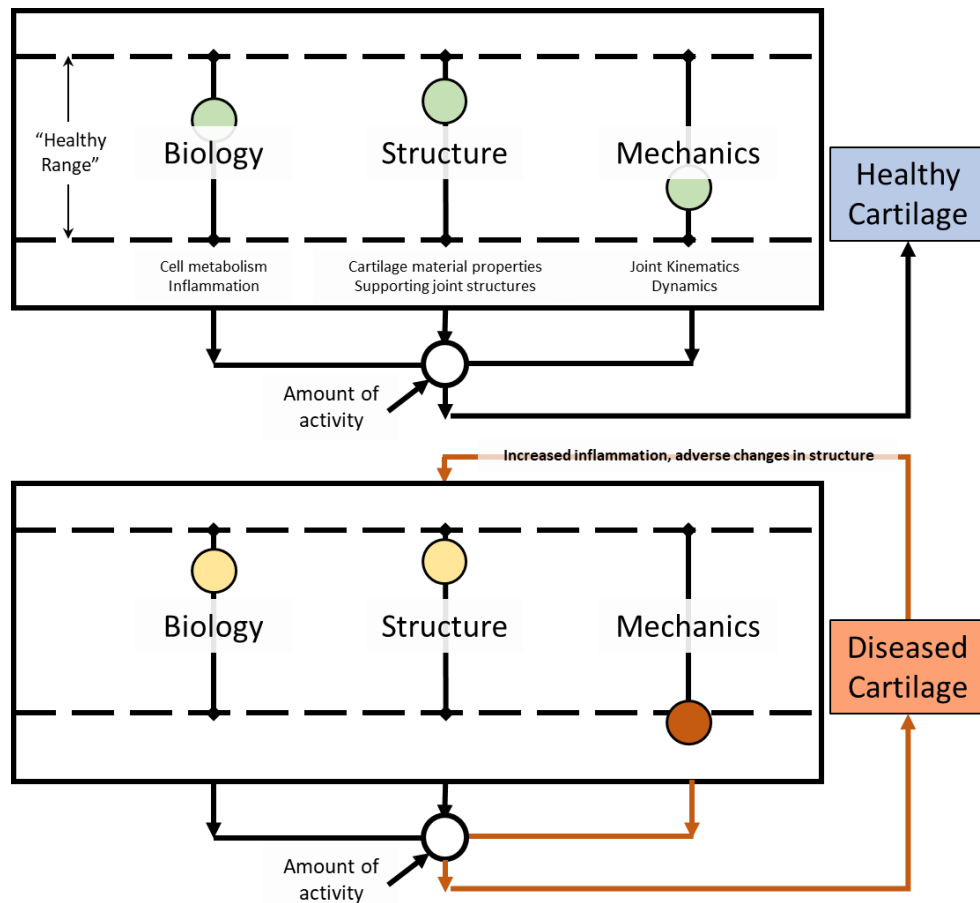


Figure 6-1: “Systems approach” to understanding OA initiation and development adapted from Andriacci et al. [278], [279]. Considering the factors of biology, structure, and mechanics, cartilage undergoes a specified amount of activity, which can lead to a healthy environment or disease cartilage. If cartilage cannot withstand activity, it is worsened through a feedback loop until end-stage OA.

More recent work has demonstrated that “OA patient-specific risks will be found if direct metrics for the tissue mechanical environmental stressors, such as [tissue] consolidation and fluid exudation, rather than indirect measures like BMI and

physical activity, are used” [182]. Because this dissertation demonstrates that the interface can quickly dehydrate and rehydrate the tissue based on timescales ranging from minutes to hours, the functionality and health of your cartilage likely depend on activity behavior reflective of an hourly timescale rather than just a daily or weekly timescale. Because activity promotes cartilage hydration and fluid pressurization, I propose that habitual activity throughout the day drives the health of cartilage (See Figure 6-2). This dissertation has only uncovered the relationship between tissue mechanics, fluid exchange, and cartilage functionality, and must be translated to more clinically relevant settings, such as the joint level or person level. It is important that future researchers work towards understanding fluid exchange within the context of whole joints so that clinicians can ultimately optimize cartilage function and engage the population in long-term OA prevention [65].

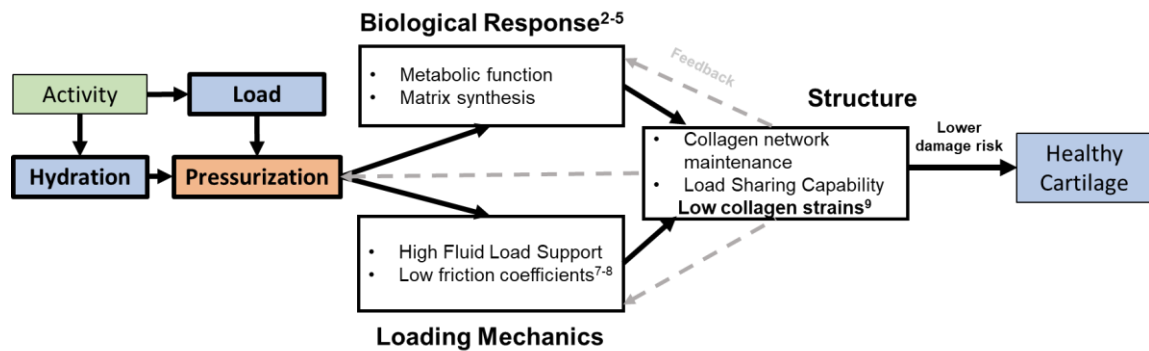


Figure 6-2: A modified “systems approach” to account for the role of activity and hydration in the responses of each system and ultimately cartilage health.

REFERENCES

- [1] R. A. Brand, "JOINT CONTACT STRESS : A REASONABLE SURROGATE FOR BIOLOGICAL PROCESSES ?," *Iowa Orthop J*, vol. 25, pp. 82–94, 2005.
- [2] J. T. Evans, R. W. Walker, J. P. Evans, A. W. Blom, A. Sayers, and M. R. Whitehouse, "How long does a knee replacement last? A systematic review and meta-analysis of case series and national registry reports with more than 15 years of follow-up," *Lancet*, vol. 393, no. 10172, pp. 655–663, 2019, doi: 10.1016/s0140-6736(18)32531-5.
- [3] A. J. Sophia Fox, A. Bedi, and S. A. Rodeo, "The basic science of articular cartilage: Structure, composition, and function," *Sports Health*, vol. 1, no. 6, pp. 461–468, Nov. 2009, doi: 10.1177/1941738109350438.
- [4] R. Shirazi and A. Shirazi-Adl, "Deep vertical collagen fibrils play a significant role in mechanics of articular cartilage," *J. Orthop. Res.*, vol. 26, no. 5, pp. 608–615, 2008, doi: 10.1002/jor.20537.
- [5] J. A. Buckwalter and H. J. Mankin, "Articular cartilage: tissue design and chondrocyte-matrix interactions," *Instr. Course Lect.*, vol. 47, pp. 477–486, 1998, [Online]. Available: <http://europepmc.org/abstract/MED/9571449>.
- [6] B. D. Elder and K. A. Athanasiou, "Hydrostatic Pressure in Articular Cartilage Tissue Engineering: From Chondrocytes to Tissue Regeneration," *Tissue Eng. Part B Rev.*, vol. 15, no. 1, pp. 43–53, 2009, doi: 10.1089/ten.teb.2008.0435.
- [7] D. L. Bader, D. M. Salter, and T. T. Chowdhury, "Biomechanical Influence of Cartilage Homeostasis in Health and Disease," *Arthritis*, vol. 2011, pp. 1–16, 2011, doi: 10.1155/2011/979032.
- [8] C. Chen, D. T. Tambe, L. Deng, and L. Yang, "Biomechanical properties and mechanobiology of the articular chondrocyte," *Am. J. Physiol. Physiol.*, vol. 305, no. 12, pp. C1202–C1208, 2013, doi: 10.1152/ajpcell.00242.2013.
- [9] J. Sanchez-Adams, H. A. Leddy, A. L. McNulty, C. J. O’Conor, and F. Guilak, "The Mechanobiology of Articular Cartilage: Bearing the Burden of Osteoarthritis," *Current Rheumatology Reports*, vol. 16, no. 10. 2014, doi: 10.1007/s11926-014-0451-6.

- [10] M. Maldonado and J. Nam, "The role of changes in extracellular matrix of cartilage in the presence of inflammation on the pathology of osteoarthritis," *Biomed Res. Int.*, vol. 2013, 2013, doi: 10.1155/2013/284873.
- [11] G. A. Ateshian, W. M. Lai, W. B. Zhu, and V. C. Mow, "An asymptotic solution for the contact of two biphasic cartilage layers," *J. Biomech.*, vol. 27, no. 11, pp. 1347–1360, 1994, doi: 10.1016/0021-9290(94)90044-2.
- [12] G. A. Ateshian and H. Wang, "A theoretical solution for the frictionless rolling contact of cylindrical biphasic articular cartilage layers," *J. Biomech.*, vol. 28, no. 11, pp. 1341–1355, 1995, doi: 10.1016/0021-9290(95)00008-6.
- [13] A. Jackson and W. Gu, "Transport Properties of Cartilaginous Tissues," *Curr. Rheumatol. Rev.*, vol. 5, no. 1, pp. 40–50, 2009, doi: 10.2174/157339709787315320.
- [14] Y. Wang, L. Wei, L. Zeng, D. He, and X. Wei, "Nutrition and degeneration of articular cartilage," *Knee Surgery, Sport. Traumatol. Arthrosc.*, vol. 21, no. 8, pp. 1751–1762, Aug. 2013, doi: 10.1007/s00167-012-1977-7.
- [15] R. Kelkar and G. A. Ateshian, "Contact creep of biphasic cartilage layers," *J. Appl. Mech. Trans. ASME*, vol. 66, no. 1, pp. 137–145, 1999, doi: 10.1115/1.2789140.
- [16] S. S. Pawaskar, Z. M. Jin, and J. Fisher, "Modelling of fluid support inside articular cartilage during sliding," 2007, doi: 10.1243/13506501JET241.
- [17] S. Park, R. Krishnan, S. B. Nicoll, and G. A. Ateshian, "Cartilage interstitial fluid load support in unconfined compression," *J. Biomech.*, vol. 36, no. 12, pp. 1785–1796, 2003, doi: 10.1016/S0021-9290(03)00231-8.
- [18] E. D. Bonnevie, V. J. Baro, L. Wang, and D. L. Burriss, "Fluid load support during localized indentation of cartilage with a spherical probe," *J. Biomech.*, vol. 45, no. 6, pp. 1036–1041, 2012, doi: 10.1016/j.jbiomech.2011.12.019.
- [19] R. Krishnan, M. Kopacz, and G. A. Ateshian, "Experimental verification of the role of interstitial fluid pressurization in cartilage lubrication," *J. Orthop. Res.*, vol. 22, no. 3, pp. 565–570, 2004, doi: 10.1016/j.orthres.2003.07.002.
- [20] M. Caligaris and G. A. Ateshian, "Effects of sustained interstitial fluid pressurization under migrating contact area, and boundary lubrication by synovial fluid, on cartilage friction," *Osteoarthr. Cartil.*, vol. 16, no. 10, pp. 1220–1227, 2008, doi: 10.1016/j.joca.2008.02.020.

- [21] G. A. Ateshian, "The role of interstitial fluid pressurization in articular cartilage lubrication," *J. Biomech.*, vol. 42, no. 9, pp. 1163–1176, 2009, doi: 10.1016/j.jbiomech.2009.04.040.
- [22] C. W. McCutchen, "The frictional properties of animal joints," *Wear*, vol. 5, pp. 1–17, 1962, doi: 10.1016/0043-1648(62)90176-X.
- [23] P. Wang, F. Zhu, N. H. Lee, and K. Konstantopoulos, "Shear-induced interleukin-6 synthesis in chondrocytes: Roles of E prostanoic acid (EP) 2 and EP3 in cAMP/protein kinase A- and PI3-K/Akt-dependent NF- κ B activation," *J. Biol. Chem.*, vol. 285, no. 32, pp. 24793–24804, 2010, doi: 10.1074/jbc.M110.110320.
- [24] D. Eyre, "Collagen of articular cartilage. - PubMed - NCBI," *Arthritis Res. Ther.*, vol. 4, no. 1, pp. 30–35, 2002, [Online]. Available: <https://www.ncbi.nlm.nih.gov/pubmed/11879535>.
- [25] T. A. Schmidt, N. S. Gastelum, Q. T. Nguyen, B. L. Schumacher, and R. L. Sah, "Boundary lubrication of articular cartilage: Role of synovial fluid constituents," *Arthritis Rheum.*, vol. 56, no. 3, pp. 882–891, 2007, doi: 10.1002/art.22446.
- [26] T. A. Schmidt and R. L. Sah, "Effect of synovial fluid on boundary lubrication of articular cartilage," *Osteoarthr. Cartil.*, vol. 15, no. 1, pp. 35–47, Jan. 2007, doi: 10.1016/j.joca.2006.06.005.
- [27] H. Forster and J. Fisher, "The influence of loading time and lubricant on the friction of articular cartilage," *Proc. Inst. Mech. Eng. Part H J. Eng. Med.*, vol. 210, no. 2, pp. 109–118, 1996, doi: 10.1243/pime_proc_1996_210_399_02.
- [28] A. C. Moore, J. L. Schrader, J. J. Ulvila, and D. L. Burris, "A review of methods to study hydration effects on cartilage friction," *Tribol. - Mater. Surfaces Interfaces*, vol. 5831, no. November, pp. 1–13, 2017, doi: 10.1080/17515831.2017.1397329.
- [29] M. Daniel, "Boundary cartilage lubrication: Review of current concepts," *Wiener Medizinische Wochenschrift*, vol. 164, no. 5–6, pp. 88–94, 2014, doi: 10.1007/s10354-013-0240-2.
- [30] J. Klein, "Hydration lubrication," *Friction*, vol. 1, no. 1, 2013, doi: 10.1007/s40544-013-0001-7.
- [31] S. Jahn, J. Seror, and J. Klein, "Lubrication of Articular Cartilage," *Annu. Rev. Biomed. Eng.*, vol. 18, 2016, doi: 10.1146/annurev-bioeng-081514-123305.

- [32] A. Wall and T. Board, “Biosynthetic response of cartilage explants to dynamic compression,” in *Classic Papers in Orthopaedics*, 2014, pp. 427–429.
- [33] J. C. Y. Hu and K. A. Athanasiou, “Structure and Function of Articular Cartilage - Handbook of Histology Methods for Bone and Cartilage,” *Handb. Histol. Methods Bone Cartil.*, pp. 73–95, 2003, [Online]. Available: https://doi.org/10.1007/978-1-59259-417-7_4.
- [34] B. T. Graham, A. C. Moore, D. L. Burriss, and C. Price, “Sliding enhances fluid and solute transport into buried articular cartilage contacts,” *Osteoarthr. Cartil.*, 2017, doi: 10.1016/j.joca.2017.08.014.
- [35] F. Eckstein, M. Tieschky, S. Faber, K. H. Englmeier, and M. Reiser, “Functional analysis of articular cartilage deformation, recovery, and fluid flow following dynamic exercise in vivo,” *Anat. Embryol. (Berl.)*, vol. 200, no. 4, pp. 419–424, 1999, doi: 10.1007/s004290050291.
- [36] D. J. Hunter and F. Eckstein, “Exercise and osteoarthritis,” *J. Anat.*, vol. 214, no. 2, pp. 197–207, 2009, doi: 10.1111/j.1469-7580.2008.01013.x.
- [37] C. S. Paranjape *et al.*, “A New Stress Test for Knee Joint Cartilage,” *Sci. Rep.*, vol. 9, no. 1, 2019, doi: 10.1038/s41598-018-38104-2.
- [38] A. T. Collins, M. Kulvaranon, C. E. Spritzer, A. L. McNulty, and L. E. DeFrate, “The Influence of Obesity and Meniscal Coverage on In Vivo Tibial Cartilage Thickness and Strain,” *Orthop. J. Sport. Med.*, vol. 8, no. 12, pp. 1–8, 2020, doi: 10.1177/2325967120964468.
- [39] S. Mizuno, T. Tateishi, T. Ushida, and J. Glowacki, “Hydrostatic fluid pressure enhances matrix synthesis and accumulation by bovine chondrocytes in three-dimensional culture,” *J. Cell. Physiol.*, vol. 193, no. 3, pp. 319–327, 2002, doi: 10.1002/jcp.10180.
- [40] Arthritis Foundation, “Osteoarthritis.” <https://www.arthritis.org/diseases/osteoarthritis>.
- [41] G. A. Hawker, “Osteoarthritis is a serious disease,” *Clinical and experimental rheumatology*, vol. 37, no. 5, pp. 3–6, 2019.
- [42] CDC, “Osteoarthritis (OA),” 2020. <https://www.cdc.gov/arthritis/basics/osteoarthritis.htm>.
- [43] C. Palazzo, C. Nguyen, M.-M. Lefevre-Colau, F. Rannou, and S. Poiraudau, “Risk factors and burden of osteoarthritis,” *Ann. Phys. Rehabil. Med.*, vol. 59,

pp. 134–138, 2016, doi: 10.1016/j.rehab.2016.01.006.

- [44] V. Silverwood, M. Blagojevic-Bucknall, C. Jinks, J. L. Jordan, J. Protheroe, and K. P. Jordan, “Current evidence on risk factors for knee osteoarthritis in older adults: A systematic review and meta-analysis,” *Osteoarthritis and Cartilage*, vol. 23, no. 4. 2015, doi: 10.1016/j.joca.2014.11.019.
- [45] I. J. Wallace *et al.*, “Knee osteoarthritis has doubled in prevalence since the mid-20th century,” *Proc. Natl. Acad. Sci. U. S. A.*, vol. 114, no. 35, pp. 9332–9336, 2017, doi: 10.1073/pnas.1703856114.
- [46] B. Antony, G. Jones, X. Jin, and C. Ding, “Do early life factors affect the development of knee osteoarthritis in later life: A narrative review,” *Arthritis Research and Therapy*, vol. 18, no. 1. Arthritis Research & Therapy, pp. 1–8, 2016, doi: 10.1186/s13075-016-1104-0.
- [47] J. B. Driban, J. M. Hootman, M. R. Sitler, K. P. Harris, and N. M. Cattano, “Is participation in certain sports associated with knee osteoarthritis? A systematic review,” *Journal of Athletic Training*, vol. 52, no. 6. pp. 497–506, 2017, doi: 10.4085/1062-6050-50.2.08.
- [48] G. H. Lo *et al.*, “Is There an Association Between a History of Running and Symptomatic Knee Osteoarthritis? A Cross-Sectional Study From the Osteoarthritis Initiative,” *Arthritis Care Res. (Hoboken)*, vol. 69, no. 2, pp. 183–191, 2017, doi: 10.1002/acr.22939.
- [49] E. Alentorn-Geli, K. Samuelsson, V. Musahl, C. L. Green, M. Bhandari, and J. Karlsson, “The Association of Recreational and Competitive Running With Hip and Knee Osteoarthritis: A Systematic Review and Meta-analysis,” *J. Orthop. Sport. Phys. Ther.*, vol. 47, no. 6, pp. 373–390, 2017, doi: 10.2519/jospt.2017.7137.
- [50] M. M. Lefèvre-Colau *et al.*, “Is physical activity, practiced as recommended for health benefit, a risk factor for osteoarthritis?,” *Annals of Physical and Rehabilitation Medicine*, vol. 59, no. 3. pp. 196–206, 2016, doi: 10.1016/j.rehab.2016.02.007.
- [51] M. Hurley *et al.*, “Exercise interventions and patient beliefs for people with hip, knee or hip and knee osteoarthritis: A mixed methods review,” *Cochrane Database of Systematic Reviews*, vol. 2018, no. 4. 2018, doi: 10.1002/14651858.CD010842.pub2.
- [52] G. Musumeci, F. C. Aiello, M. A. Szychlinska, M. Di Rosa, P. Castrogiovanni, and A. Mobasher, “Osteoarthritis in the XXIst century: Risk factors and

- behaviours that influence disease onset and progression,” *International Journal of Molecular Sciences*, vol. 16, no. 3. pp. 6093–6112, 2015, doi: 10.3390/ijms16036093.
- [53] S. G. Muthuri, D. F. McWilliams, M. Doherty, and W. Zhang, “History of knee injuries and knee osteoarthritis: A meta-analysis of observational studies,” *Osteoarthr. Cartil.*, vol. 19, no. 11, pp. 1286–1293, 2011, doi: 10.1016/j.joca.2011.07.015.
- [54] D. W. Dunstan, B. Howard, G. N. Healy, and N. Owen, “Too much sitting - A health hazard,” *Diabetes Res. Clin. Pract.*, vol. 97, no. 3, pp. 368–376, 2012, doi: 10.1016/j.diabres.2012.05.020.
- [55] J. A. Levine, S. K. Mccrady, S. Boyne, J. Smith, K. Cargill, and T. Forrester, “Non-exercise Physical Activity in Agricultural and Urban People,” vol. 48, no. August, pp. 2417–2427, 2011, doi: 10.1177/0042098010379273.
- [56] D. A. Raichlen *et al.*, “Sitting, squatting, and the evolutionary biology of human inactivity,” *Proc. Natl. Acad. Sci. U. S. A.*, vol. 117, no. 13, pp. 7115–7121, 2020, doi: 10.1073/pnas.1911868117.
- [57] R. C. Brownson, T. K. Boehmer, and D. A. Luke, “Declining rates of physical activity in the United States: What are the contributors?,” *Annual Review of Public Health*, vol. 26. pp. 421–443, 2005, doi: 10.1146/annurev.publhealth.26.021304.144437.
- [58] M. T. Hamilton, G. N. Healy, D. W. Dunstan, T. W. Zderic, and N. Owen, “Too little exercise and too much sitting: Inactivity physiology and the need for new recommendations on sedentary behavior,” *Curr. Cardiovasc. Risk Rep.*, vol. 2, no. 4, pp. 292–298, 2008, doi: 10.1007/s12170-008-0054-8.
- [59] K. E. Barbour *et al.*, “Meeting physical activity guidelines and the risk of incident knee osteoarthritis: A population-based prospective cohort study,” *Arthritis Care Res.*, vol. 66, no. 1, pp. 139–146, 2014, doi: 10.1002/acr.22120.
- [60] L. S. Gates *et al.*, “Recreational Physical Activity and Risk of Incident Knee Osteoarthritis: An International Meta-Analysis of Individual Participant–Level Data,” *Arthritis Rheumatol.*, vol. 74, no. 4, pp. 612–622, 2022, doi: 10.1002/art.42001.
- [61] P. T. Williams, “Effects of running and walking on osteoarthritis and hip replacement risk,” *Med. Sci. Sports Exerc.*, vol. 45, no. 7, pp. 1292–1297, 2013.
- [62] R. H. Miller, “Joint loading in runners does not initiate knee osteoarthritis,”

Exerc. Sport Sci. Rev., vol. 45, no. 2, pp. 87–95, 2017, doi: 10.1249/JES.000000000000105.

- [63] G. H. Lo *et al.*, “Running does not increase symptoms or structural progression in people with knee osteoarthritis: data from the osteoarthritis initiative,” *Clin. Rheumatol.*, vol. 37, pp. 2497–2504, 2018, doi: 10.1007/s10067-018-4121-3.
- [64] N. J. Bosomworth, “Exercise and knee osteoarthritis: Benefit or hazard?,” *Canadian Family Physician*, vol. 55, no. 9, pp. 871–878, 2009.
- [65] D. Voinier and D. K. White, “Walking, running, and recreational sports for knee osteoarthritis: An overview of the evidence,” *Eur. J. Rheumatol.*, no. Figure 1, 2022, doi: 10.5152/eurjrheum.2022.21046.
- [66] A. Bricca, C. B. Juhl, M. Steultjens, W. Wirth, and E. M. Roos, “Impact of exercise on articular cartilage in people at risk of, or with established, knee osteoarthritis: A systematic review of randomised controlled trials,” *Br. J. Sports Med.*, 2018, doi: 10.1136/bjsports-2017-098661.
- [67] A. Bricca *et al.*, “Moderate physical activity may prevent cartilage loss in women with knee osteoarthritis: data from the Osteoarthritis Initiative,” *Arthritis Care Res. (Hoboken)*, Oct. 2018, doi: 10.1002/acr.23791.
- [68] B. Vanwanseele, F. Eckstein, H. Knecht, A. Spaepen, and E. St??ssis, “Longitudinal Analysis of Cartilage Atrophy in the Knees of Patients with Spinal Cord Injury,” *Arthritis Rheum.*, vol. 48, no. 12, pp. 3377–3381, 2003, doi: 10.1002/art.11367.
- [69] R. B. Souza *et al.*, “Effects of Unloading on Knee Articular Cartilage T1rho and T2 Magnetic Resonance Imaging Relaxation Times: A Case Series,” *J. Orthop. Sport. Phys. Ther.*, vol. 42, no. 6, pp. 511–520, 2012, doi: 10.2519/jospt.2012.3975.
- [70] J. S. Willey *et al.*, “Spaceflight-Relevant Challenges of Radiation and/or Reduced Weight Bearing Cause Arthritic Responses in Knee Articular Cartilage,” *Radiat. Res.*, vol. 186, no. 4, pp. 333–344, 2016, doi: 10.1667/RR14400.1.
- [71] A. Liphardt *et al.*, “The Effect of Immobility and Microgravity on Cartilage Metabolism,” *Ann. Rheum. Dis.*, vol. 74, no. Suppl 2, p. 919, 2015, doi: 10.1136/annrheumdis-2015-eular.3390.
- [72] A. Niehoff *et al.*, “Long-duration space flight and cartilage adaptation: First results on changes in tissue metabolism,” *Osteoarthr. Cartil.*, vol. 24, no. 2016,

pp. S144–S145, 2016, doi: 10.1016/j.joca.2016.01.282.

- [73] F. C. Linn, “Lubrication of animal joints: I. The arthrotripsometer,” *JBJS*, vol. 49, no. 6, pp. 1079–1098, 1967.
- [74] F. C. Linn, “Lubrication of animal joints. II. The mechanisms,” *J. Biomech.*, vol. 1, pp. 193–205, 1968, doi: 10.1115/1.3554927.
- [75] C. W. McCutchen, “Mechanism of animal joints,” *Nature*, vol. 183, pp. 1654–1655, 1959, doi: 10.1038/1831654a0.
- [76] V. C. Mow, “The Role of Lubrication in Biomechanical Joints,” *J. Lubr. Technol.*, vol. 91, no. 2, p. 320, 1969, doi: 10.1115/1.3554924.
- [77] A. F. Mak, W. M. Lai, and V. C. Mow, “Biphasic indentation of articular cartilage-I. Theoretical analysis,” *Journal of Biomechanics*, vol. 20, no. 7, pp. 703–714, 1987, doi: 10.1016/0021-9290(87)90036-4.
- [78] C. G. Armstrong, W. M. Lai, and V. C. Mow, “An Analysis of the Unconfined Compression of Articular Cartilage,” *J. Biomech. Eng.*, vol. 106, no. 2, p. 165, 1984, doi: 10.1115/1.3138475.
- [79] V. C. Mow and W. M. Lai, “Recent Developments in Synovial Joint Biomechanics,” *SIAM Rev.*, vol. 22, no. 3, pp. 275–317, 1980, doi: 10.1137/1022056.
- [80] S. A. Maas, B. J. Ellis, G. A. Ateshian, and J. A. Weiss, “FEBio: Finite Elements for Biomechanics,” 2012, doi: 10.1115/1.4005694.
- [81] A. Maroudas, “Balance between swelling pressure and collagen tension in normal and degenerate cartilage Growth of algal symbionts in regenerating hydra,” *Nature*, vol. 260, pp. 808–809, 1976.
- [82] G. A. Ateshian, M. A. Soltz, R. L. Mauck, I. M. Basalo, C. T. Hung, and W. M. Lai, “The Role of Osmotic Pressure and Tension-Compression Nonlinearity in the Frictional Response of Articular Cartilage,” 2003.
- [83] A. C. Moore and D. L. Burris, “An analytical model to predict interstitial lubrication of cartilage in migrating contact areas,” *J. Biomech.*, vol. 47, no. 1, pp. 148–153, 2014, doi: 10.1016/j.jbiomech.2013.09.020.
- [84] V. C. Mow, S. C. Kuei, W. M. Lai, and C. G. Armstrong, “Biphasic Creep and Stress Relaxation of Articular Cartilage in Compression: Theory and Experiments,” *J. Biomech. Eng.*, vol. 102, no. 1, p. 73, 1980, doi:

10.1115/1.3138202.

- [85] X. L. Lu and V. C. Mow, “Biomechanics of articular cartilage and determination of material properties,” *Med. Sci. Sports Exerc.*, vol. 40, no. 2, pp. 193–199, 2008, doi: 10.1249/mss.0b013e31815cb1fc.
- [86] F. G. Donnan, “The theory of membrane equilibria,” *Chem. Rev.*, vol. 1, no. 1, pp. 73–90, 1924, doi: 10.1021/cr60001a003.
- [87] A. C. Moore, B. K. Zimmerman, X. Chen, X. L. Lu, and D. L. Burris, “Experimental characterization of biphasic materials using rate-controlled Hertzian indentation,” *Tribol. Int.*, vol. 89, pp. 2–8, 2015, doi: 10.1016/j.triboint.2015.02.001.
- [88] J. E. Greenleaf, R. Bulbulian, E. M. Bernauer, W. Haskell, and T. Moore, “Exercise-training protocols for astronauts in microgravity,” *J. Appl. Physiol.*, vol. 67, no. 6, pp. 2191–2204, 1989, doi: 10.1152/jappl.1989.67.5.1820.
- [89] R. Krishnan, E. N. Mariner, and G. A. Ateshian, “Effect of dynamic loading on the frictional response of bovine articular cartilage,” *J. Biomech.*, vol. 38, no. 8, pp. 1665–1673, 2005, doi: 10.1016/j.jbiomech.2004.07.025.
- [90] M. Soltz and G. A. Ateshian, “A Conewise Linear Elasticity Mixture Model for the Analysis of Tension-Compression Nonlinearity in Articular Cartilage,” 2000. Accessed: Jan. 23, 2020. [Online]. Available: https://asmedigitalcollection.asme.org/biomechanical/article-pdf/122/6/576/5484464/576_1.pdf.
- [91] M. J. Carter, I. M. Basalo, and G. A. Ateshian, “The Temporal Response of the Friction Coefficient of Articular Cartilage Depends on the Contact Area,” *J. Biomech.*, vol. 40, no. 14, pp. 3257–3260, 2007, Accessed: Dec. 19, 2018. [Online]. Available: <https://www.ncbi.nlm.nih.gov/udel.idm.oclc.org/pmc/articles/PMC2094001/pdf/nihms-33344.pdf>.
- [92] P. A. Smyth, R. E. Rifkin, R. L. Jackson, and R. R. Hanson, “A surface roughness comparison of cartilage in different types of synovial joints,” *J. Biomech. Eng.*, vol. 134, no. 2, pp. 1–6, 2012, doi: 10.1115/1.4005934.
- [93] B. K. Zimmerman *et al.*, “Role of interstitial fluid pressurization in TMJ lubrication,” *J. Dent. Res.*, vol. 94, no. 1, pp. 85–92, 2015, doi: 10.1177/0022034514553626.
- [94] V. K. Shekhawat, M. P. Laurent, C. Muehleman, and M. A. Wimmer, “Surface topography of viable articular cartilage measured with scanning white light

- interferometry,” *Osteoarthr. Cartil.*, vol. 17, no. 9, pp. 1197–1203, 2009, doi: 10.1016/j.joca.2009.03.013.
- [95] Y. Wu and S. J. Ferguson, “The influence of cartilage surface topography on fluid flow in the intra-articular gap,” *Comput. Methods Biomech. Biomed. Engin.*, vol. 20, no. 3, pp. 250–259, 2017, doi: 10.1080/10255842.2016.1215438.
- [96] J. J. Liao, D. W. Smith, S. Miramini, N. Thibbotuwawa, B. S. Gardiner, and L. Zhang, “The investigation of fluid flow in cartilage contact gap,” *J. Mech. Behav. Biomed. Mater.*, vol. 95, pp. 153–164, 2019, doi: 10.1016/j.jmbbm.2019.04.008.
- [97] T. Macirowski, S. Tepic, and R. W. Mann, “Cartilage Stresses in the Human Hip Joint,” vol. 116, no. February, 1994, [Online]. Available: http://www.asme.org/terms/Terms_Use.cfm.
- [98] D. E. Kenyon, “A model for surface flow in cartilage,” *J. Biomech.*, vol. 13, no. 2, pp. 129–134, 1980, doi: 10.1016/0021-9290(80)90186-4.
- [99] J. A. Gustafson, J. J. Elias, R. E. Debski, and S. Farrokhi, “Development and validation of a kinematically-driven discrete element model of the patellofemoral joint,” *J. Biomech.*, vol. 88, pp. 164–172, 2019, doi: 10.1016/j.jbiomech.2019.03.032.
- [100] A. Erdemir *et al.*, “Deciphering the ‘Art’ in Modeling and Simulation of the Knee Joint: Overall Strategy,” *J. Biomech. Eng.*, vol. 141, no. 7, pp. 1–10, 2019, doi: 10.1115/1.4043346.
- [101] N. K. Lad *et al.*, “Effect of normal gait on in vivo tibiofemoral cartilage strains,” *J. Biomech.*, vol. 49, no. 13, pp. 2870–2876, 2016, doi: 10.1016/j.jbiomech.2016.06.025.
- [102] F. Eckstein, M. Hudelmaier, and R. Putz, “The effects of exercise on human articular cartilage,” *J. Anat.*, vol. 208, no. 4, pp. 491–512, 2006, doi: 10.1111/j.1469-7580.2006.00546.x.
- [103] E. G. Sutter, M. R. Widmyer, G. M. Utturkar, C. E. Spritzer, W. E. Garrett, and L. E. DeFrate, “In Vivo Measurement of Localized Tibiofemoral Cartilage Strains in Response to Dynamic Activity,” *Am. J. Sports Med.*, vol. 43, no. 2, pp. 370–376, 2015, doi: 10.1177/0363546514559821.
- [104] A. T. Collins, M. Kulvaranon, C. E. Spritzer, A. L. McNulty, and L. E. DeFrate, “The Influence of Obesity and Meniscal Coverage on In Vivo Tibial Cartilage

- Thickness and Strain,” *Orthop. J. Sport. Med.*, vol. 8, no. 12, pp. 1–8, 2020, doi: 10.1177/2325967120964468.
- [105] J. M. Benson, C. Kook, A. C. Moore, S. Voinier, C. Price, and D. L. Burris, “Range-of-motion affects cartilage fluid load support: functional implications for prolonged inactivity,” *Osteoarthr. Cartil.*, vol. 29, no. 1, pp. 134–142, 2021, doi: 10.1016/j.joca.2020.11.005.
- [106] J. L. Coleman *et al.*, “Diurnal variations in articular cartilage thickness and strain in the human knee,” *J. Biomech.*, vol. 46, no. 3, 2013, doi: 10.1016/j.jbiomech.2012.09.013.
- [107] M. R. Widmyer *et al.*, “High Body Mass Index Is Associated With Increased Diurnal Strains in the Articular Cartilage of the Knee,” *ARTHRITIS Rheum.*, vol. 65, no. 10, pp. 2615–2622, 2013, doi: 10.1002/art.38062.
- [108] C. E. Matthews *et al.*, “Amount of time spent in sedentary behaviors in the United States, 2003–2004,” *Am. J. Epidemiol.*, vol. 167, no. 7, pp. 875–881, 2008, doi: 10.1093/aje/kwm390.
- [109] T. Rantalainen, A. J. Pesola, M. Quittner, N. D. Ridgers, and D. L. Belavy, “Are habitual runners physically inactive?,” *J. Sports Sci.*, vol. 36, no. 16, pp. 1793–1800, 2018, doi: 10.1080/02640414.2017.1420452.
- [110] W. J. Anderst and S. Tashman, “A method to estimate in vivo dynamic articular surface interaction,” *J. Biomech.*, vol. 36, no. 9, pp. 1291–1299, 2003, doi: 10.1016/S0021-9290(03)00157-X.
- [111] T. A. Moro-Oka *et al.*, “Dynamic activity dependence of in vivo normal knee kinematics,” *J. Orthop. Res.*, vol. 26, no. 4, pp. 428–434, 2008, doi: 10.1002/jor.20488.
- [112] Y. Hoshino and S. Tashman, “Internal tibial rotation during in vivo, dynamic activity induces greater sliding of tibio-femoral joint contact on the medial compartment,” *Knee Surgery, Sport. Traumatol. Arthrosc.*, vol. 20, no. 7, pp. 1268–1275, 2012, doi: 10.1007/s00167-011-1731-6.
- [113] J. S. Li, A. Hosseini, L. Cancre, N. Ryan, H. E. Rubash, and G. Li, “Kinematic characteristics of the tibiofemoral joint during a step-up activity,” *Gait Posture*, vol. 38, no. 4, pp. 712–716, 2013, doi: 10.1016/j.gaitpost.2013.03.004.
- [114] B. Akpınar, E. Thorhauer, S. Tashman, J. J. Irrgang, F. H. Fu, and W. J. Anderst, “Tibiofemoral Cartilage Contact Differences Between Level Walking and Downhill Running,” *Orthop. J. Sport. Med.*, vol. 7, no. 4, pp. 1–7, 2019,

doi: 10.1177/2325967119836164.

- [115] M. H. Holmes and V. C. Mow, “The nonlinear characteristics of soft gels and hydrated connective tissues in ultrafiltration,” *J. Biomech.*, vol. 23, no. 11, pp. 1145–1156, 1990, doi: 10.1016/0021-9290(90)90007-P.
- [116] A. C. Moore and D. L. Burris, “Tribological rehydration of cartilage and its potential role in preserving joint health,” *Osteoarthr. Cartil.*, vol. 25, no. 1, pp. 99–107, 2017, doi: 10.1016/j.joca.2016.09.018.
- [117] D. L. Burris, · L Ramsey, · B T Graham, · C Price, and · A C Moore, “How Sliding and Hydrodynamics Contribute to Articular Cartilage Fluid and Lubrication Recovery,” *Tribol. Lett.*, vol. 67, p. 46, 2019, doi: 10.1007/s11249-019-1158-7.
- [118] A. W. Eberhardt, L. M. Keer, J. L. Lewis, and V. Vithoontien, “An analytical model of joint contact,” *J. Biomech. Eng.*, vol. 112, no. 4, pp. 407–413, 1990, doi: 10.1115/1.2891204.
- [119] L. Guoan, M. Sakamoto, and E. Y. S. Chao, “A comparison of different methods in predicting static pressure distribution in articulating joints,” *J. Biomech.*, vol. 30, no. 6, pp. 635–638, 1997, doi: 10.1016/S0021-9290(97)00009-2.
- [120] I. Argatov and G. Mishuris, *Contact Mechanics of Articular Cartilage Layers*. 2015.
- [121] A. W. Eberhardt, J. L. Lewis, and L. M. Keer, “Normal Contact of Elastic Spheres With Two Elastic Layers as a Model of Joint Articulation,” 1991. Accessed: Oct. 21, 2018. [Online]. Available: <http://biomechanical.asmedigitalcollection.asme.org>.
- [122] S. Federico and W. Herzog, “Towards an analytical model of soft biological tissues,” *J. Biomech.*, vol. 41, no. 16, pp. 3309–3313, 2008, doi: 10.1016/j.jbiomech.2008.05.039.
- [123] S.-K. Han, S. Federico, M. Epstein, and W. Herzog, “An articular cartilage contact model based on real surface geometry,” *J. Biomech.*, vol. 38, pp. 179–184, 2005, doi: 10.1016/j.jbiomech.2004.03.010.
- [124] P. S. Donzelli and R. L. Spilker, “Computer methods in applied mechanics and engineering A contact finite element formulation for biological soft hydrated tissues,” *Comput. Methods Appl. Mech. Engrg.*, vol. 153, pp. 63–79, 1998, Accessed: Feb. 12, 2019. [Online]. Available: <https://ac.els->

cdn.com/S0045782597000650/1-s2.0-S0045782597000650-
main.pdf?_tid=364eb50d-c1b3-4837-8be1-
d8d170d86d5b&acdnat=1550000359_b26d92c3b356f417920b7dd79592a14e.

- [125] T. L. H. Donahue, M. L. Hull, M. M. Rashid, and C. R. Jacobs, “A finite element model of the human knee joint for the study of tibio-femoral contact,” *J. Biomech. Eng.*, vol. 124, no. 3, pp. 273–280, 2002, doi: 10.1115/1.1470171.
- [126] S. A. Maas, B. J. Ellis, D. S. Rawlins, and J. A. Weiss, “Finite element simulation of articular contact mechanics with quadratic tetrahedral elements,” *J. Biomech.*, vol. 49, no. 5, pp. 659–667, 2016, doi: 10.1016/j.jbiomech.2016.01.024.
- [127] G. A. Ateshian, C. R. Henak, and J. A. Weiss, “Toward patient-specific articular contact mechanics,” *J. Biomech.*, vol. 48, no. 5, pp. 779–786, 2015, doi: 10.1016/j.jbiomech.2014.12.020.
- [128] J. Z. Wu, W. Herzog, and J. Ronsky, “MODELING AXI-SYMMETRICAL JOINT CONTACT WITH BIPHASIC CARTILAGE LAYERS-AN ASYMPTOTIC SOLUTION,” 1996.
- [129] J. J. Liao, D. W. Smith, S. Miramini, B. S. Gardiner, and L. Zhang, “A coupled contact model of cartilage lubrication in the mixed-mode regime under static compression,” *Tribol. Int.*, vol. 145, no. November 2019, p. 106185, 2020, doi: 10.1016/j.triboint.2020.106185.
- [130] T. M. Griffin and F. Guilak, “The Role of Mechanical Loading in the Onset and Progression of Oestoarthritis: Exercise and Sport Sciences Reviews,” *Exerc. Sport Sci. Rev.*, vol. 33, no. 4, pp. 195–200, 2005, [Online]. Available: https://journals.lww.com/acsm-essr/Fulltext/2005/10000/The_Role_of_Mechanical_Loading_in_the_Onset_and.8.aspx.
- [131] T. P. Andriacchi and A. Mü Ndermann, “The role of ambulatory mechanics in the initiation and progression of knee osteoarthritis,” Lippincott Williams & Wilkins, 2006. Accessed: Dec. 28, 2018. [Online]. Available: <https://udel-illiad-oclc-org.udel.idm.oclc.org/illiad/illremoteauth/illiad.dll?Action=10&Form=75&Value=644123>.
- [132] T. L. Vincent and A. K. T. Wann, “Mechanoadaptation: articular cartilage through thick and thin,” *Journal of Physiology*, vol. 597, no. 5, pp. 1271–1281, 2019, doi: 10.1113/JP275451.

- [133] R. H. Miller and R. L. Krupenevich, “Medial knee cartilage is unlikely to withstand a lifetime of running without positive adaptation: a theoretical biomechanical model of failure phenomena,” *PeerJ*, vol. 8, p. e9676, 2020, doi: 10.7717/peerj.9676.
- [134] N. A. Segal *et al.*, “Baseline Articular Contact Stress Levels Predict Incident Symptomatic Knee Osteoarthritis Development in the MOST Cohort,” *J Orthop Res*, vol. 27, no. 12, pp. 1562–1568, 2009, doi: 10.1002/jor.20936.
- [135] S. J. Lee *et al.*, “Tibiofemoral contact mechanics after serial medial meniscectomies in the human cadaveric knee,” *Am. J. Sports Med.*, 2006, doi: 10.1177/0363546506286786.
- [136] G. S. Nunes, R. Scattone Silva, A. F. dos Santos, R. A. S. Fernandes, F. V. Serrão, and M. de Noronha, “Methods to assess patellofemoral joint stress: A systematic review,” *Gait Posture*, vol. 61, no. June 2017, pp. 188–196, 2018, doi: 10.1016/j.gaitpost.2017.12.018.
- [137] C. R. Henak, A. L. Kapron, A. E. Anderson, B. J. Ellis, S. A. Maas, and J. A. Weiss, “Specimen-specific predictions of contact stress under physiological loading in the human hip: Validation and sensitivity studies,” *Biomech. Model. Mechanobiol.*, vol. 13, no. 2, 2014, doi: 10.1007/s10237-013-0504-1.
- [138] G. A. Ateshian, B. J. Ellis, and J. A. Weiss, “Equivalence Between Short-Time Biphase and Incompressible Elastic Material Responses,” 2007, doi: 10.1115/1.2720918.
- [139] M. Freutel, H. Schmidt, L. Dürselen, A. Ignatius, and F. Galbusera, “Finite element modeling of soft tissues: Material models, tissue interaction and challenges,” 2014, doi: 10.1016/j.clinbiomech.2014.01.006.
- [140] R. J. Cooper, R. K. Wilcox, and A. C. Jones, “Finite element models of the tibiofemoral joint: A review of validation approaches and modelling challenges,” *Med. Eng. Phys.*, vol. 74, pp. 1–12, 2019, doi: 10.1016/j.medengphy.2019.08.002.
- [141] Z. Trad, A. Barkaoui, and M. Chafra, “A three dimensional finite element analysis of mechanical stresses in the human knee joint: Problem of cartilage destruction,” *J. Biomimetics, Biomater. Biomed. Eng.*, vol. 32, no. April, pp. 29–39, 2017, doi: 10.4028/www.scientific.net/JBBBE.32.29.
- [142] N. H. Yang, H. Nayeb-Hashemi, P. K. Canavan, and A. Vaziri, “Effect of frontal plane tibiofemoral angle on the stress and strain at the knee cartilage during the stance phase of gait,” *J. Orthop. Res.*, vol. 28, no. 12, pp. 1539–

1547, 2010, doi: 10.1002/jor.21174.

- [143] M. L. Hull, M. M. Rashid, and C. R. Jacobs, “A Finite Element Model of the Human Knee Joint for the Study of Tibio-Femoral Contact,” 2002, doi: 10.1115/1.1470171.
- [144] S. Hirokawa, “Three-dimensional mathematical model analysis of the patellofemoral joint,” *J. Biomech.*, vol. 24, no. 8, pp. 659–671, 1991, doi: 10.1016/0021-9290(91)90331-G.
- [145] K. S. and A. T.P., “A comparison of the influence of global functional loads vs. local contact anatomy on articular cartilage thickness at the knee,” *Journal of Biomechanics*, vol. 40, no. 13. pp. 2961–2966, 2007, doi: 10.1016/j.jbiomech.2007.02.005 LK - http://sfx-bcu.unil.ch/sfx_local?sid=EMBASE&issn=00219290&id=doi:10.1016%2Fj.jbiomech.2007.02.005&atitle=A+comparison+of+the+influence+of+global+functional+loads+vs.+local+contact+anatomy+on+articular+cartilage+thickness+at+the+knee&stitle=J.+Biomech.&title=Journal+of+Biomechanics&volume=40&issue=13&spage=2961&epage=2966&aualast=Koo&aufirst=Seungbum&aunit=S.&aufull=Koo+S.&coden=JBMCB&isbn=&pages=2961-2966&date=2007&aunit1=S&aunitm=.
- [146] M. S. Renani, M. Rahman, A. Cil, and A. P. Stylianou, “Calibrating multibody ulno-humeral joint cartilage using a validated finite element model,” *Multibody Syst. Dyn.*, vol. 44, no. 1, pp. 81–91, 2018, doi: 10.1007/s11044-018-9622-y.
- [147] Y. Bei and B. J. Fregly, “Multibody dynamic simulation of knee contact mechanics,” *Med. Eng. Phys.*, vol. 26, pp. 777–789, 2004, doi: 10.1016/j.medengphy.2004.07.004.
- [148] D. D. Anderson, K. S. Iyer, N. A. Segal, J. A. Lynch, and T. D. Brown, “Implementation of discrete element analysis for subject-specific, population-wide investigations of habitual contact stress exposure,” *J. Appl. Biomech.*, vol. 26, no. 2, pp. 215–223, 2010, doi: 10.1123/jab.26.2.215.
- [149] R. H. Miller and R. L. Krupenevich, “Medial knee cartilage is unlikely to withstand a lifetime of running without positive adaptation: a theoretical biomechanical model of failure phenomena,” *PeerJ*, vol. 8, p. e9676, 2020, doi: 10.7717/peerj.9676.
- [150] I. Argatov and G. Mishuris, *Contact Mechanics of Articular Cartilage Layers*. 2015.
- [151] A. E. Peters, R. Akhtar, E. J. Comerford, and K. T. Bates, “Tissue material

properties and computational modelling of the human tibiofemoral joint: A critical review,” *PeerJ*, vol. 2018, no. 1. PeerJ Inc., 2018, doi: 10.7717/peerj.4298.

- [152] A. E. Anderson, B. J. Ellis, S. A. Maas, C. L. Peters, and J. A. Weiss, “Validation of finite element predictions of cartilage contact pressure in the human hip joint,” *J. Biomech. Eng.*, vol. 130, no. 5, pp. 1–10, 2008, doi: 10.1115/1.2953472.
- [153] D. Shepherd, “The ‘instantaneous’ compressive modulus of human articular cartilage in joints of the lower limb,” *Rheumatology*, vol. 38, no. 2, pp. 124–132, 2002, doi: 10.1093/rheumatology/38.2.124.
- [154] A. C. Moore and D. L. Burris, “Tribological and material properties for cartilage of and throughout the bovine stifle: support for the altered joint kinematics hypothesis of osteoarthritis,” *Osteoarthr. Cartil.*, vol. 23, no. 1, pp. 161–169, Jan. 2015, doi: 10.1016/j.joca.2014.09.021.
- [155] A. C. Swann and B. B. Seedhom, “The stiffness of normal articular cartilage and the predominant acting stress levels: Implications for the aetiology of osteoarthritis,” *Rheumatology*, vol. 32, no. 1, pp. 16–25, 1993, doi: 10.1093/rheumatology/32.1.16.
- [156] J. M. Deneweth, K. E. Newman, S. M. Sylvia, S. G. McLean, and E. M. Arruda, “Heterogeneity of tibial plateau cartilage in response to a physiological compressive strain rate,” *J. Orthop. Res.*, vol. 31, no. 3, pp. 370–375, 2013, doi: 10.1002/jor.22226.
- [157] J. M. Deneweth, S. G. McLean, and E. M. Arruda, “Evaluation of hyperelastic models for the non-linear and non-uniform high strain-rate mechanics of tibial cartilage,” *J. Biomech.*, vol. 46, no. 10, pp. 1604–1610, 2013, doi: 10.1016/j.jbiomech.2013.04.014.
- [158] M. Stevanovic, M. M. Yovanovich, and J. R. Culham, “Modeling contact between rigid sphere and elastic layer bonded to rigid substrate,” *IEEE Trans. Components Packag. Technol.*, vol. 24, no. 2, pp. 207–212, Jun. 2001, doi: 10.1109/6144.926384.
- [159] G. E. Kempson, M. A. R. Freeman, and S. A. V. Swanson, “The determination of a creep modulus for articular cartilage from indentation tests on the human femoral head,” *J. Biomech.*, vol. 4, no. 4, pp. 239–250, 1971, doi: 10.1016/0021-9290(71)90030-3.
- [160] A. C. Moore, J. F. DeLucca, D. M. Elliott, and D. L. Burris, “Quantifying

Cartilage Contact Modulus, Tension Modulus, and Permeability With Hertzian Biphase Creep,” *J. Tribol.*, vol. 138, no. 4, p. 041405, 2016, doi: 10.1115/1.4032917.

- [161] S. Gilbert *et al.*, “Dynamic contact mechanics on the tibial plateau of the human knee during activities of daily living,” *J. Biomech.*, vol. 47, no. 9, pp. 2006–2012, 2014, doi: 10.1016/j.jbiomech.2013.11.003.
- [162] W. Wilson, J. M. Huyghe, and C. C. Van Donkelaar, “Depth-dependent compressive equilibrium properties of articular cartilage explained by its composition,” *Biomech. Model. Mechanobiol.*, vol. 6, no. 1–2, pp. 43–53, 2007, doi: 10.1007/s10237-006-0044-z.
- [163] M. Fortin, J. Soulhat, A. Shirazi-Adl, E. B. Hunziker, and M. D. Buschmann, “Unconfined compression of articular cartilage: Nonlinear behavior and comparison with a fibril-reinforced biphasic model,” *J. Biomech. Eng.*, vol. 122, no. 2, pp. 189–195, 2000, doi: 10.1115/1.429641.
- [164] E. Langelier and M. D. Buschmann, “Increasing strain and strain rate strengthen transient stiffness but weaken the response to subsequent compression for articular cartilage in unconfined compression,” *J. Biomech.*, vol. 36, no. 6, pp. 853–859, 2003, doi: 10.1016/S0021-9290(03)00006-X.
- [165] L. P. Li and W. Herzog, “Strain-rate dependence of cartilage stiffness in unconfined compression: The role of fibril reinforcement versus tissue volume change in fluid pressurization,” *J. Biomech.*, vol. 37, no. 3, pp. 375–382, 2004, doi: 10.1016/S0021-9290(03)00263-X.
- [166] L. A. Setton, W. Y. Gu, W. M. Lai, and V. C. Mow, “Pre-stress in articular cartilage due to internal swelling pressure,” in *Winter Annual Meeting of the American Society of Mechanical Engineers*, 1992, pp. 485–488.
- [167] J. Mizrahi, A. Maroudas, Y. Lanir, I. Ziv, and T. J. Webber, “The ‘instantaneous’ deformation of cartilage: effects of collagen fiber orientation and osmotic stress,” *Biorheology*, vol. 23, no. 4, pp. 311–330, 1986.
- [168] J. M. Deneweth, E. M. Arruda, and S. G. McLean, “Hyperelastic modeling of location-dependent human distal femoral cartilage mechanics,” *Int. J. Non. Linear. Mech.*, vol. 68, pp. 146–156, 2015, doi: 10.1016/j.ijnonlinmec.2014.06.013.
- [169] R. M. Schinagl, D. Gurskis, A. C. Chen, and R. L. Sah, “Depth-dependent confined compression modulus of full-thickness bovine articular cartilage,” *J. Orthop. Res.*, vol. 15, no. 4, pp. 499–506, 1997, doi: 10.1002/jor.1100150404.

- [170] S. Manzano *et al.*, “Inhomogeneous response of articular cartilage: A three-dimensional multiphasic heterogeneous study,” *PLoS ONE*, vol. 11, no. 6, 2016, doi: 10.1371/journal.pone.0157967.
- [171] S. S. Chen, Y. H. Falcovitz, R. Schneiderman, A. Maroudas, and R. L. Sah, “Depth-dependent compressive properties of normal aged human femoral head articular cartilage: relationship to fixed charge density,” *Osteoarthr. Cartil.*, vol. 9, pp. 561–569, 2001, doi: 10.1053/joca.2001.0424.
- [172] I. J. Hill and W. G. Sawyer, “Energy, adhesion, and the elastic foundation,” *Tribol. Lett.*, vol. 37, no. 2, pp. 453–461, 2010, doi: 10.1007/s11249-009-9537-0.
- [173] A. F. Mak, W. M. Lai, and V. C. Mow, “Biphasic indentation of articular cartilage-I. Theoretical analysis,” *J. Biomech.*, vol. 20, no. 7, pp. 703–714, 1987, doi: 10.1016/0021-9290(87)90036-4.
- [174] T. L. H. Donahue, M. L. Hull, M. M. Rashid, and C. R. Jacobs, “A finite element model of the human knee joint for the study of tibio-femoral contact,” *J. Biomech. Eng.*, vol. 124, no. 3, pp. 273–280, 2002, doi: 10.1115/1.1470171.
- [175] Y. Bei and B. J. Fregly, “Multibody dynamic simulation of knee contact mechanics,” *Med. Eng. Phys.*, vol. 26, pp. 777–789, 2004, doi: 10.1016/j.medengphy.2004.07.004.
- [176] R. Y. Hori and L. F. Mockros, “Indentation tests of human articular cartilage,” *J. Biomech.*, vol. 9, no. 4, pp. 259–268, 1976, doi: 10.1016/0021-9290(76)90012-9.
- [177] M. MacHado, P. Moreira, P. Flores, and H. M. Lankarani, “Compliant contact force models in multibody dynamics: Evolution of the Hertz contact theory,” *Mech. Mach. Theory*, vol. 53, pp. 99–121, 2012, doi: 10.1016/j.mechmachtheory.2012.02.010.
- [178] M. G. Pandy, K. Sasaki, and S. Kim, “A three-dimensional musculoskeletal model of the human knee joint. Part 1: Theoretical construction,” *Comput. Methods Biomech. Biomed. Engin.*, vol. 1, no. 2, pp. 87–108, 1997, doi: 10.1080/01495739708936697.
- [179] C. R. Smith *et al.*, “Efficient computation of cartilage contact pressures within dynamic simulations of movement,” *Comput. Methods Biomech. Biomed. Eng. Imaging Vis.*, vol. 6, no. 5, pp. 491–498, 2018, doi: 10.1080/21681163.2016.1172346.

- [180] A. E. Peters, R. Akhtar, E. J. Comerford, and K. T. Bates, “The effect of ageing and osteoarthritis on the mechanical properties of cartilage and bone in the human knee joint,” *Sci. Rep.*, vol. 8, no. 1, 2018, doi: 10.1038/s41598-018-24258-6.
- [181] T. T. Dao and P. Pouletaut, “A Hertzian Integrated Contact Model of the Total Knee Replacement Implant for the Estimation of Joint Contact Forces,” *J. Comput. Med.*, vol. 2015, pp. 1–9, 2015, doi: 10.1155/2015/945379.
- [182] B. S. Gardiner *et al.*, “Predicting Knee Osteoarthritis,” *Ann. Biomed. Eng.*, vol. 44, no. 1, 2016, doi: 10.1007/s10439-015-1393-5.
- [183] L. Yang *et al.*, “Trends in Sedentary Behavior among the US Population, 2001-2016,” *JAMA - J. Am. Med. Assoc.*, vol. 321, no. 16, pp. 1587–1597, 2019, doi: 10.1001/jama.2019.3636.
- [184] W. M. Lai, V. C. Mow, and V. Roth, “Effects of nonlinear strain-dependent permeability and rate of compression on the stress behavior of articular cartilage,” *J. Biomech. Eng.*, vol. 103, no. 2, pp. 61–66, 1981, doi: 10.1115/1.3138261.
- [185] J. M. Mansour and V. C. Mow, “The permeability of articular cartilage under compressive strain and at high pressures,” *J. Bone Jt. Surg. - Ser. A*, vol. 58, no. 4, pp. 509–516, 1976, doi: 10.2106/00004623-197658040-00014.
- [186] X. L. Lu, D. D. N. Sun, X. E. Guo, F. H. Chen, W. M. Lai, and V. C. Mow, “Indentation determined mechanochemical properties and fixed charge density of articular cartilage,” *Ann. Biomed. Eng.*, vol. 32, no. 3, pp. 370–379, 2004, doi: 10.1023/B:ABME.0000017534.06921.24.
- [187] W. M. Lai, J. S. Hou, and V. C. Mow, “A triphasic theory for the swelling and deformation behaviors of articular cartilage,” *J. Biomech. Eng.*, vol. 113, no. 3, pp. 245–258, 1991, doi: 10.1115/1.2894880.
- [188] J. S. Hou, V. C. Mow, W. M. Lai, and M. H. Holmes, “An analysis of the squeeze-film lubrication mechanism for articular cartilage,” *J. Biomech.*, vol. 25, no. 3, pp. 247–259, 1992, doi: 10.1016/0021-9290(92)90024-U.
- [189] P. S. Walker, D. Dowson, M. D. Longfield, and V. Wright, “‘‘Boosted lubrication’ in synovial joints by fluid entrapment and enrichment.,” *Ann. Rheum. Dis.*, vol. 27, no. 6, pp. 512–520, 1968, doi: 10.1136/ard.27.6.512.
- [190] M. A. Soltz, I. M. Basalo, and G. A. Ateshian, “Hydrostatic Pressurization and Depletion of Trapped Lubricant Pool During Creep Contact of a Rippled

- Indenter Against a Biphasic Articular Cartilage Layer,” *J. Biomech. Eng.*, vol. 125, no. 5, pp. 585–593, 2003, doi: 10.1115/1.1610020.
- [191] S. Federico, G. La Rosa, W. Herzog, and J. Z. Wu, “Effect of Fluid Boundary Conditions on Joint Contact Mechanics and Applications to the Modeling of Osteoarthritic Joints,” *J. Biomech. Eng.*, vol. 126, no. 2, pp. 220–225, 2004, doi: 10.1115/1.1691445.
- [192] M. N. Moghadam, P. Abdel-Sayed, V. M. Camine, and D. P. Pioletti, “Impact of synovial fluid flow on temperature regulation in knee cartilage,” *J. Biomech.*, vol. 48, no. 2, pp. 370–374, 2015, doi: 10.1016/j.jbiomech.2014.11.008.
- [193] S. J. Ferguson, J. T. Bryant, R. Ganz, and K. Ito, “The acetabular labrum seal: A poroelastic finite element model,” *Clin. Biomech.*, vol. 15, no. 6, pp. 463–468, 2000, doi: 10.1016/S0268-0033(99)00099-6.
- [194] S. S. Pawaskar, J. Fisher, and Z. Jin, “Robust and general method for determining surface fluid flow boundary conditions in articular cartilage contact mechanics modeling,” *J. Biomech. Eng.*, vol. 132, no. 3, pp. 1–8, 2010, doi: 10.1115/1.4000869.
- [195] D. W. Smith, B. S. Gardiner, L. Zhang, and A. J. Grodzinsky, *Articular cartilage dynamics*. 2018.
- [196] C. E. Henderson, J. S. Higginson, and P. J. Barrance, “Comparison of mri-based estimates of articular cartilage contact area in the tibiofemoral joint,” *J. Biomech. Eng.*, vol. 133, no. 1, pp. 1–4, 2011, doi: 10.1115/1.4002938.
- [197] S. Hinterwimmer *et al.*, “In vivo contact areas of the knee in patients with patellar subluxation,” *J. Biomech.*, vol. 38, no. 10, pp. 2095–2101, 2005, doi: 10.1016/j.jbiomech.2004.09.008.
- [198] S. Voinier, A. C. Moore, J. M. Benson, C. Price, and D. L. Burriss, “The modes and competing rates of cartilage fluid loss and recovery,” *Acta Biomater.*, vol. 138, pp. 390–397, 2021, doi: 10.1016/j.actbio.2021.11.014.
- [199] S. Kobayashi, S. Yonekubo, and Y. Kurogouchi, “Cryoscanning electron microscopy of loaded articular cartilage with special reference to the surface amorphous layer,” *J. Anat.*, vol. 188 (Pt 2, pp. 311–22, 1996, [Online]. Available: <http://www.ncbi.nlm.nih.gov/pubmed/8621329><http://www.pubmedcentral.nih.gov/articlerender.fcgi?artid=PMC1167566>.
- [200] J. J. Liao, S. Miramini, X. Liu, and L. Zhang, “Computational study on synovial

- fluid flow behaviour in cartilage contact gap under osteoarthritic condition,” *Comput. Biol. Med.*, vol. 123, no. June, p. 103915, 2020, doi: 10.1016/j.compbiomed.2020.103915.
- [201] J. J. Liao, D. W. Smith, S. Miramini, B. S. Gardiner, and L. Zhang, “A Probabilistic Failure Risk Approach to The Problem of Articular Cartilage Lubrication,” *Comput. Methods Programs Biomed.*, vol. 203, p. 106053, 2021, doi: 10.1016/j.cmpb.2021.106053.
- [202] K. Boettcher, S. Kienle, J. Nachtsheim, R. Burgkart, T. Hugel, and O. Lieleg, “The structure and mechanical properties of articular cartilage are highly resilient towards transient dehydration,” *Acta Biomater.*, vol. 29, 2016, doi: 10.1016/j.actbio.2015.09.034.
- [203] H. C. Cutcliffe and L. E. DeFrate, “Comparison of Cartilage Mechanical Properties Measured During Creep and Recovery,” *Sci. Rep.*, vol. 10, no. 1, p. 1547, 2020, doi: 10.1038/s41598-020-58220-2.
- [204] Z. Ugray, L. Lasdon, J. Plummer, F. Glover, J. Kelly, and R. Marti, “Scatter Search and Local Nlp Solvers: A Multistart Framework for Global Optimization,” *SSRN Electron. J.*, no. May, 2011, doi: 10.2139/ssrn.886559.
- [205] W. M. Lai and V. C. Mow, “DRAG-INDUCED COMPRESSION OF ARTICULAR CARTILAGE DURING A PERMEATION EXPERIMENT,” *Biorheology*, vol. 17, no. 10, pp. 111–123, 1980, doi: 10.1111/j.1365-2133.1896.tb16883.x.
- [206] M. A. Soltz and G. A. Ateshian, “Experimental verification and theoretical prediction of cartilage interstitial fluid pressurization at an impermeable contact interface in confined compression,” in *Journal of Biomechanics*, 1998, vol. 31, no. 10, pp. 927–934, doi: 10.1016/S0021-9290(98)00105-5.
- [207] C. G. Armstrong, “An analysis of the stresses in a thin layer of articular cartilage in a synovial joint,” *Eng. Med.*, vol. 15, no. 2, pp. 55–61, 1986, doi: 10.1243/EMED_JOUR_1986_015_018_02.
- [208] D. L. Burris and A. C. Moore, “Cartilage and Joint Lubrication: New Insights Into the Role of Hydrodynamics,” *Biotribology*, vol. 12, no. May, pp. 8–14, 2017, doi: 10.1016/j.biotri.2017.09.001.
- [209] I. Argatov and G. Mishuris, “Articular Contact Mechanics from an Asymptotic Modeling Perspective: A Review,” *Front. Bioeng. Biotechnol.*, vol. 4, no. NOV, p. 1, 2016, doi: 10.3389/fbioe.2016.00083.

- [210] M. E. Kupratis, A. E. Gure, J. M. Benson, K. F. Ortved, D. L. Burris, and C. Price, “Comparative tribology II—Measurable biphasic tissue properties have predictable impacts on cartilage rehydration and lubricity,” *Acta Biomater.*, vol. 138, pp. 375–389, 2022, doi: 10.1016/j.actbio.2021.10.049.
- [211] A. Maroudas, P. Bullough, S. A. V Swanson, and M. A. R Freeman, “THE PERMEABILITY OF ARTICULAR CARTILAGE I 66 THE JOURNAL OF BONE AND JOINT SURGERY.” Accessed: Nov. 01, 2018. [Online]. Available: <https://pdfs.semanticscholar.org/176a/4c528ca7cc794af77464512c2f75d55254bc.pdf>.
- [212] B. K. Zimmerman, R. J. Nims, A. Chen, C. T. Hung, and G. A. Ateshian, “Direct Osmotic Pressure Measurements in Articular Cartilage Demonstrate Nonideal and Concentration-Dependent Phenomena,” *J. Biomech. Eng.*, vol. 143, no. 4, pp. 1–15, 2021, doi: 10.1115/1.4049158.
- [213] S. Graindorge *et al.*, “Biphasic surface amorphous layer lubrication of articular cartilage,” *Med. Eng. Phys.*, vol. 27, no. 10, pp. 836–844, 2005, doi: 10.1016/j.medengphy.2005.05.001.
- [214] Z. Peng and M. Wang, “Three dimensional surface characterization of human cartilages at a micron and nanometre scale,” *Wear*, vol. 301, no. 1–2, pp. 210–217, 2013, doi: 10.1016/j.wear.2012.11.056.
- [215] S. S. Lee, C. T. Duong, S. H. Park, Y. Cho, S. Park, and S. Park, “Frictional response of normal and osteoarthritic articular cartilage in human femoral head,” *Proc. Inst. Mech. Eng. Part H J. Eng. Med.*, vol. 227, no. 2, pp. 129–137, 2013, doi: 10.1177/0954411912462815.
- [216] M. Wang and Z. Peng, “Investigation of the nano-mechanical properties and surface topographies of wear particles and human knee cartilages,” *Wear*, vol. 324–325, pp. 74–79, 2015, doi: 10.1016/j.wear.2014.11.033.
- [217] F. Boschetti and G. M. Peretti, “Tensile and compressive properties of healthy and osteoarthritic human articular cartilage,” *Biorheology*, vol. 45, no. 3–4, pp. 337–344, 2008.
- [218] L. A. Setton, V. C. Mow, F. J. Müller, J. C. Pita, and D. S. Howell, “Mechanical Properties of Canine Articular Cartilage Are Significantly Altered Following Transection of the Anterior Cruciate Ligament,” *J. Orthop. Res.*, vol. 12, no. 4, pp. 451–463, 1994, doi: 10.1002/jor.1100120402.
- [219] J. T. A. Mäkelä, S. K. Han, W. Herzog, and R. K. Korhonen, “Very early

- osteoarthritis changes sensitively fluid flow properties of articular cartilage,” *J. Biomech.*, vol. 48, no. 12, pp. 3369–3376, Sep. 2015, doi: 10.1016/j.jbiomech.2015.06.010.
- [220] J. Hwang, W. C. Bae, W. Shieu, C. W. Lewis, W. D. Bugbee, and R. L. Sah, “Increased hydraulic conductance of human articular cartilage and subchondral bone plate with progression of osteoarthritis,” *Arthritis Rheum.*, vol. 58, no. 12, pp. 3831–3842, 2008, doi: 10.1002/art.24069.
- [221] J. Kosel, I. Giouroudi, C. Scheffer, E. Dillon, and P. Erasmus, “Anatomical Study of the Radius and Center of Curvature of the Distal Femoral Condyle,” *J. Biomech. Eng.*, 2010, doi: 10.1115/1.4002061.
- [222] T. Röstlund, L. Carlsson, B. Albrektsson, and T. Albrektsson, “Morphometrical studies of human femoral condyles,” *J. Biomed. Eng.*, vol. 11, no. 6, pp. 442–448, 1989, doi: 10.1016/0141-5425(89)90037-X.
- [223] S. Demirci, A. Jubel, J. Andermahr, and J. Koebke, “Chondral thickness and radii of curvature of the femoral condyles and talar trochlea,” *Int. J. Sports Med.*, vol. 29, no. 4, pp. 327–330, 2008, doi: 10.1055/s-2007-965361.
- [224] S. Nozaki, K. Watanabe, T. Kato, T. Miyakawa, T. Kamiya, and M. Katayose, “Radius of curvature at the talocrural joint surface: inference of subject-specific kinematics,” *Surg. Radiol. Anat.*, vol. 41, no. 1, pp. 53–64, 2019, doi: 10.1007/s00276-018-2098-x.
- [225] F. Boschetti, M. Colombo, G. M. Peretti, G. Frascini, and R. Pietrabissa, “Direct and indirect measurement of human articular cartilage permeability .,” *Trans. Orthop. Res. Soc.*, vol. 28, p. 293, 2003, [Online]. Available: <https://www.ors.org/Transactions/49/0293.pdf>.
- [226] F. Boschetti *et al.*, “An experimental study on human articular cartilage permeability,” in *Annual International Conference of the IEEE Engineering in Medicine and Biology - Proceedings*, 2002, vol. 3, pp. 2581–2582, doi: 10.1109/iembs.2002.1053436.
- [227] M. S. Farnham, K. F. Ortved, J. S. Horner, N. J. Wagner, D. L. Burris, and C. Price, “Lubricant Effects on Articular Cartilage Sliding Biomechanics Under Physiological Fluid Load Support,” *Tribol. Lett.*, vol. 69, no. 2, pp. 1–14, 2021, doi: 10.1007/s11249-021-01430-0.
- [228] J. J. Liao, Z. Liu, S. Miramini, and L. Zhang, “Influence of variability and uncertainty in vertical and horizontal surface roughness on articular cartilage lubrication,” *Comput. Biol. Med.*, 2022.

- [229] B. Reynaud and T. M. Quinn, “Anisotropic hydraulic permeability in compressed articular cartilage,” *J. Biomech.*, vol. 39, no. 1, pp. 131–137, 2006, doi: 10.1016/j.jbiomech.2004.10.015.
- [230] H. Fujie and K. Imade, “Effects of low tangential permeability in the superficial layer on the frictional property of articular cartilage,” *Biosurface and Biotribology*, vol. 1, no. 2, pp. 124–129, 2015, doi: 10.1016/j.bsbt.2015.06.001.
- [231] M. K. Barker and B. B. Seedhom, “The relationship of the compressive modulus of articular cartilage with its deformation response to cyclic loading: Does cartilage optimize its modulus so as to minimize the strains arising in it due to the prevalent loading regime?,” *Rheumatology*, vol. 40, no. 3, pp. 274–284, 2001, doi: 10.1093/rheumatology/40.3.274.
- [232] L. Zhang, S. Miramini, D. W. Smith, B. S. Gardiner, and A. J. Grodzinsky, “Time Evolution of Deformation in a Human Cartilage Under Cyclic Loading,” *Ann. Biomed. Eng.*, vol. 43, no. 5, 2015, doi: 10.1007/s10439-014-1164-8.
- [233] H. Guo, S. A. Maher, and P. A. Torzilli, “A biphasic finite element study on the role of the articular cartilage superficial zone in confined compression,” *J. Biomech.*, vol. 48, no. 1, pp. 166–170, 2015, doi: 10.1016/j.jbiomech.2014.11.007.
- [234] P. A. Torzilli and S. N. Allen, “Effect of Articular Surface Compression on Cartilage Extracellular Matrix Deformation,” *J. Biomech. Eng.*, vol. 144, no. 9, pp. 1–11, 2022, doi: 10.1115/1.4054108.
- [235] L. A. Setton, W. Zhu, and V. C. Mow, “The biphasic poroviscoelastic behavior of articular cartilage: Role of the surface zone in governing the compressive behavior,” *J. Biomech.*, vol. 26, no. 4–5, pp. 581–592, 1993, doi: 10.1016/0021-9290(93)90019-B.
- [236] J. R. Owen and J. S. Wayne, “Contact models of repaired articular surfaces: Influence of loading conditions and the superficial tangential zone,” *Biomech. Model. Mechanobiol.*, vol. 10, no. 4, pp. 461–471, 2011, doi: 10.1007/s10237-010-0247-1.
- [237] V. C. Mow, M. H. Holmes, and W. Michael Lai, “Fluid transport and mechanical properties of articular cartilage: A review,” *J. Biomech.*, vol. 17, no. 5, pp. 377–394, 1984, doi: 10.1016/0021-9290(84)90031-9.
- [238] C. Herberhold *et al.*, “In situ measurement of articular cartilage deformation in intact femoropatellar joints under static loading,” *J. Biomech.*, vol. 32, no. 12, pp. 1287–1295, 1999, doi: 10.1016/S0021-9290(99)00130-X.

- [239] G. S. Beaupré, S. S. Stevens, and D. R. Carter, “Mechanobiology in the development, maintenance, and degeneration of articular cartilage,” 2000. doi: 10.1068/d9909.
- [240] V. C. Mow, M. C. Gibbs, W. M. Lai, W. B. Zhu, and K. A. Athanasiou, “Biphasic indentation of articular cartilage-II. A numerical algorithm and an experimental study,” *J. Biomech.*, vol. 22, no. 8–9, pp. 853–861, 1989, doi: 10.1016/0021-9290(89)90069-9.
- [241] K. A. Athanasiou, A. Agarwal, and F. J. Dzida, “Comparative study of the intrinsic mechanical properties of the human acetabular and femoral head cartilage,” *J. Orthop. Res.*, vol. 12, no. 3, pp. 340–349, 1994, doi: 10.1002/jor.1100120306.
- [242] D. D. Chan, L. Cai, K. D. Butz, S. B. Trippel, E. A. Nauman, and C. P. Neu, “In vivo articular cartilage deformation: Noninvasive quantification of intratissue strain during joint contact in the human knee,” *Sci. Rep.*, vol. 6, no. August 2015, 2016, doi: 10.1038/srep19220.
- [243] B. T. Graham, A. C. Moore, D. L. Burris, and C. Price, “Detrimental effects of long sedentary bouts on the biomechanical response of cartilage to sliding,” *Connect. Tissue Res.*, pp. 1–14, Jan. 2020, doi: 10.1080/03008207.2019.1673382.
- [244] R. Dumas, F. Moissenet, and L. Cheze, “Fluoroscopy-based subject-specific knee joint constraints for the estimation of prosthesis kinematics and contact velocities during gait,” *Comput. Methods Biomech. Biomed. Engin.*, vol. 23, no. sup1, pp. S91–S93, 2020, doi: 10.1080/10255842.2020.1812170.
- [245] M. S. Farnham, R. E. Larson, D. L. Burris, and C. Price, “Effects of mechanical injury on the tribological rehydration and lubrication of articular cartilage,” *J. Mech. Behav. Biomed. Mater.*, vol. 101, no. August 2018, p. 103422, 2020, doi: 10.1016/j.jmbbm.2019.103422.
- [246] M. S. Farnham, K. F. Ortved, J. S. Horner, N. J. Wagner, D. L. Burris, and C. Price, “Lubricant Effects on Articular Cartilage Sliding Biomechanics Under Physiological Fluid Load Support,” *Tribol. Lett.*, vol. 69, no. 2, pp. 1–14, 2021, doi: 10.1007/s11249-021-01430-0.
- [247] J. Klein, “Molecular mechanisms of synovial joint lubrication,” *Proc. Inst. Mech. Eng. Part J J. Eng. Tribol.*, vol. 220, no. 8, pp. 691–710, 2006, doi: 10.1243/13506501JET143.
- [248] C. Putignano, D. Burris, A. Moore, and D. Dini, “Cartilage rehydration: The

- sliding-induced hydrodynamic triggering mechanism,” *Acta Biomater.*, vol. 125, pp. 90–99, 2021.
- [249] D. R. Carter, G. S. Beaupré, M. Wong, R. L. Smith, T. P. Andriacchi, and D. J. Schurman, “The mechanobiology of articular cartilage development and degeneration,” *Clin. Orthop. Relat. Res.*, no. 427 SUPPL., pp. 69–77, 2004, doi: 10.1097/01.blo.0000144970.05107.7e.
- [250] L. F. Mellor, A. J. Steward, R. C. Nordberg, M. A. Taylor, and E. G. Lobo, “Comparison of simulated microgravity and hydrostatic pressure for chondrogenesis of hASC,” *Aerosp. Med. Hum. Perform.*, vol. 88, no. 4, pp. 377–384, 2017, doi: 10.3357/AMHP.4743.2017.
- [251] J. N. Todd, T. G. Maak, G. A. Ateshian, S. A. Maas, and J. A. Weiss, “Hip chondrolabral mechanics during activities of daily living: Role of the labrum and interstitial fluid pressurization,” *J. Biomech.*, vol. 69, pp. 113–120, Mar. 2018, doi: 10.1016/j.jbiomech.2018.01.001.
- [252] C. O. Dyrby, S. Koo, T. P. Andriacchi, R. L. Smith, A. Mündermann, and E. J. Alexander, “A Framework for the in Vivo Pathomechanics of Osteoarthritis at the Knee,” *Ann. Biomed. Eng.*, vol. 32, no. 3, pp. 447–457, 2004, doi: 10.1023/b:abme.0000017541.82498.37.
- [253] G. Bergmann *et al.*, “Hip forces and gait patterns from routine activities,” *J. Biomech.*, vol. 34, pp. 859–871, 2001.
- [254] G. N. de Boer, N. Raske, S. Soltanahmadi, D. Dowson, M. G. Bryant, and R. W. Hewson, “A porohyperelastic lubrication model for articular cartilage in the natural synovial joint,” *Tribol. Int.*, no. July 2018, p. 105760, 2019, doi: 10.1016/j.triboint.2019.04.044.
- [255] G. N. de Boer, N. Raske, S. Soltanahmadi, M. G. Bryant, and R. W. Hewson, “Compliant-poroelastic lubrication in cartilage-on-cartilage line contacts,” *Tribol. - Mater. Surfaces Interfaces*, vol. 14, no. 3, pp. 151–165, 2020, doi: 10.1080/17515831.2020.1720381.
- [256] B. Graham, “Novel Approaches To Determine the Role of Diffusive and Convective Transport Environments in Articular Cartilage Function,” 2018, [Online]. Available: <https://search.proquest.com/docview/2191586207?pq-origsite=gscholar>.
- [257] B. T. Graham, A. C. Moore, D. L. Burris, and C. Price, “Mapping the spatiotemporal evolution of solute transport in articular cartilage explants reveals how cartilage recovers fluid within the contact area during sliding,” *J.*

Biomech., pp. 1–6, 2018, doi: 10.1016/j.jbiomech.2018.01.041.

- [258] J. P. Gleghorn and L. J. Bonassar, “Lubrication mode analysis of articular cartilage using Stribeck surfaces,” *J. Biomech.*, vol. 41, no. 9, pp. 1910–1918, Jan. 2008, doi: 10.1016/j.jbiomech.2008.03.043.
- [259] C. P. Neu, K. Komvopoulos, and A. H. Reddi, “The interface of functional biotribology and regenerative medicine in synovial joints,” *Tissue Engineering - Part B: Reviews*, vol. 14, no. 3, pp. 235–247, 2008, doi: 10.1089/ten.teb.2008.0047.
- [260] B. Graham, “NOVEL APPROACHES TO DETERMINE THE ROLE OF DIFFUSIVE AND CONVECTIVE TRANSPORT ENVIRONMENTS IN ARTICULAR CARTILAGE FUNCTION,” 2018. [Online]. Available: <https://search.proquest.com/docview/2191586207?pq-origsite=gscholar>.
- [261] A. C. Moore, “Independent and Competing Roles of Fluid Exudation and Rehydration in Cartilage Mechanics and Tribology,” 2017, [Online]. Available: <https://udspace.udel.edu/handle/19716/24506>.
- [262] “five-parameter logistic equation.” https://www.graphpad.com/guides/prism/latest/curve-fitting/reg_asymmetric_dose_response_ec_2.htm.
- [263] M. E. Kupratis, A. E. Gure, K. F. Ortved, D. L. Burris, and C. Price, “Comparative Tribology: Articulation-induced Rehydration of Cartilage Across Species,” *Biotribology*, vol. 25, no. September 2020, p. 100159, 2021, doi: 10.1016/j.biotri.2020.100159.
- [264] D. Dowson and Zhong-Min Jin, “Micro-elastohydrodynamic lubrication of synovial joints,” *Eng. Med.*, vol. 15, no. 2, pp. 63–65, 1986, doi: 10.1243/EMED_JOUR_1986_015_019_02.
- [265] B. J. Hamrock and D. Dowson, “Elastohydrodynamic Lubrication of Elliptical Contacts for Materials of Low Elastic Modulus,” *Am. Soc. Mech. Eng.*, vol. 100, no. 78-Lub-1, 1978.
- [266] Z. M. Jin and D. Dowson, “Elastohydrodynamic lubrication in biological systems,” *Proc. Inst. Mech. Eng. Part J J. Eng. Tribol.*, vol. 219, no. 5, pp. 367–380, 2005, doi: 10.1243/135065005X33982.
- [267] E. D. Bonnevie and L. J. Bonassar, “A Century of Cartilage Tribology Research Is Informing Lubrication Therapies,” *J. Biomech. Eng.*, vol. 142, no. 3, 2020, doi: 10.1115/1.4046045.

- [268] J. A. Buckwalter, D. D. Anderson, T. D. Brown, Y. Tochigi, and J. A. Martin, "The Roles of Mechanical Stresses in the Pathogenesis of Osteoarthritis: Implications for Treatment of Joint Injuries," *Cartilage*, vol. 4, no. 4, pp. 286–294, Oct. 2013, doi: 10.1177/1947603513495889.
- [269] T. P. Andriacchi and J. Favre, "The nature of in vivo mechanical signals that influence cartilage health and progression to knee osteoarthritis," *Current rheumatology reports*, vol. 16, no. 11. 2014, doi: 10.1007/s11926-014-0463-2.
- [270] D. Simon, R. Mascarenhas, B. M. Saltzman, M. Rollins, B. R. Bach, and P. MacDonald, "The Relationship between Anterior Cruciate Ligament Injury and Osteoarthritis of the Knee," *Advances in Orthopedics*, vol. 2015. Hindawi Limited, 2015, doi: 10.1155/2015/928301.
- [271] J. E. Bischof *et al.*, "In vivo cartilage contact strains in patients with lateral ankle instability," *J. Biomech.*, vol. 43, no. 13, pp. 2561–2566, 2010, doi: 10.1016/j.jbiomech.2010.05.013.
- [272] S. K. Van De Velde *et al.*, "Increased tibiofemoral cartilage contact deformation in patients with anterior cruciate ligament deficiency," *Arthritis Rheum.*, vol. 60, no. 12, pp. 3693–3702, 2009, doi: 10.1002/art.24965.
- [273] K. J. Vazquez, J. T. Andrae, and C. R. Henak, "Cartilage-on-cartilage cyclic loading induces mechanical and structural damage," *J. Mech. Behav. Biomed. Mater.*, vol. 98, pp. 262–267, 2019, doi: 10.1016/j.jmbbm.2019.06.023.
- [274] T. S. Atkinson, R. C. Haut, and N. J. Altiero, "An investigation of biphasic failure criteria for impact-induced fissuring of articular cartilage," *J. Biomech. Eng.*, vol. 120, no. 4, pp. 536–537, 1998, doi: 10.1115/1.2798025.
- [275] R. L. Trevino, C. A. Pacione, A.-M. Malfait, S. Chubinskaya, and M. A. Wimmer, "Development of a Cartilage Shear-Damage Model to Investigate the Impact of Surface Injury on Chondrocytes and Extracellular Matrix Wear.," *Cartilage*, vol. 8, no. 4, pp. 444–455, Oct. 2017, doi: 10.1177/1947603516681133.
- [276] B. Kurz, A. K. Lemke, J. Fay, T. Pufe, A. J. Grodzinsky, and M. Schünke, "Pathomechanisms of cartilage destruction by mechanical injury," *Ann. Anat.*, vol. 187, no. 5–6, pp. 473–485, 2005, doi: 10.1016/j.aanat.2005.07.003.
- [277] F. Zhu, P. Wang, N. H. Lee, M. B. Goldring, and K. Konstantopoulos, "Prolonged Application of High Fluid Shear to Chondrocytes Recapitulates Gene Expression Profiles Associated with Osteoarthritis," *PLoS One*, vol. 5, no. 12, 2010, doi: 10.1371/journal.pone.0015174.

- [278] T. P. Andriacchi, J. Favre, J. C. Erhart-Hledik, and C. R. Chu, "A Systems View of Risk Factors for Knee Osteoarthritis Reveals Insights into the Pathogenesis of the Disease," *Ann. Biomed. Eng.*, vol. 43, no. 2, pp. 376–387, 2015, doi: 10.1007/s10439-014-1117-2.
- [279] C. R. Chu and T. P. Andriacchi, "Dance between biology, mechanics, and structure: A systems-based approach to developing osteoarthritis prevention strategies," *J. Orthop. Res.*, vol. 33, no. 7, pp. 939–947, 2015, doi: 10.1002/jor.22817.
- [280] L. Petrigna, F. Roggio, B. Trovato, M. Zangh, C. Guglielmino, and G. Musumeci, "How Physical Activity Affects Knee Cartilage and a Standard Intervention Procedure for an Exercise Program : A Systematic Review," 2022.
- [281] R. Krishnan, S. Park, F. Eckstein, and G. A. Ateshian, "Inhomogeneous Cartilage Properties Enhance Superficial Interstitial Fluid Support and Frictional Properties, But Do Not Provide a Homogeneous State of Stress," *J. Biomech. Eng.*, vol. 125, no. 5, pp. 569–577, 2003, doi: 10.1115/1.1610018.
- [282] A. L. Clark, L. D. Barclay, J. R. Matyas, and W. Herzog, "In situ chondrocyte deformation with physiological compression of the feline patellofemoral joint," *J. Biomech.*, vol. 36, no. 4, pp. 553–568, 2003, doi: 10.1016/S0021-9290(02)00424-4.

Appendix A

SUPPLEMENTAL METHODS

A.1 Darcy Flow Model Development

The development of the squeeze film exudation model is dependent on Darcy's Law and conservation of mass flow through the permeable tissue and contact interface. Refer to Figure A. 1 for flow analysis through the tissue. To calculate the fluid pressurization in the tissue, lateral transmission of the fluid was assumed per unconfined compression analysis. The total fluid exudation included the summation of the fluid being ejected through the tissue and the contact gap. The pressure drop from point 1 to point 2 was assumed ~ 0 , as demonstrated by previous numerical analyses of fluid flow stream lines within cartilage (see appendix B in [17] and Figure 3 in [281] and Figure 10 in [194]).

Using conservation of flow within a small section of the tissue, the following relationship is given:

$$2\pi i \cdot r \cdot dh \cdot V(r) = 2\pi i \cdot r \cdot ds \cdot \delta$$
$$V(@r) = \frac{ds \cdot \delta}{dh}$$

Because of the symmetry of streamlines in the squeeze film analysis, the following relationship between a change 'dh' and 'ds' is provided:

$$2 \cdot \frac{dh}{h} = \frac{ds}{a}$$

And therefore:

$$V(@r) = \frac{2a \cdot \dot{\delta}}{h}$$

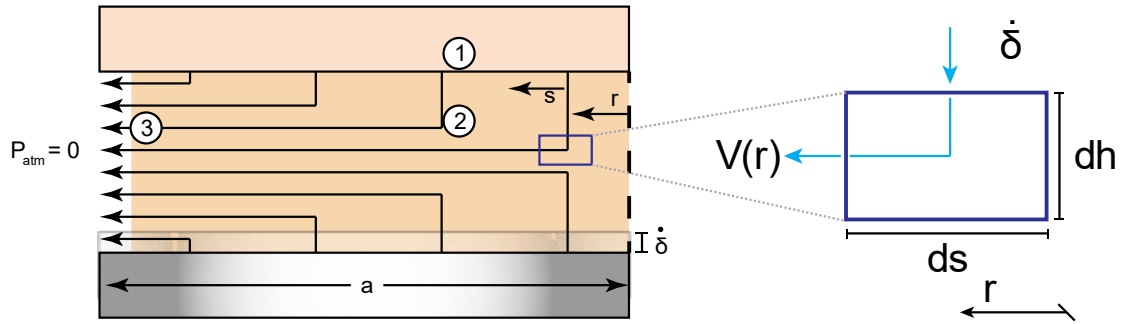


Figure A. 1: The squeeze film analysis of fluid flow for a given time step. The change in strain ($\dot{\delta}$) manifests as streamlines as shown. 'r' represents the distance from the center of contact to each streamline. 's' is the axis that accounts for the distance each streamline must travel to be laterally ejected. For an infinitely small section of the tissue (shown on the right), the velocity ($V(r)$) of streamline starting at distance 'r' can be calculated for a given $\dot{\delta}$. 'dh' represents the change in thickness, or thickness, of the tissue.

The velocity relationship $V(r) = \frac{2a \cdot \dot{\delta}}{h}$ can be used with the conservation of flow expanding out radially as shown in the contact area Figure A. 2. The following relationship can be provided:

$$r \cdot d\theta \cdot V(@r) = V(r + s) \cdot (r + s) \cdot d\theta$$

And thus, the velocity of a stream line originating at distance 'r' along axis 's' can be defined:

$$V(r, s) = \frac{2a \cdot \dot{\delta}}{h} \cdot \frac{r}{r + s}$$

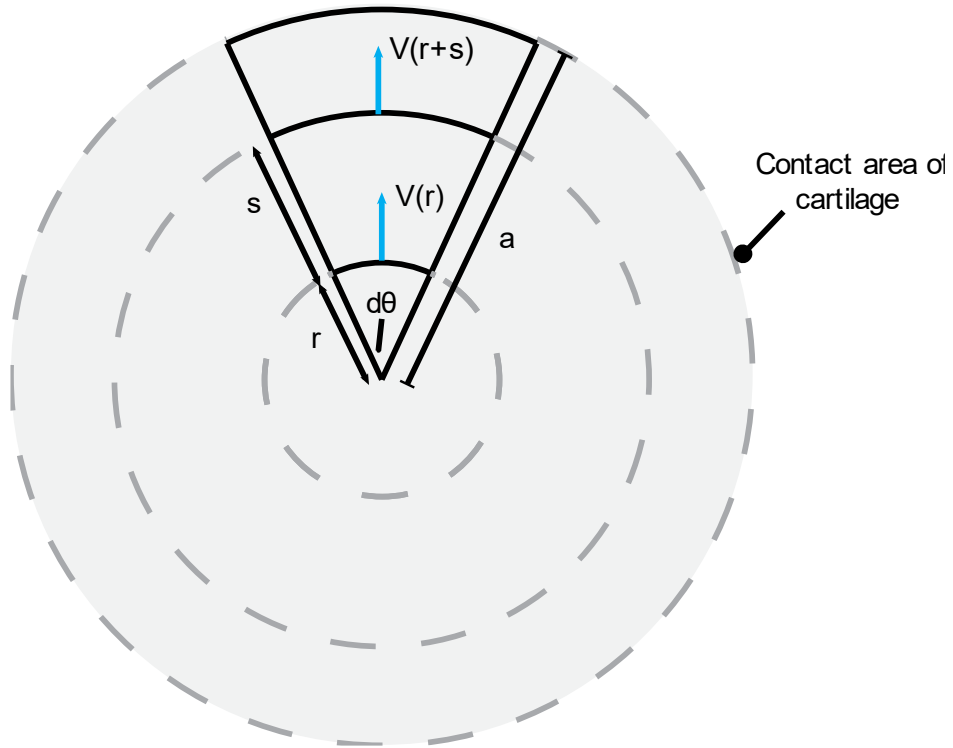


Figure A. 2: Looking at the contact area of cartilage, conservation of flow requires that the flow rate for any slice defined by $d\theta$ must equate. Using the relationship, $V(r) = \frac{2a \cdot \dot{\delta}}{h}$, the flow velocity at point $V(r+s)$ can be defined.

Darcy's law states that $\nabla P_{2-3} = V/k$, and therefore the pressure at distance 'r' can be calculated:

$$P(r) = \int_0^{a-r} \frac{V(s, r)}{k} \cdot ds = \frac{2 \cdot \dot{\delta} \cdot a \cdot r}{h \cdot k} (\ln(a) - \ln(r))$$

The average pressure within a cartilage at a given timepoint, P_{ave} , can be calculated with the known values of contact radius (a), permeability (k), and strain rate ($\dot{\epsilon}$).

$$P_{ave} = \frac{1}{a-0} \int_0^a P(r) \cdot dr = \frac{4 \cdot a^2}{9 \cdot k} \cdot \dot{\epsilon}$$

A.2 Model Iterative Algorithm and Fit

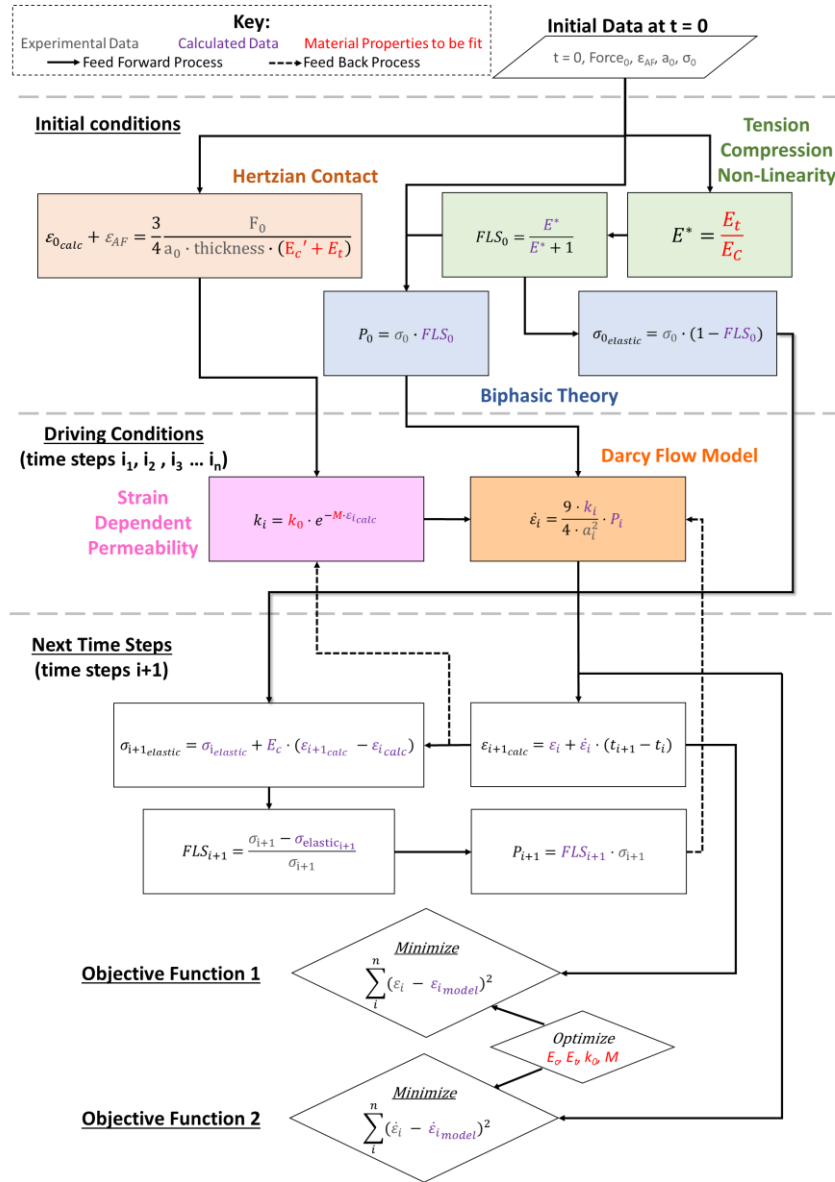


Figure A. 3: The algorithm to compute the model strain. The model starts at the initial conditions and computes the permeability and strain rate at each time step. The next time steps are then used in subsequent time steps to update permeability and strain rate. The material properties are optimized based on the two objective functions.

A.3 Exudation Model Image processing

Because of the potential change in image darkness from initial contact to final contact, an adaptive algorithm was applied to calculate the contact area. First, image intensities were adjusted such that grayer pixels would be saturated near the fringe of the contact area. Then were binarized with an adaptive threshold, including a sensitivity of 0.9. Binarized images were dilated via orthogonal flat linear structuring elements (length = 4 pixels) to fill in any generated holes. An active contour was then applied to the binary images based on the original image (N = 15 iterations). Finally the area was then calculated based on the calibration constant of .018243 mm/pixel. Figure A. 4 showcases the contact area at initial contact and the equilibrium contact area from a single 3N static load test.

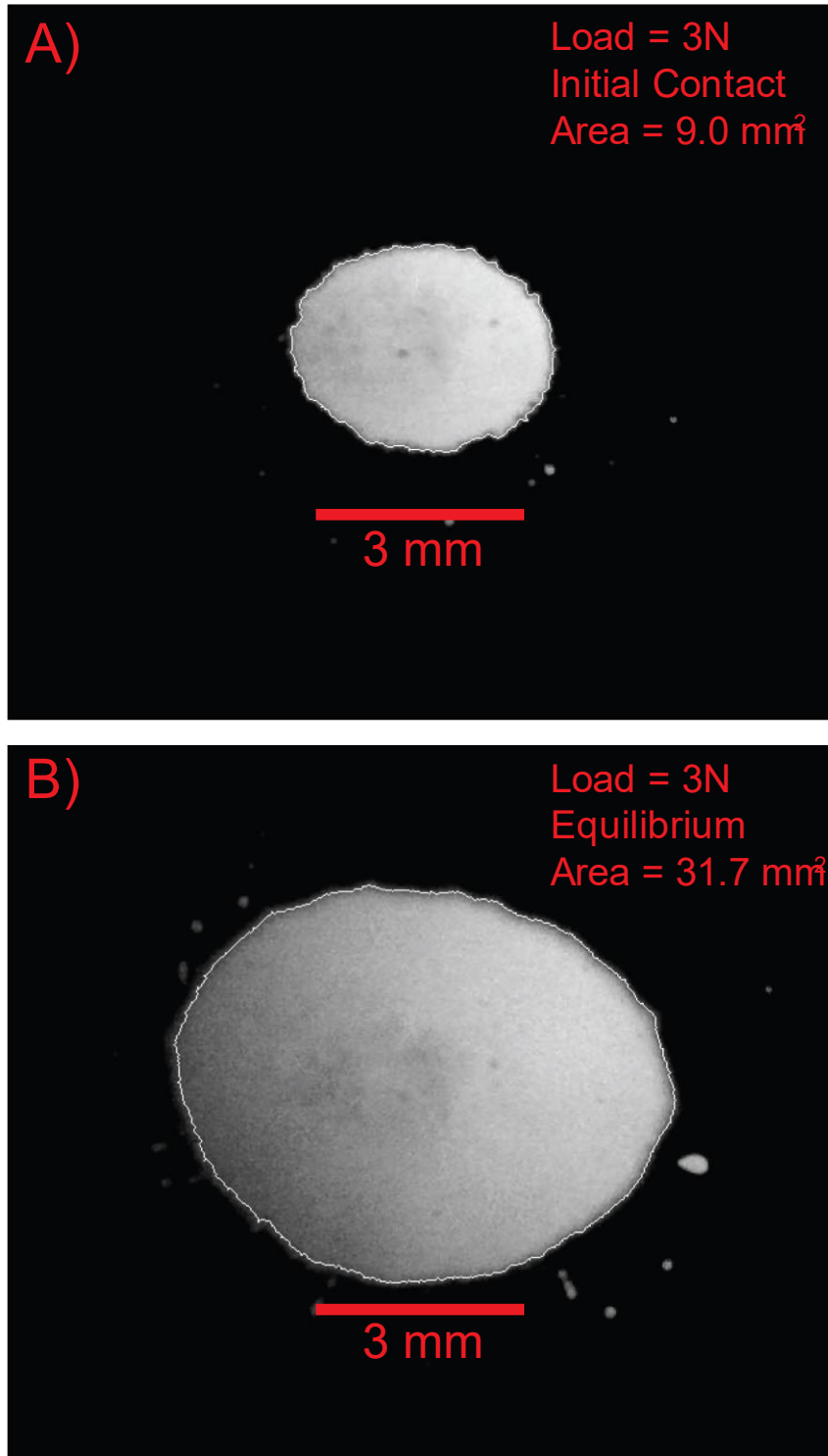


Figure A. 4: The calculated area for two images in a single test. All data within the white outlines shown was considered the contact area.

Appendix B

SUPPLEMENTAL RESULTS

B.1 Exudation Model Results

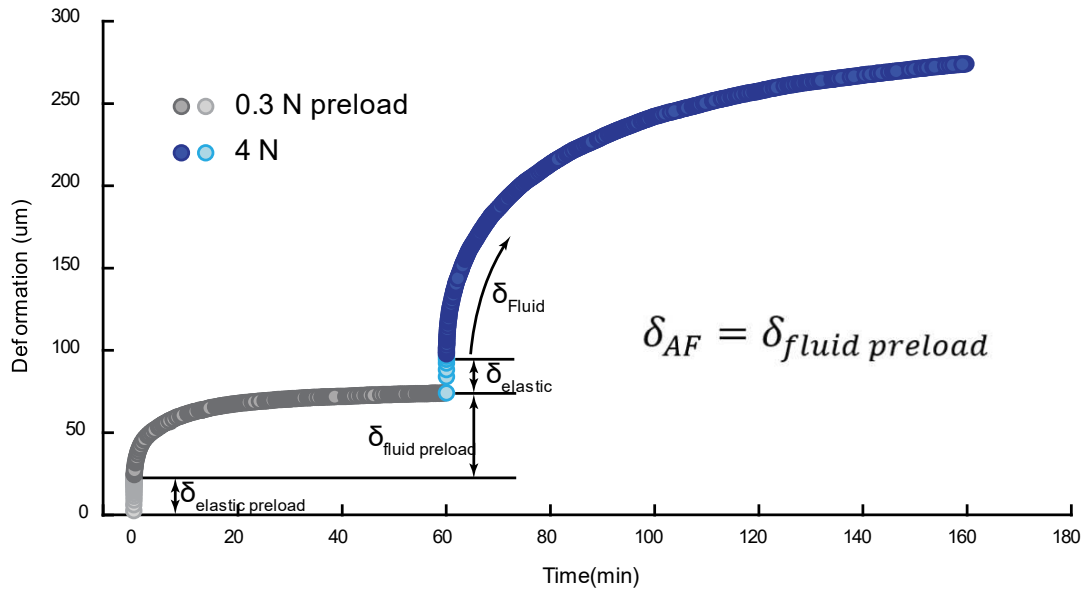


Figure B. 1: A representative preload at 0.3N is shown before at a 4N load. The preload causes an elastic deformation ($\delta_{elastic\ preload}$) and fluid deformation ($\delta_{fluid\ preload}$). If the accumulated fluid is not accounted for the exudation model (Section 3.2.4), the effective tensile modulus is calculated much softer and the fluid pressurization will be undercalculated. Thus, the $\delta_{fluid\ preload} = \epsilon_{AF}$ for Equation 11 calculations.

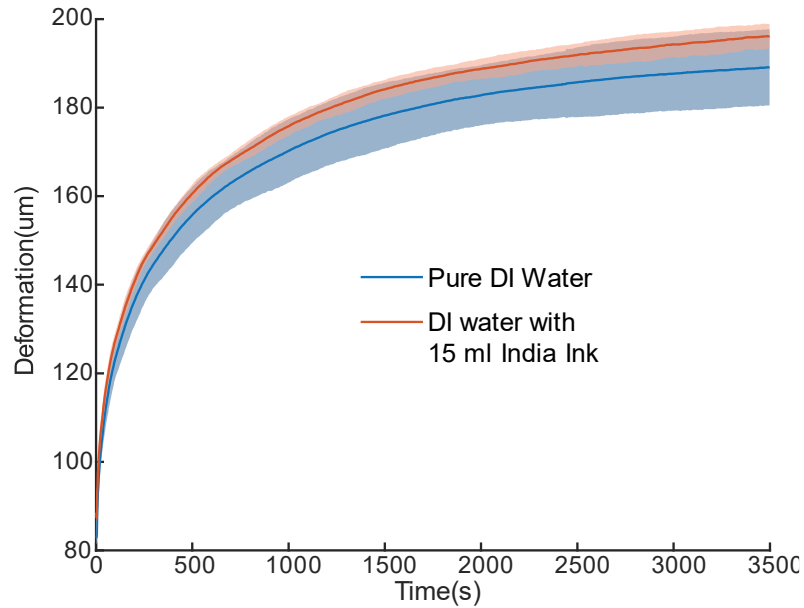


Figure B. 2: The mean characteristic curves of exudation are compared between pure DI water and same volume of water with 15ml of India Ink (n = 3 repeat tests for each condition, 5 N load for all tests). The overlap of the 2 standard deviation (shaded portions) indicate that the inclusion of India Ink did not significantly alter the exudation mechanics of the cartilage layer.

B.2 Rehydration Rates Comparison

B.2.1 Comparing Cartilage-on-Cartilage rehydration vs. Free Swelling and Passive Swelling

We used a cartilage-on-glass contact to enforce a zero-flow boundary for passive swelling measurements. This is consistent with the zero-flow boundary used in biphasic theory. The experiment was repeated with a cartilage-on-cartilage contact to demonstrate that passive recovery against glass represents the physiological situation. The challenge, in this case, is that two surfaces recover fluid with unknowable relative

contributions. We divided the total recovery of both surfaces by two to obtain the average passive swelling rate for each. While we cannot measure the contact area, the contact between two identical elastic spheres is approximately equal to the contact between one elastic sphere against a 'rigid' (glass) flat according to Hertz contact theory.

Figure **Error! Reference source not found.** demonstrates the testing configurations for the representative sample, including the total fluid recovery and rate of fluid recovery. For these experiments, the cartilage sample was loaded at 5N of load until a deformation of 315 +/- 20 um. As illustrated, the cartilage-on-cartilage recovery response was comparable to the cartilage-on-glass passive swelling response and many times slower than free swelling against a porous indenter. The important takeaway is that the recovery of cartilage is slowed significantly by contact with glass, cartilage, or any other 'low permeability' surface.

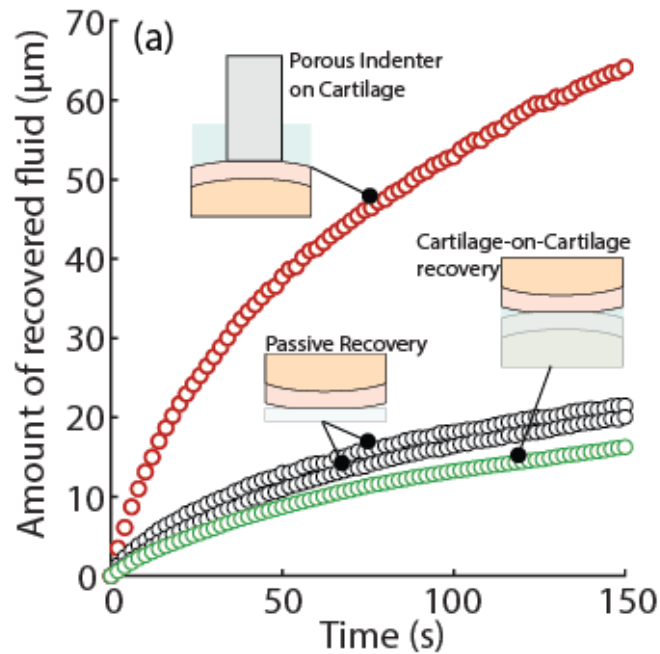


Figure B. 3: Comparing the rehydration characteristics of unloaded cartilage-on-cartilage with free swelling and passive swelling measurements described in methods Section 4.2. The amount of fluid recovered by the cartilage surface are plotted versus time. In the cartilage-on-cartilage experiment, the total recovery was divided by 2 surfaces to obtain the average rate. A second passive recovery repeat measurement performed after free swelling to demonstrate that contact with the porous indentation had no significant effect on the passive swelling response.

B.2.2 Quantifying Applied Contact Pressures

To rehydrate the tissue, cartilage must overcome the exudation due to the contact pressure. Although the contact pressure is not explicitly reported for all the data sets, the contact area was measured for some representative samples through the glass slide in the experimental configuration. Contact pressures during loaded

exudation (5N) and static unloading (passive swelling at 0.1 N) are compared at the same total deformation in Figure B. 4. For this representative sample, the initial contact stress during static loading was 0.30 MPa and decreased to 0.12 due to relaxation of the tissue (i.e. increase in contact diameter). During static unloading, the contact area remained large and contact stresses decreased in proportion to the change in load; in this case, contact stress decreased by $\sim 10\times$ and remained extremely low throughout the rehydration process. In the case of free swelling, the nominal contact area is equal to the area of the indenter.

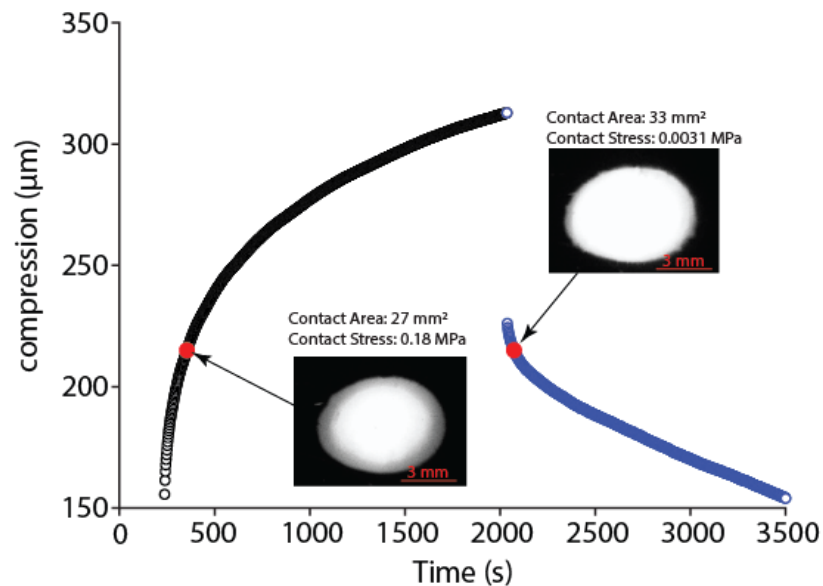


Figure B. 4: An example comparison of the contact area and contact pressure between static loading and static unloading. Cartilage maintained a relatively constant contact area during unloading. Recovery following exudation is promoted by the reduction in contact pressure but impeded by the contact area. The contact area decreased during recovery such that the contact pressure increased from 0.003 to 0.005 MPa by the end of the experiment.

Contact pressures were also measured for a second representative sample for a static load (5N) followed by sliding at 100 mm/s under constant load (tribological rehydration), as shown in Figure B. 5. During loaded sliding, cartilage recovered fluid despite increased contact pressures compared to static loading.

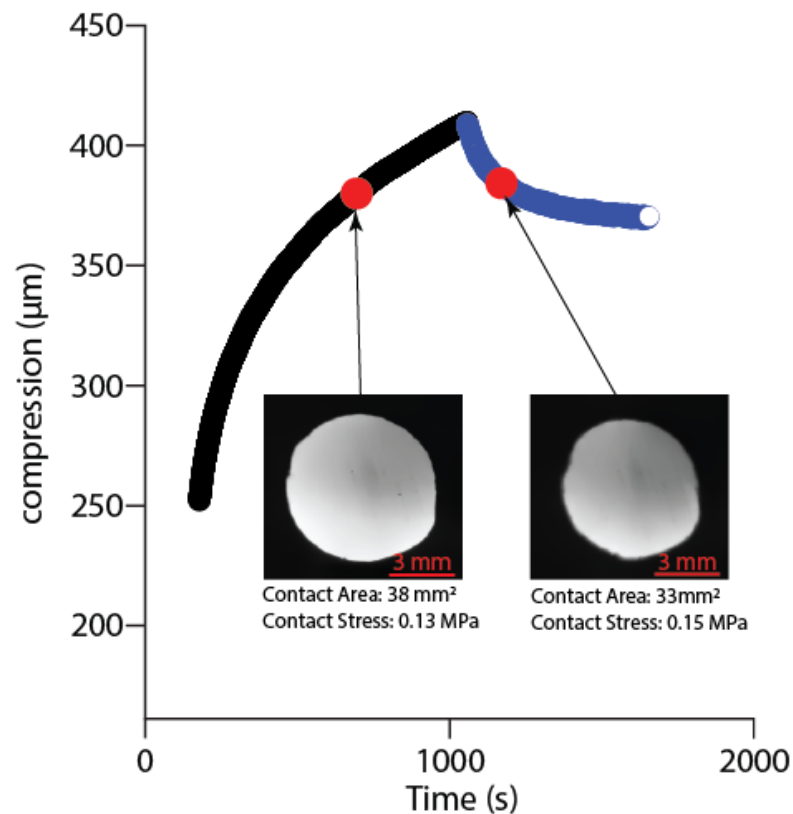


Figure B. 5: An example comparison of the contact area and contact pressure between static loading and loaded sliding. Cartilage maintains relatively constant contact pressure during sliding conditions, but tribological rehydration allows for bulk tissue hydration, which stiffens the tissue, reduces the contact area, and increases the contact pressure. Throughout the tribological rehydration process, the contact stress was between 0.15 and 0.16 MPa.

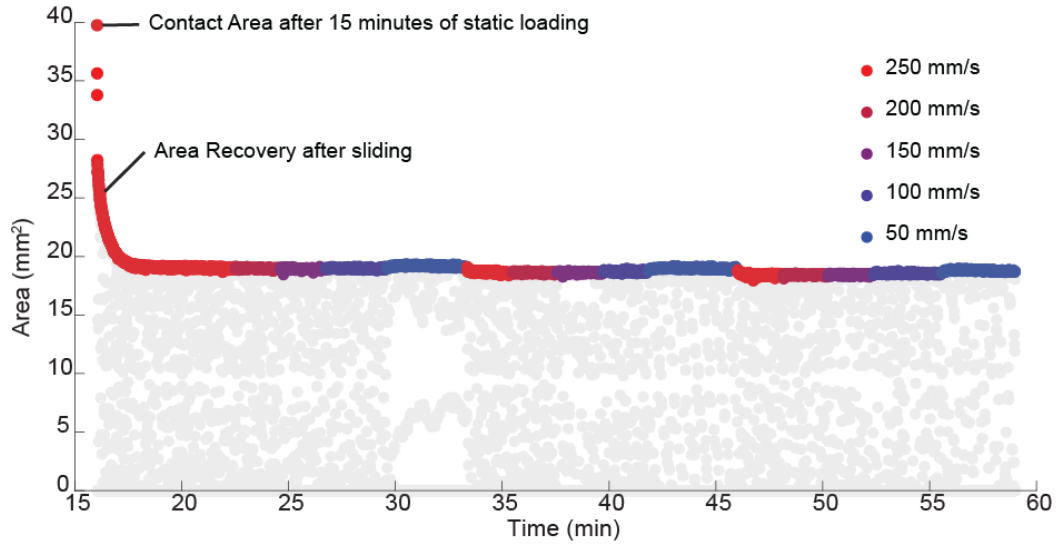


Figure B. 6: Quantification of area during sliding experiments after 15 minutes of static loading. Images of contact area during sliding were captured every 0.1 seconds. Because images were taken during through a port in the POD tribometer, the area was not always well defined (see grey data points). The true area was computed as the maximum area during each rotation, as illustrated by the colored array.